UNIVERSITÀ DEGLI STUDI DI MILANO

Scuola di Dottorato in Fisica, Astrofisica e Fisica Applicata

Dipartimento di Fisica

Corso di Dottorato in Fisica, Astrofisica e Fisica Applicata

Ciclo XXV

Renormalization Effects in Nuclei

Settore Scientifico Disciplinare FIS/04

Supervisore: Professor Ricardo A. BROGLIA

Coordinatore: Professor Marco BERSANELLI

Tesi di Dottorato di:

Andrea IDINI

Anno Accademico 2012

Commission of the final examination:

External Referee:
Professor Kalrheinz LANGANKE

External Member:
Professor Francesco PEDERIVA

Internal Members:
Professor Ricardo A. BROGLIA

Professor Davide GALLI

Final examination:

Date 04-02-2012

Università degli Studi di Milano, Dipartimento di Fisica, Milano, Italy

Cover illustration:
Andrea Zanzani
Internal illustrations:
Andrea Idini
Template Design:
Annalisa Varri, Ph.D.

MIUR subjects:
FIS/04

PACS:
...

Contents

Abstract

"You can't say A is made of B or vice versa: all mass is interaction"
-Richard P. Feynman

Renormalization effects in nuclei, namely the calculation of the field theoretical processes which dress single-particle and collective degrees of freedom, lead to observable quantal states which constitute the main manifestation of the nuclear structure to external fields, among them inelastic and one- and two- particle transfer reactions, aside from decay processes. They result from the (nuclear) Field Theory (NFT) orthogonalization of the associated product basis states, and are thus intimately connected not only with a static, but also with a dynamic requirement of selfconsistency between mean field and density, allowing also for scattering processes (vertices). Such requirements are fulfilled through the diagonalization of the particle-vibration coupling Hamiltonian, properly supplemented by four point vertices, leading, among other things, to a single, unified source of ground state correlations (quantal zero point fluctuations). Through them, single-particle and collective degrees of freedom melt together into the physical states which display both features, emphasizing their common, complementary origin, closely related to the fact that nuclei respond elastically to rapid solicitations (shell model) and plastically over longer periods of time (liquid drop). It is found that renormalization effects are important in the description of both superfluid and normal nuclei. In particular, they contribute to 50% of the value of the pairing gap of ^{120}Sn, and reduce by 40% the single-particle content of specific valence states of the exotic, closed shell nucleus ^{132}Sn.

Further progress in the systematic implementation of the renormalization program will be related to: i) the development of a bare NN-force which allows for an accurate and economic determination of both single-particle and collective degrees of freedom within the framework of HFB and QRPA respectively, thus providing the non-orthogonal, overcomplete basis of NFT with which to work out the variety of couplings; ii) development of experimental techniques which eventually brings the study of nuclear spin modes to the same level as that of density modes studies. The reaching of these two objetives are likely to constitute milestones in making operative renormalization processes as standard elements of nuclear structure calculations.

CHAPTER 1

Renormalization of the properties of the superfluid nucleus ^{120}Sn

"Anything that happens, happens.
Anything that, in happening, causes something else to happen, causes something else to happen.
Anything that, in happening, causes itself to happen again, happens again.
It doesn't necessarily do it in chronological order, though."
-Douglas Adams

1.1 Introduction

Collective and single-particle (quasiparticle) degrees of freedom constitute the elementary modes of nuclear excitation which relate theory directly to experiment, that is, to the outcome of elastic, inelastic, Coulomb excitation and γ–decay processes, as well as one-, two- and multi-particle transfer and knock-out reactions. A central theme in the development of the modern view of nuclear structure has been that of achieving a proper balance in the use of the above mentioned apparently contrasting aspects of nuclear dynamics. The development of nuclear field theory (NFT) (cf., e.g., [1, 2, 3, 4, 5, 6, 7] and references therein) provided a rigorous theoretical framework to describe nuclear structure in terms of elementary modes of excitation. It was also instrumental to show that collective and quasiparticle degrees of freedom are complementary facets of nuclear dynamics, as evidenced by their interweaving and by the associated renormalization effects. This is in keeping with the fact that collective and quasiparticle degrees of freedom constitute a basis that is overcomplete. Vibrations and rotations are built out of the same quasiparticle degrees of freedom as those involved in independent particle motion. As a consequence, there is a (coupling) term H_C in the NFT Hamiltonian, which is linear in both the single- particle and the collective coordinates. NFT provides the rules to work out, one at a time, the different processes dressing quasiparticle and collective modes. Summing up the different contributions (diagrams) to any order of perturbation, eventually also to infinite order, one can diagonalize H_C to the chosen accuracy and thus renormalize the variety of elementary modes of nuclear excitation.

The results of the calculations can be directly used as input in working out the absolute differential cross sections and transition probabilities, which can be compared to the corresponding experimental data. Also to calculate optical potentials as needed to describe the elastic channels, as well as the different direct reaction channels.

Although much work has been done concerning this program in connection with one-particle transfer (cf. e.g. [8, 9]) as well particle-hole channels (mostly in connection with the studies of giant resonances cf. e.g. [10, 11]), little has been done regarding the role renormalization (medium polarization) effects have on nuclear interactions in general, and on pairing correlations in particular.

The basic scope of the present thesis was that of studying and systematically calculate, in the case of a superfluid nucleus, pairing correlations taking properly into account renormalization effects. In particular, not only the bare but also the induced pairing interaction arizing from the exchange of collective density and spin vibrations between nucleons moving in time reversal states close to the Fermi energy, properly corrected by self-energy (correlation (CO) and polarization (PO)) processes and vertex corrections [12]. The final scope of the thesis was that of using these results as input to reaction software aimed at calculating absolute cross sections which can be directly compared to observables. In particular absolute two-particle transfer differential cross section, specific probe of pairing in nuclei, thus avoiding the use of spectroscopic factors, difficult to justify theoretically in the case of one-particle transfer processes, let alone in the case of Cooper pair transfer [8, 9, 13].

It did not escape my attention that such a program was tantamount to solving, at least to a large extent, the many-body nuclear problem, taking properly into account both bound and continuum states, as well as the $\omega-$dependence of the different renormalization processes, working out microscopically effective charges, masses and interactions resulting from the interweaving of quasiparticle and density and spin modes. Although in my three year PhD work I was not able to bring to completion this program, I have come close to having developed all the elements to do so on short call, as documented below. These elements have been worked out also considering the possibility of implementing them within the most exotic scenario of the inner crust of neutron stars, allowing for the presence of finite nuclei immersed in the sea of free neutrons (see e.g. [14] and refs. therein).

I am using as input a (Skyrme-based) mean field and a bare pairing interaction. Once these elements are introduced, one can proceed to calculate the bare quasiparticles (BCS solution of pairing) and, in the corresponding two quasiparticle basis, the collective vibrational modes (QRPA). In this way one obtains the basic matrix element (processes) defining H_C, namely the scattering of a quasiparticle from an initial to a final state through the creation of a collective mode. The corresponding formfactors and strengths determine the particle-vibration coupling vertex.

A powerful technique to propagate the variety of elementary, lowest- order NFT diagrams such as single-particle and collective vibration dressing processes, as well as induced (phonon- mediated) interactions, e.g. pairing induced interaction (eventually taking properly into account vertex corrections and tadpole processes), is through Dyson's equation, or, in the case in which the system under consideration is superfluid (superconducting), through the Nambu-Gor'kov equations (see e.g. ref. [15] and refs. therein). With the help of these equations, which allow for the calculation of energy-dependent normal and abnormal self-energies, one can take into account the effect of medium polarization effects on the pairing interaction. In other words the contribution induced by the exchange of collective vibrations between members of Cooper pairs. The output of such calculations not only allows for a detailed, self-consistent description of the nuclear spectrum, but also provide the structure elements needed for a consistent calculation of reaction processes.

This thesis presents the results discussed above, calculated by solving the Nambu-Gor'kov equation in the case of the nucleus ^{120}Sn, which can be considered a typical example of superfluid nucleus. Within this context see [16].

To carry out the calculations we have:

- developed a general scheme to solve the Nambu-Gor'kov equation based on a HFB mean field instead of BCS as previously done. The extension to the general case allows to properly treat the coupling with the continuum states.The details of the formalism are

given in Appendix A, where the BCS limit is also discussed.

- recasted the formalism of continuous strength functions (cf. Appendix D) in a way that makes it possible to iterate the solution of the Nambu-Gor'kov equation to convergence. This scheme is more efficient than the algorithms used in [16], algorithms which becomes very heavy to consider the coupling between many single-particle levels and phonons.

- implemented the coupling to spin modes, known to play a dominant role in infinite nuclear matter. Due to the fact that spin modes are, as a rule, not very collective in nuclei, let alone the fact that their properties are poorly constrained by the empirical evidence, they have seldom been considered in these systems. In previous exploratory calculations (see in particular [17]) it was found that this coupling leads, in finite nuclei, to a non negligible ($\approx 25\%$) reduction of the attractive pairing induced by the density modes. While in [17] only a lowest order calculation of the pairing induced interaction was performed, in the present work I have calculated these renormalization effects solving the Nambu-Gor'kov equation.

- considered vertex correction (cf. App. B) as well as tadpole processes (cf. also [16]), although they have not been fully implemented.

We have also applied the formalism to the study of the renormalization processes associated with the dressing of single-particle states in a closed shell system, in which case $\Delta \rightarrow 0$. The system chosen for such a study is the newly discovered, unstable doubly magic exotic nucleus ^{132}Sn.

1.2 Summary of the formalism and outline of the calculations

In what follows we present the strategy used to implement the NFT rules and sum to all orders the associated renormalizing processes in terms of the the Nambu-Gor'kov equation in the case of spherical superfluid nuclei.

One starts by selecting a mean field and a residual interaction appropriate to describe correlations in the particle-particle (pairing) channel. One then diagonalizes this Hamiltonian in the BCS approximation thus determining a pairing gap and a Fermi energy, and the corresponding quasiparticle energies and occupation amplitudes u_a and v_a. In the associated two quasiparticle basis, and within the framework of the Quasiparticle Random Phase Approximation (QRPA) formalism, one calculates, making use of a residual interaction appropriate to correlate particle-hole (two quasiparticle) excitations, the vibrational modes of the superfluid nucleus under study.

In the present case, we concentrate on ^{120}Sn, making use of Skyrme force (SLy4) both to calculate the mean field in the Hartree-Fock (HF) approximation, and the collective QRPA modes, that is, the Time Dependent HF (TDHF) modes of the mean field. An alternative to this last choice, to the extent that QRPA phonons are not renormalized by self-energy and vertex correction processes (as is the case in the present calculation), is to use a separable interaction, adjusting the coupling constants to reproduce the experimental properties of the collective modes. This can essentially be done only in the case of density modes, in keeping with the fact that spin modes are little collective, let alone the fact that the corresponding experimental information regarding this channel is scarce. Concerning the particle-particle channel a schematic pairing force with constant matrix elements has been used, adjusting the coupling strength so as to reproduce, within the single-particle subspace, the same value of the pairing gap [1] ($\Delta \approx 1$ MeV)

[1] It is of notice that once renormalization processes are set in, this value decreases to about 0.7 MeV, in keeping with the breaking and shift in the centroids energy of the valence single-particle orbitals.

obtained in the HF-Bogolyubov approximation making use of the effective interaction SLy4 to determine the mean field and the v_{14} Argonne NN-interaction in the pairing channel (allowing for scattering processes up to 800 MeV [16, 18]). The above choices (mean field, residual force in the particle-hole channel, bare NN-pairing force), conclude the first step in the NFT treatment of the nuclear structure of superfluid nuclei, and define the "bare" elementary modes of nuclear excitation, namely quasiparticle and vibrational modes which contain most of the correlations at the level of HFB mean field. The corresponding formfactors (transition densities) and strengths provide the input to calculate the matrix elements of H_C which characterize the, as a rule, weak coupling between quasiparticles and collective modes. From now on the whole approach follows totally consistent, well defined rules, based on the NFT formalism, tailored after general principles of effective field theories in general and Quantum ElectroDynamics (QED) in particular (see e.g. [6]). Making use of them one can design the basic NFT diagrams (processes) to any given order of perturbation theory in the particle-vibration coupling vertex.

With this input, the corresponding (Dyson) Nambu-Gor'kov equation can be written down (cf. Appendix D.3.3, expecially the diagrams in Figs. D.7 and D.10). Its solution propagates the elementary NFT processes (Fig. D.9) to infinite order. The outcome provides detailed information concerning the breaking of the quasiparticle strength as well as of the collective modes response function, and associated shifts in energy centroids, together with the renormalization of the pairing interaction. In other words, the solution of the Nambu-Gor'kov equation leads to the dressed elementary modes of nuclear excitation, whose properties provide the structure input (effective deformations, one-, two-, etc- particle transfer amplitudes) to calculate the inelastic, Coulomb excitations and γ–decay transition probabilities, as well as one- and two- particle absolute differential cross sections, to be directly compared to the experimental data.

The fact that the first step is not totally selfconsistent as required by rule (II) of NFT (bare NN-interaction is to be used to calculate the mean field single-particle levels as well as the particle-hole like (two quasiparticle) collective modes, and to act as a four-point-vertex in higher order renormalization processes, see [6]) is to be adscribed to the fact that we are still not in possess of a NN-potential which allows for such requirements to be fullfilled. Within this context it is of notice the progress made in terms of v_{low-k} [19] and of renormalization group constrained interactions [20].

We then compute modes of ^{120}Sn within the QRPA formalism, using the same SLy4 interaction used to produce the mean field. The calculation follows the steps of ref. [17]. The vibrational modes λ^π_ν are characterized by their multipolarity λ and parity π. We consider both natural ($\pi = (-1)^\lambda$) and non-natural ($\pi = -(-1)^\lambda$) parity modes, with λ =1,2,3,4 and 5 (we have left out the giant dipole resonance). The associated transition densities are given by

$$\delta\rho^\nu_{\lambda^\pi}(r) = \frac{1}{\sqrt{2\lambda+1}} \sum_{ab} (X_{ab}(\nu,\lambda^\pi) + Y_{ab}(\nu,\lambda^\pi)) \\ (u_a v_b + u_b v_a) < a||i^\lambda Y_\lambda||b > \phi_a(r)\phi_b(r), \tag{1.1}$$

and

$$\delta\rho^\nu_{\lambda^\pi L}(r) = \frac{1}{\sqrt{2\lambda+1}} \sum_{ab} (X_{ab}(\nu,\lambda^\pi) - Y_{ab}(\nu,\lambda^\pi)) \\ (u_a v_b + u_b v_a) < a||i^\lambda [Y_L \times \sigma]_\lambda||b > \phi_a(r)\phi_b(r), \tag{1.2}$$

where ϕ_a denotes the single-particle wavefunction and X_{ab},Y_{ab} denote the QRPA amplitudes. The transition density $\delta\rho^{\nu}_{\lambda^{\pi}}$ is associated with density oscillations and vanishes for phonons of non-natural parity. The transition density $\delta\rho^{\nu}_{\lambda^{\pi}L}$ is instead associated with spin-dependent modes, that is, with phonons of both non-natural (when $\lambda \neq L$) and natural (when $\lambda = L$) parity. The index ν labels the different vibrational modes of a given multipolarity and parity.

The particle-hole residual interaction is derived in a self-consistent way from the Skyrme energy functional, with the exception of the spin-orbit and the Coulomb part (cf. [21] for details), neglecting the momentum-dependent part of the interaction in the calculation of the particle-vibration coupling [22]. The particle-hole interaction can then be written as

$$v_{ph}(\vec{r},\vec{r}') = \delta(\vec{r}-\vec{r}')[(F_0 + F_0'\vec{\tau}\cdot\tau')] + [(G_0 + G_0'\vec{\tau}\cdot\tau')\vec{\sigma}\cdot\vec{\sigma}']. \tag{1.3}$$

Concerning the $\tau\cdot\tau'$ part, we shall only consider the $\tau_z\cdot\tau_z$ term, in keeping with the fact that here we are interested in the neutron-neutron pairing interaction. Off-diagonal terms are associated with charge-exchange modes. Thus, in lowest order, they do not contribute to the neutron-neutron interaction but are expected to be of relevance in the discussion of the proton-neutron pairing interaction. The functions $F_0(r), F_0'(r), G_0(r)$, and $G_0'(r)$ are generalized Landau-Migdal parameters controlling the isoscalar and isovector (spin-independent and spin-dependent) channels.

The transition densities are then the formfactors entering the particle-vibration coupling vertex. The spin independent part of the interaction (1.3) leads to the matrix elements

$$f(a,b,\lambda^{\pi}_{\nu}) = \langle am_a|(F_0(r) + F_0'(r')\tau\cdot\tau')\delta(r-r')||[b\otimes\lambda^{\pi}_{\nu}]_{j_a m_a}\rangle. \tag{1.4}$$

Making use of the multipole expansion of the δ-function one can write,

$$\begin{aligned} f(a,b,\lambda^{\pi}_{\nu}) =& \frac{1}{\sqrt{2j_a+1}}\langle a||i^{\lambda}Y_{\lambda}||b\lambda^{\pi}\rangle \int_0^{+\infty}\phi_a(r)[(F_0(r)+F_0'(r))\delta\rho^{\nu}_{\lambda^{\pi}\ n}(r) \\ &+ (F_0(r)-F_0'(r))\delta\rho^{\nu}_{\lambda^{\pi}\ p}(r)]\phi_b(r)\mathrm{d}r, \end{aligned} \tag{1.5}$$

where $\rho^{\nu}_{\lambda^{\pi}\ n}$ and $\rho^{\nu}_{\lambda^{\pi}\ p}$ are the neutron and proton transition densities.

The spin dependent part leads to

$$g(a,b,\lambda^{\pi}_{\nu}L) = \langle am_a|(G_0(r) + G_0'(r')\tau\cdot\tau')\times\sigma\cdot\sigma'\delta(r-r')||[b\otimes\lambda^{\pi}_{\nu}L]_{j_a m_a}\rangle, \tag{1.6}$$

an expression which is recasted, through the multipole expansion of the $\delta-$function, in the form

$$\begin{aligned} g(a,b,\lambda^{\pi}_{\nu}L) =& \frac{1}{\sqrt{2j_a+1}}\langle a||i^{L}[Y_L\times\sigma]_{\lambda}||b\lambda^{\pi}L\rangle \int_0^{+\infty}\phi_a(r)[(G_0(r)+G_0'(r))\delta\rho^{\nu}_{\lambda^{\pi}L\ n}(r) \\ &+ (G_0(r)-G_0'(r))\delta\rho^{\nu}_{\lambda^{\pi}L\ p}(r)]\phi_b(r)\mathrm{d}r. \end{aligned} \tag{1.7}$$

The angular momentum L takes the values $L=\lambda$ for natural parity phonons, and $\lambda\pm1$ for non-natural parity phonons. In the following $g(a,b,\lambda^{\pi}_{\nu})$ and $(f\pm g)(a,b,\lambda^{\pi}_{\nu})$ indicate $\sum_L g(a,b,\lambda^{\pi}_{\nu}L)$ and $f(a,b,\lambda^{\pi}_{\nu})\pm\sum_L g(a,b,\lambda^{\pi}_{\nu}L)$ respectively.

In the case of natural parity modes the $f-$ terms are, as a rule, the dominant ones. Furthermore, the spin-dependent $g-$ terms vanish in the diagonal case ($a=b$). This

is the reason why in what follows we usually denote the natural and non-natural parity modes as 'density modes' and 'spin modes' respectively. This terminology is reminiscent of that adopted in infinite matter, where, in the absence of a spin-orbit term, spin is a good quantum number and density and spin excitations decouple.

The quasiparticle-phonon vertices can now be used to compute the basic NFT processes which renormalize the quasiparticle properties (see Fig. A.2). The resulting energy-dependent self-energy processes (see Fig. A.1) will then be inserted in the Nambu-Gor'kov equations, which will then be solved by iteration (cf. Fig. D.10). The Green's function of the system are computed (D.3.13), and the strength functions are obtained from its imaginary component (D.1.23) (cf. Eq. (D.1.13)). In this way one obtains information about the occupation factors, the distribution of single-particle strength and the pairing gap.

Our results are based on the solution of the Nambu-Gor'kov equation providing information concerning the properties of the dressed quasiparticles of the system, which reads

$$\widetilde{G}(a,\omega+i\eta)=\Big(\omega+i\eta-E_a\otimes\tau_3-\hat{\Sigma}(a,\omega+i\eta)\Big)^{-1}, \tag{1.8}$$

where a stands for the spherical quantum numbers $\{nlj\}$, the quantity E_a denotes the quasiparticle energy and τ_3 is the (third) 2×2 Pauli matrix (cf. Appendix D.3.4). The Green's function $\widetilde{G}(i_1,\omega+i\eta)$ is obtained by inverting a 2×2 matrix which has as components the normal and anomalous self-energy $\hat{\Sigma}$ (cf. the discussion in Appendix A and D). The explicit expression of the components of the self-energy are

$$\Sigma^{11}(a,\omega)=\sum_{b,\lambda^\pi_\nu}\int_0^{+\infty}\mathrm{d}\omega'\frac{V^2(a,b,\lambda^\pi_\nu,\omega')}{\omega-\omega'-\hbar\omega_{\lambda^\pi_\nu}}+\frac{W^2(a,b,\lambda^\pi_\nu,\omega')}{\omega+\omega'+\hbar\omega_{\lambda^\pi_\nu}}, \tag{1.9}$$

$$\Sigma^{22}(a,\omega)=\sum_{b,\lambda^\pi_\nu}\int_0^{+\infty}\mathrm{d}\omega'\frac{V^2(a,b,\lambda^\pi_\nu,\omega')}{\omega+\omega'+\hbar\omega_{\lambda^\pi_\nu}}+\frac{W^2(a,b,\lambda^\pi_\nu,\omega')}{\omega-\omega'-\hbar\omega_{\lambda^\pi_\nu}}, \tag{1.10}$$

$$\Sigma^{12}(a,\omega)=\sum_{b,\lambda^\pi_\nu}\int_0^{+\infty}\mathrm{d}\omega' VW(a,b,\lambda^\pi_\nu,\omega')\left[\frac{1}{\omega+\omega'+\hbar\omega_{\lambda^\pi_\nu}}-\frac{1}{\omega-\omega'-\hbar\omega_{\lambda^\pi_\nu}}\right]. \tag{1.11}$$

The vertices coupling quasiparticles and phonons are denoted V and W; their squares, which contain the corresponding strength functions, read

$$\begin{aligned}V^2(a,b,\lambda^\pi_\nu,\omega)=&\ (f(a,b,\lambda^\pi_\nu)+g(a,b,\lambda^\pi_\nu))^2u^2aS^+(b,\omega)\\ &+\ (f(a,b,\lambda^\pi_\nu)-g(a,b,\lambda^\pi_\nu))^2v_a^2S^-(b,\omega)\\ &-2(f(a,b,\lambda^\pi_\nu)+g(a,b,\lambda^\pi_\nu))(f(a,b,\lambda^\pi_\nu)-g(a,b,\lambda^\pi_\nu))u_av_a\widetilde{S}(b,\omega)\end{aligned} \tag{1.12}$$

(1.13)

$$\begin{aligned}W^2(a,b,\lambda^\pi_\nu,\omega)=&\ (f(a,b,\lambda^\pi_\nu)-g(a,b,\lambda^\pi_\nu))^2u_a^2S^-(b,\omega)\\ &+\ (f(a,b,\lambda^\pi_\nu)+g(a,b,\lambda^\pi_\nu))^2v_a^2S^+(b,\omega)\\ &-2(f(a,b,\lambda^\pi_\nu)-g(a,b,\lambda^\pi_\nu))(f(a,b,\lambda^\pi_\nu)+g(a,b,\lambda^\pi_\nu))u_av_a\widetilde{S}(b,\omega)\end{aligned} \tag{1.14}$$

and

$$\begin{aligned}VW(a,b,\lambda^\pi_\nu,\omega)=&\ (f(a,b,\lambda^\pi_\nu)+g(a,b,\lambda^\pi_\nu))^2u_av_aS^+(b,\omega)\\ &-(f(a,b,\lambda^\pi_\nu)-g(a,b,\lambda^\pi_\nu))^2u_av_aS^-(b,\omega)\\ +(f(a,b,\lambda^\pi_\nu)+g(a,&b,\lambda^\pi_\nu))(f(a,b,\lambda^\pi_\nu)-g(a,b,\lambda^\pi_\nu))(u_a^2-u_a^2)\widetilde{S}(b,\omega)\end{aligned} \tag{1.15}$$

The expressions for V and W depend on the normal and on the anomalous strength functions S and $\widetilde{S}$. The particle and hole part of the normal strength function are respectively denoted

$$S^{+}(a,\omega) = S(a,\omega) \qquad \text{and} \qquad S^{-}(a,\omega) = S(a,-\omega). \tag{1.16}$$

The strength functions are directly related to the imaginary part of the Green's functions. The normal strength function is given by

$$S(a,\omega) = -\Im m\{u_a^2 \widetilde{G}_{11}(a,\omega+i\eta) + v_a^2 \widetilde{G}_{22}(a,\omega+i\eta) - 2u_a v_a \widetilde{G}_{12}(a,\omega+i\eta)\}/\pi, \tag{1.17}$$

while the anomalous strength function can be written as

$$\widetilde{S}(a,\omega) = -\Im m\{u_a v_a(\widetilde{G}_{11}(a,\omega+i\eta) - \widetilde{G}_{22}(a,\omega+i\eta)) + (u_a^2 - v_a^2)\widetilde{G}_{12}(a,\omega+i\eta)\}/\pi. \tag{1.18}$$

Strength functions are, as a rule, peaked at the energies of the corresponding dressed quasiparticle fragments.

1.2.1 Pairing gap renormalization

An important consequence of the renormalization of the quasiparticles is that in turns modifies the original value of the pairing gap due to both fragmentation and medium polarization interactions. In fact, the coupling to phonons gives rise to an induced interaction via phonon exchange between particles in time reversal states. Another consequence of the coupling to phonons (c.f. Appendix A and D) is the fragmentation of the single-particle strength, which also affects the pairing field. These two aspects of the renormalization process are reflected in the expression for the renormalized gap which reads,

$$\tilde{\Delta}(a,\omega) = Z(a,\omega)\left(\Delta_a^{BCS} + \widetilde{\Sigma}^{12}(a,\omega)\right) \equiv \tilde{\Delta}^{bare}(a,\omega) + \tilde{\Delta}^{ind}(a,\omega), \tag{1.19}$$

where Δ_a^{BCS} is the pairing gap corresponding to level a before the coupling to phonons, and $\widetilde{\Sigma}^{12}$ is the corresponding gap associated to the mentioned induced interaction, which is obtained from the 2×2 $\hat{\Sigma}$-matrix as

$$\widetilde{\Sigma}^{12}(a,\omega) = \Sigma^{12}(a,\omega)(u_a^2 - v_a^2) + u_a v_a(\Sigma^{11}(a,\omega) - \Sigma^{22}(a,\omega)), \tag{1.20}$$

Of notice that this is also the BCS gap-like expression associated with v_{ind}, namely

$$\tilde{\Sigma}^{12}(a,\omega) = -\sum_b \int_0^{+\infty} d\omega' \frac{(2j_b+1)}{2} v_{ind}(a,\omega,b,\omega')\widetilde{S}(b,\omega'), \tag{1.21}$$

where v_{ind} is the induced interaction

$$\begin{aligned} v_{ind}(a,\omega,b,\omega') = &\sum_{\lambda,\nu} \frac{2[(f+g)(ab\lambda\nu)][(f-g)(ab\lambda\nu)]}{(2j_b+1)} \\ &\times \left[\frac{1}{\omega-\omega'-\hbar\omega_{\lambda\nu}} - \frac{1}{\omega+\omega'+\hbar\omega_{\lambda\nu}}\right]. \end{aligned} \tag{1.22}$$

The factor Z in (1.19) accounts for the fragmentation of quasiparticles around the Fermi energy, and is obtained from the 2x2 Σ-matrix as

$$Z(a,\omega) = \left(1 - \frac{\tilde{\Sigma}^{odd}(a,\omega)}{\omega}\right)^{-1}, \tag{1.23}$$

where

$$\tilde{\Sigma}^{odd}(a,\omega) = \frac{\tilde{\Sigma}^{11}(a,\omega) - \tilde{\Sigma}^{11}(a,-\omega)}{2}. \tag{1.24}$$

1.3 Results for ^{120}Sn

1.3.1 Mean Field and QRPA

As stated before, the first step in the calculation is the solution of the HF equations using the SLy4 interaction. The energies of the five single-particle levels lying closest to the Fermi energy are shown in Fig. C.1. For simplicity this will be the explicit single-particle space used in the effective field theory (NFT) calculations.

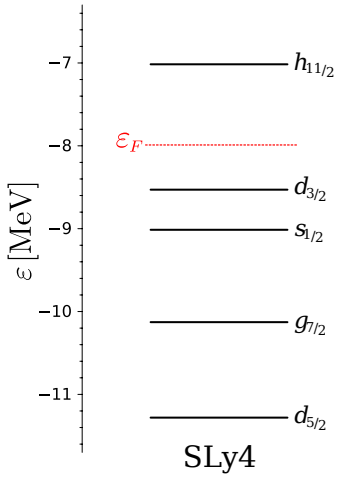

Figure 1.1: Energies of single-particle levels in ^{120}Sn obtained in a HF calculation using the SLy4 interaction. They constitute the independent-particle degrees of freedom. The BCS Fermi energy ε_F is also reported.

We then perform a BCS calculation with a monopole force. The pairing coupling constant G_0 is adjusted so as to obtain a pairing gap equal to $\Delta = 1$ MeV that corresponds to the result obtained by the bare Argonne v_{14} force in this mean field [16]. Based on these HF+BCS results, collective excitations are calculated in form of phonons of the various multipolarities of natural and not natural parity using Quasi Random Phase Approximation (QRPA). The associated electromagnetic transition probabilities $B(E\lambda)$ and $B(M\lambda)$ are shown in Fig. 1.2.

1.3.2 Particle-Vibration interweaving leads to levels fragmentation

Self-energy processes increase, as a rule, the density of levels around the Fermi energy (cf. Fig. 1.3). Moreover the coupling to collective excitations of the system and to virtual states implies a fragmentation of the quasiparticle strength which can be conveniently taken into account in terms of strength functions (see Eq. (1.17)). In Figs. 1.4 and 1.5 we compare these functions with that obtained by making use of the experimental spectroscopic factors associated with the ^{120}Sn$(d,p)^{121}$Sn, ^{120}Sn$(p,d)^{119}$Sn and ^{120}Sn$(^3$He,$\alpha)^{119}$Sn [23, 24, 25]

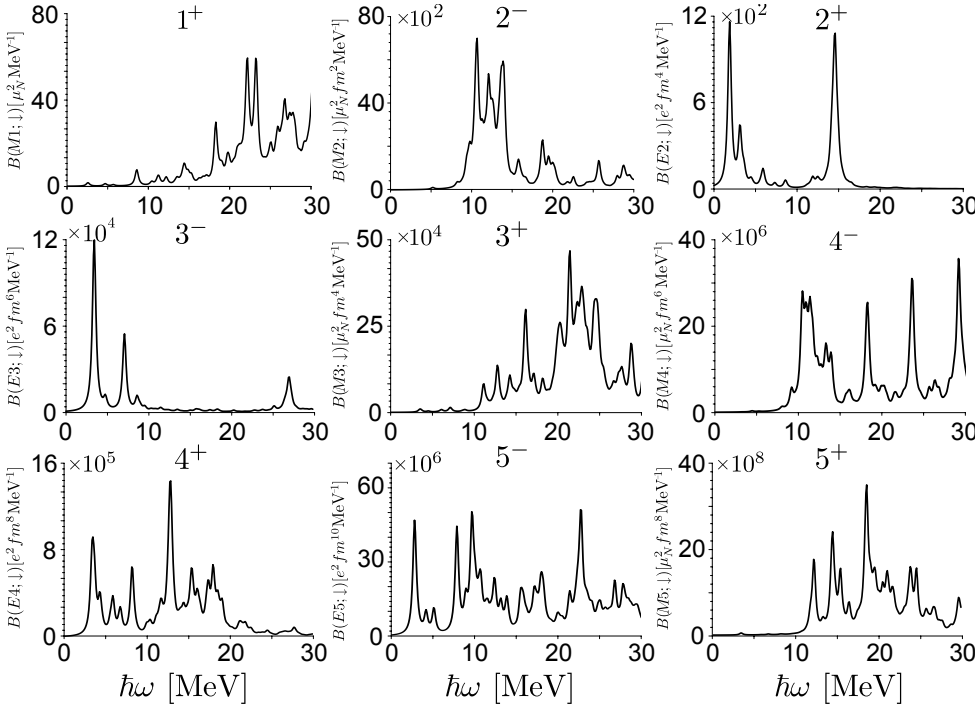

Figure 1.2: Phonon spectra for different multipolarities calculated making use of the QRPA based on a Skyrme SLy4 interaction, convoluted with a Lorentzian of width 0.5 MeV. The output of the QRPA calculation (phonon spectra and associated transition densities) characterize the collective degrees of freedom and the coupling to quasiparticle states.

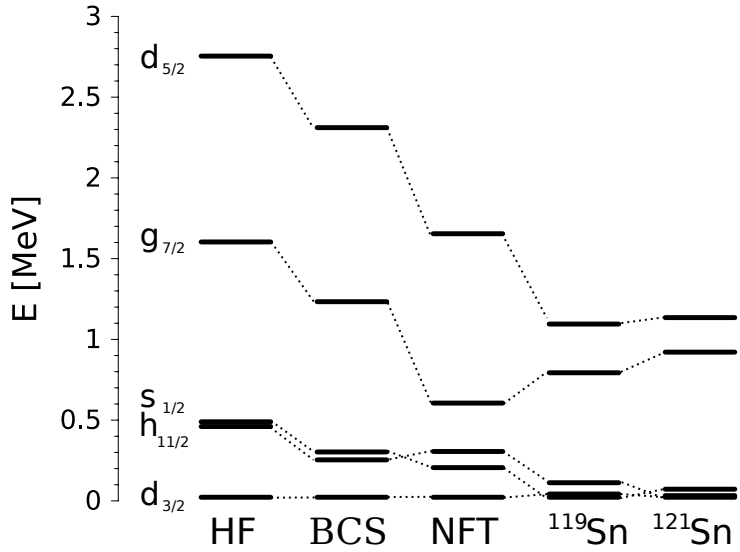

Figure 1.3: The theoretical quasiparticle spectra obtained at the various steps of the calculation are compared to the experimental data. One starts from an Hartree-Fock calculation (HF), adding then a monopole pairing interaction, with a strength tuned so as to reproduce the output of calculations performed with the bare Argonne N-N interaction (BCS). Afterwards one works out the contribution arising from the self-energy processes (NFT). The experimental energies derived from one particle transfer experiments on ^{120}Sn and leading to ^{119}Sn and ^{121}Sn, are also shown. For details cf. ref. [16]

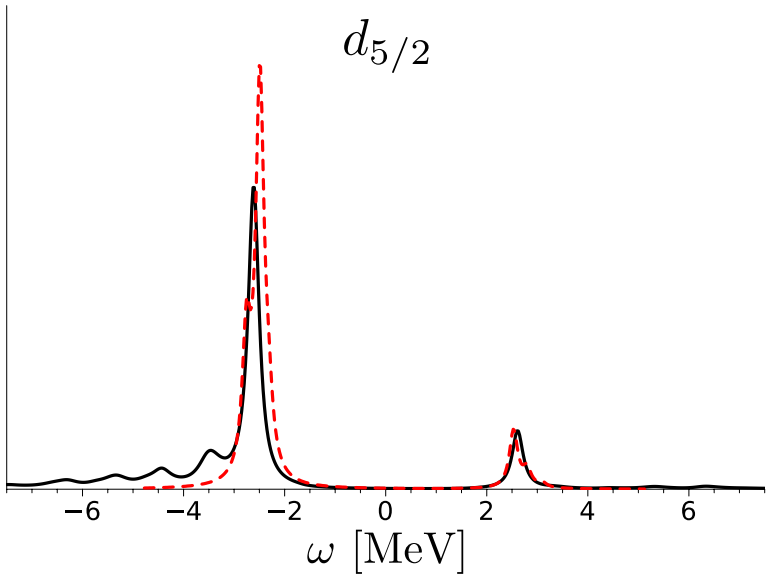

Figure 1.4: The calculated (NFT) strength function $S(d_{5/2}, \omega)$ (1.17) of the $d_{5/2}$ state (solid line) is compared to a convolution, with a Lorentzian of $FWHM = 0.2$ MeV, of the respective experimental spectroscopic factors (dashed lines) obtained from the analysis of stripping and pick-up one-particle transfer reactions on ^{120}Sn [23, 24, 25].

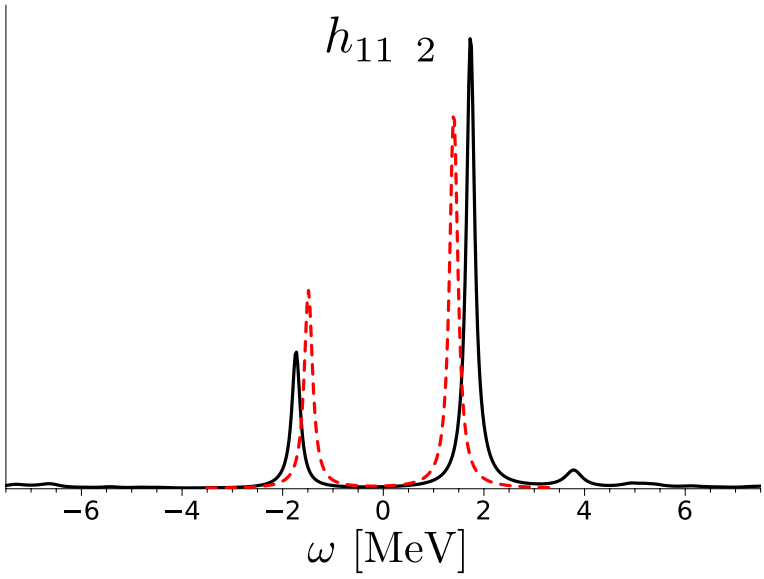

Figure 1.5: The calculated (NFT) strength function $S(h_{11/2}, \omega)$ (1.17) of the $h_{11/2}$ state (solid line) is compared to a convolution, with a Lorentzian of $FWHM = 0.2$ MeV, of the respective experimental spectroscopic factors (dashed lines) obtained from the analysis of stripping and pick-up one-particle transfer reactions on ^{120}Sn [23, 24, 25].

1.3.3 Effect on pairing correlations

Pairing correlations are modified by the change of the quasiparticle properties mentioned above, namely density of levels and quasiparticle fragmentation. Also by medium polarization effects arizing from the exchange of phonons between particles moving in time reversal states, processes which modify the off diagonal term of the self energy $\hat{\Sigma}$ (1.11). The state dependent pairing gap is then calculated taking into account both the contribution of the bare NN interaction and of the induced interaction, modified by the factor Z defined in Eq. (1.23), factor which includes the renormalization (1.19) of the quasiparticle properties of the system (cf. Fig. 1.6). The resulting average value of the state-dependent pairing gap (1.50 MeV) is to be compared with the experimental value $\Delta = 1.46$ MeV, calculated making use of the binding energies within the framework of the so called three point-formula.

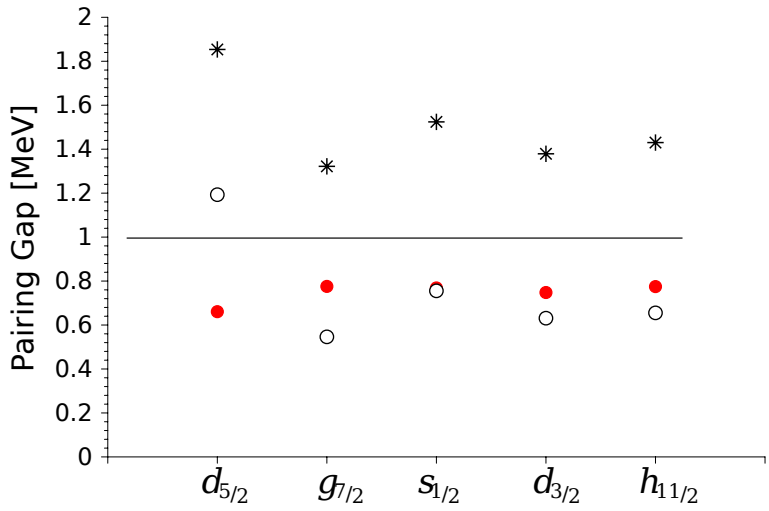

Figure 1.6: State-dependent pairing gap (stars) calculated solving the Nambu-Gor'kov equation, including both spin-dependent g and spin-independent f matrix elements for every multipolarity. The initial pairing gap obtained in the BCS calculation, $\Delta^{BCS} = 1$ MeV (horizontal line), is renormalized by the Z-factor, $\tilde{\Delta}^{bare} = Z(a, \widetilde{E}_a)\Delta^{BCS}$ (full dots). The contribution of the pairing induced interaction $\tilde{\Delta}^{ind} = Z(a, \widetilde{E}_a)\Sigma^{12}(a, \widetilde{E}_a)$ (empty circles) accounts for about 50% to the total gap $\tilde{\Delta} = \Delta^{bare} + \tilde{\Delta}^{ind}$ (stars).

Considering both the coupling with density and spin modes is mandatory. In fact, as seen from Fig. C.13, the contribution arizing from the coupling to density modes is very important, and can hardly be ignored. On the other hand, the proper inclusion of the coupling to spin-dependent modes screens out part of the density modes contributions (in keeping with the fact that the spin-dependent matrix element g are, as rule, repulsive (cf. App. C.1.3)), bringing theory in overall agreement with the experimental findings (Fig 1.6).

In a similar way in which the shape of nuclei results from a delicate balance in the competition between the paired (high degeneracy) and the aligned (Jahn-Teller like) coupling scheme, the importance of medium polarization effects on the nuclear superfluidity reflects the contrasting role spin-flip and density modes, exchanged between Cooper pair partners, play in binding these systems, and indirectly, through Cooper pair con-

densation, on the overall nuclear ground state correlation.

1.3.4 Absolute cross sections

The above nuclear structure results can be used as input in the calculation of, among other things, one- and two-particle transfer processes. The first one provides specific information concerning the occupation numbers, centroids and lifetimes of the quasiparticle states, while Cooper pair transfer sheds light on pairing correlations in nuclei. Concerning one-particle transfer reactions, the strength functions shown in Figs. 1.4 and 1.5 can be integrated locally or globally, depending on the energy resolution of the experiments to be analyzed, to obtain renormalized $\tilde{u}, \tilde{v}$ quasiparticle amplitudes and energies to be used as spectroscopic amplitudes (and ω-values) for the calculation of single-particle transfer absolute cross section which can be directly compared to the experimental absolute differential cross sections. Inversely, if such an analysis has already been carried out starting from the measured cross sections and excitation functions, one can directly compare the resulting strength functions as done in e.g. Figs. 1.4 and 1.5.

In keeping with the fact that in the case of two-nucleon transfer reactions one is, as a rule, probing the structure of coherent states, resulting from Cooper pair correlated over many two-particle configurations, this inverse protocol is non-operative. In fact in this case one has to use the $\tilde{u}, \tilde{v}$ factors to calculate the two-nucleon spectroscopic amplitudes, e.g. those associated with the ^{122}Sn$(p,t)^{120}$Sn(gs) reaction ($= B(j^2(0); gs(122) \rightarrow gs(120)) = \sqrt{(2j+1)/2}\ \tilde{u}_j\tilde{v}_j$), to calculate the associated absolute differential cross section, quantities which can be directly compared with the experimental findings (see Fig. 1.7).

It could be argued that the result displayed in this figure depends only on the value of the pairing gap, and not on the variety of mechanism (self-energy, Z-values, induced interactions contributing to $\tilde{\Delta}^{ind}$, etc.) leading to it, and that one could do equally well with a standard, schematic pairing force adjusting G to reproduce the empirical three-point Δ-value. Superficially this is true, in the same way that the fact that the quadrupole vibrational state has an energy of $\hbar\omega_{2_1^+} = 1.2$ MeV measured from the ground state, whether one considers that this mode contributes a ground state (ZPF) energy of $1/2\hbar\omega_{2_1^+}$ for each of it five degrees of freedom or not. On the other hand, this fact has important consequences on the predicted value of e.g. the mean square radius of ^{120}Sn.

In fact, it is the whole picture which provides the confirmation or less of the validity of the NFT approach to nuclear structure: density of levels (Fig. 1.3), single particle strength functions (Figs. 1.4 and 1.5), absolute value of the two-particle transfer cross sections, etc., and not a single quantity like the pairing gap.

Important steps forward in the quest to test NFT are expected to come from research eventually providing a bare NN, eventually including also three-body effects, to be used for all the steps of a low-energy nuclear structure calculation (mean field (HFB), QRPA, four-point vertices (NFT),etc.). Also from the measurement, through e.g. the determination of the Density of State (DOS), of the dependence of the pairing gap with the (intrinsic) nuclear excitation energy (temperatures T). In this case one expect a very different variation of $\tilde{\Delta}^{bare}(T)$ as compared with $\tilde{\Delta}^{ind}(T)$.

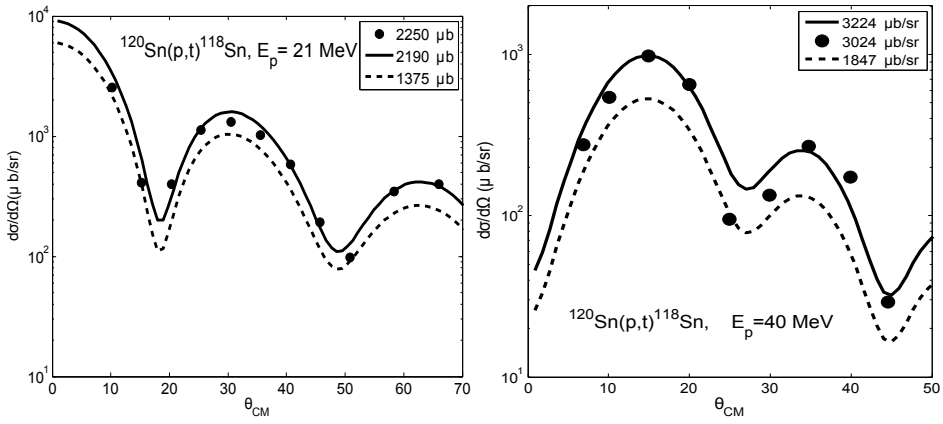

Figure 1.7: Two-particle transfer absolute cross section obtained with a second order DWBA software (which include simultaneous, successive and non-orthogonality processes) [26], calculated with two-nucleon spectroscopic amplitudes input corresponding to the total pairing gap ($\tilde{\Delta} = \tilde{\Delta}^{bare} + \tilde{\Delta}^{ind} = 1.45$ MeV) (solid curve) or with only one component of the pairing gap ($\tilde{\Delta}^{bare} \simeq \tilde{\Delta}^{ind} \simeq 0.725$ MeV) (dashed curve), in comparison with the experimental data (solid dots) [27, 28, 29]. In the inset the integrated cross sections are shown.

CHAPTER 2

Renormalization of the properties of the valence, single particle states of closed shell nuclei

2.1 The newly discovered, double magic exotic ^{132}Sn

The processes which are at the basis of the renormalization of elementary modes of nuclear excitation find (weak-coupling) textbook examples in the case of doubly magic nuclei (see Table 2.1). This is because (pairing) correlations in such nuclei, although not strong so as to win over the single-particle gap and induce superfluidity (deformation in gauge space), are nonetheless sufficiently strong to stabilize the spherical shape against the drive of quadrupole correlations (aligned coupling scheme).

A central theme concerning renormalization processes around closed shells is that of the role played by the neutron excess on magic numbers. This is, among other things, in keeping with the phenomenon of parity inversion and of the associated emergence of the $N = 6$ magic number in detriment of the standard $N = 8$ magicity (observed e.g. in Li and Be nuclei). Within this context, the recent experimental study of the single-particle structure of $^{132}_{50}\mathrm{Sn}_{82}$ making use of inverse kinematics, provides an important input [30, 31].

2.2 Single-particle strength Functions and fragmentation

Following Sect. 1.2 we start by calculating the mean field making use of an effective interaction. As seen from Fig. 2.1 and Tables 2.2 and 2.3 the resulting density of levels is considerably lower than experimentally observed, and reflects the value $m_k = 0.75m$ of the SLy4 k-mass used in the calculations.

With the help of the the particle-hole basis related to a standard $m_k = 1m$ mean field, we have calculated the collective vibrations of the system within the RPA (linear response function), making use of a separable multipole-multipole interaction (cf. Appendix E), adjusting the coupling constant k_λ in each case, so as to fulfill the experimental constrains associated with the polarizabilities $\alpha_{\lambda_1} = B(E\lambda_1)/\hbar\omega_1$. In particular, the value of α_{2_1} associated with the lowest quadrupole mode is experimentally constrained in the range $44e^2\mathrm{fm}^4\mathrm{MeV}^{-1} \leq \alpha_{2_1} \leq 90e^2\mathrm{fm}^4\mathrm{MeV}^{-1}$ [32, 33], while the collectivity of the 3^- low-lying phonon is constrained by only a lower bound $B(E3) > 7.1$ Weisskopf Units (WU) [34]. In the calculations discussed below we have used the experimental energies of the lowest quadrupole and octupole states (see Table 2.4). For the first one we have chosen the upper limit of the polarizability, corresponding to $B(E2_1 \downarrow) = 9.3$ WU while for the second one we have chosen $B(E3_1 \downarrow) = 14.1$ WU, which corresponds to the RPA value of the SLy4 interaction. This is also the choice made for the 4^+ (cf. [35]) and 5^- modes (see Table 2.4 and Fig. 2.2).

Nucleus	$\frac{N}{Z}$	$\frac{N-Z}{A}$	
$^{4}_{2}\mathrm{He}_{2}$	1	0	stable
$^{16}_{8}\mathrm{O}_{8}$	1	0	stable
$^{40}_{20}\mathrm{Ca}_{20}$	1	0	stable
$^{56}_{28}\mathrm{Ni}_{28}$	1	0	unstable
$^{48}_{20}\mathrm{Ca}_{28}$	1.40	0.167	stable
$^{132}_{50}\mathrm{Sn}_{82}$	1.64	0.242	unstable
$^{208}_{82}\mathrm{Pb}_{126}$	1.54	0.212	stable

Table 2.1: A selection of the doubly closed shell nuclei observed to date. Also reported are the neutron(N)-proton(Z) ratio, as well as the neutron excess, normalized with respect to the mass number A. Although these nuclei are essentially spherical in their ground state, the situation is rather special concerning the case of $N = Z$ nuclei. In fact, in these systems, $\lambda^{\pi} = 0^{+}$ 4particle-4hole like states can exist at relatively low excitation energies, due to α-like ($^{4}_{2}\mathrm{He}_{2}$) correlations. Because of the anisotropy of the single-particle orbitals, these states display a conspicuous quadrupole deformation (Jahn-Teller-like degeneracy breaking mechanism) a fact which emerges naturally in terms of the cluster model (made out of a string of two α-like particles), deformation which also affects in an important way the ground state of the system as well as the valence single-particle orbitals. This is the case for ^{16}O and ^{40}Ca, the nucleus ^{4}He being more a few-body system than a many-body one.

Making use of the HF and RPA results and of the formalism described in Ch. 1 (cf. also App. A and D) in the limit of $\Delta \to 0$, we have calculated the interweaving between single-particle (HF) and collective (RPA) vibrations (NFT). The resulting spectrum is considerably more concentrated around the Fermi energy than that associated with HF theory (see Fig. 2.1) and reproduces the experimental data within statistical errors (see Table 2.3), consistent with an effective mass $m^{*} = m_{k}m_{\omega}/m \approx 0.9m (= 0.75 \cdot 1.2m)$ (see Table 2.2).

Making use of the values of $Z_{\omega} \equiv (m/m_{\omega})$, the associated single-particle ($^{133}\mathrm{Sn}(j)$) and single-hole ($^{131}\mathrm{Sn}(j^{-1})$) strength functions have been calculated. They are displayed in Figs. 2.3 and 2.4. Also shown in Fig. 2.3 are the HF-results, as well as the Q-value spectrum for the ^{132}Sn(^{2}H,^{1}H)^{133}Sn inverse kinematic reaction.

The experimental results are consistent with spectroscopic factors of value $1(\pm 0.2)$ NFT predicts a value of 0.8 when the calculated spectroscopic factors are averaged over the observed ($j = f_{7/2}, f_{5/2}, p_{3/2}, p_{1/2}$) valence single-particle states of $^{133}\mathrm{Sn}(j)$, and of ≈ 0.6 when they are averaged over the (hole) valence orbitals ($j = d^{-1}_{3/2}, d^{-1}_{5/2}, h^{-1}_{11/2}, s^{-1}_{1/2}, g^{-1}_{7/2}$) of $^{131}\mathrm{Sn}(j^{-1})$ (see Fig. 2.4 and Table 2.5).

While theory provides an overall account of the experimental findings, conspicuous deviations are observed concerning the position of individual levels, in particular the splitting between the $h_{11/2}$ and the $d_{3/2}$ and $s_{1/2}$ levels (≈ 0.33 MeV experimental, ≈ 1.9 MeV theoretical). Wether this (local) discrepancy is the result of "accidental" effects related to the specific mean field chosen [36], or whether it reflects the lack of some physical, specific process is, at the moment, an open question. In an attempt of eventually shedding light on such a question, results as those collected in Table 2.6 may be used

	HF (SLy4)	NFT				Exp	
	ε_a [MeV]	$\Delta\varepsilon_a$ [MeV]	$\tilde{\varepsilon}_a$ [MeV]	S	m_ω/m	ε_a [MeV]	S
$i_{13/2}$	2.31	-1.66	0.65	0.53	1.25	0.19	
$h_{9/2}$	0.91	-0.82	0.09	0.74	1.16	-0.88	
$f_{5/2}$	0.70	-1.01	-0.32	0.75	1.13	-0.44	1.1 ± 0.2
$p_{1/2}$	0.42	-0.87	-0.45	0.80	1.08	-1.04	1.1 ± 0.3
$p_{3/2}$	-0.17	-1.01	-1.19	0.77	1.12	-1.58	0.92 ± 0.18
$f_{7/2}$	-1.99	-0.53	-2.52	0.83	1.17	-2.44	0.86 ± 0.16
$h_{11/2}$	-7.68	0.74	-6.95	0.78	1.20	-7.52	
$d_{3/2}$	-9.12	0.61	-8.52	0.75	1.26	-7.35	
$s_{1/2}$	-9.39	1.21	-8.19	0.69	1.30	-7.68	
$g_{7/2}$	-11.36	1.28	-10.07	0.62	1.20	-9.78	
$d_{5/2}$	-11.73	2.09	-9.63	0.47	1.38	-9.05	

Table 2.2: Properties of the valence single-particle levels of ^{132}Sn as calculated in HF theory (in which case $Z_\omega = S(a,\omega) = 1$ by definition) and those resulting from renormalization effects (NFT), the associated energy shifts being $\Delta\varepsilon_a = \tilde{\varepsilon}_a - \varepsilon_a$, while the factors $Z(\omega)$ are equal to the inverse of the relative, state dependent ω-mass m_ω/m. The experimental values are taken from [30, 37].

	$\rho_{sp}(\varepsilon_F)$ [MeV^{-1}]		
	HF	NFT	Exp
particle	10.4	13.9	16.7 ± 3.3
hole	7.9	10.2	13.2 ± 2.6
total	5.4	7.1	7.6 ± 1.5

Table 2.3: Density $\rho_{sp}(\varepsilon_F)$ of single-particle levels of ^{132}Sn lying around the Fermi energy. In the two first columns the Hartree-Fock and the renormalized (NFT) results are displayed in comparison with the experimental data (third column) [30, 37]. In the first two lines the particle and hole values are reported, while in the last line the total density of levels is given.

at profit.

	Exp		RPA		
	$\hbar\omega_1$ [MeV]	$B(E\lambda_1)$ [W.U.]	$\hbar\omega_1$ [MeV]	$B(E\lambda_1)$ [W.U.]	β_{λ_1}
2^+	4.04	≈ 7	3.35	7.6	0.09
3^-	4.35	> 7.1	4.50	14.1	0.11
4^+	4.42	≈ 8	4.05	6.0	0.08
5^-	4.89		4.71	13.3	0.13

Table 2.4: Properties of the low-lying density modes of ^{132}Sn corresponding to different multipolarities, calculated within the framework of the RPA, in comparison with the experimental data.

	NFT	Exp
particle (f,p)	0.79	1.0 ± 0.2
hole	0.67	–

Table 2.5: Average spectroscopic factors for the valence single-particle states of ^{132}Sn lying above and below the Fermi energy. It is of notice that for the particle states, only the (f,p) orbitals ($\equiv f_{5/2}, p_{1/2}, p_{3/2}, f_{7/2}$) were considered, in keeping with the fact that $h_{9/2}$ state was not significatly populated in the ^{132}Sn(^{2}H,^{1}H)^{133}Sn reaction and therefore was not included in the Q-value spectrum fit (see Table 2.2 and Fig. 2.3).

interm. / renorm.	$d_{5/2}$	$g_{7/2}$	$s_{1/2}$	$d_{3/2}$	$h_{11/2}$	$f_{7/2}$	$p_{3/2}$	$h_{9/2}$	$f_{5/2}$	$p_{1/2}$
$d_{5/2}$	-0.100	-0.061	-0.075	-0.192	-1.508	0.053	0.021	-0.003	0.051	0.012
$g_{7/2}$	-0.104	-0.305	-0.157	-0.267	-0.377	-0.038	-0.041	0.086	0.009	-0.030
$s_{1/2}$	-0.124	-0.118	–	-0.167	-0.812	0.202	–	0.158	0.143	–
$d_{3/2}$	-0.221	-0.286	-0.180	-0.141	-0.257	0.131	-0.025	0.223	0.072	–
$h_{11/2}$	-0.231	-0.076	-0.143	-0.070	-0.584	0.107	-0.040	0.026	–	-0.018
$f_{7/2}$	-0.116	-0.077	-0.122	-0.166	-0.166	0.201	0.110	-0.025	–	0.008
$p_{3/2}$	-0.016	-0.002	–	-0.044	-0.045	0.407	0.060	0.011	0.129	0.043
$p_{1/2}$	-0.036	-0.090	–	–	0.094	0.498	0.103	–	0.144	–
$f_{5/2}$	-0.120	-0.012	-0.087	-0.032	–	0.119	0.103	-0.040	0.137	-0.007
$h_{9/2}$	-0.095	-0.207	-0.110	-0.204	-0.044	0.025	-0.057	0.404	0.012	–

Table 2.6: Energy shifts affecting the (NFT) renormalized states (renorm.) through correlation and polarization processes, eliminating intermediate states, appearing in the correlation and polarization diagrams, and containg the single-particle states (interm.). For example, not considering the contribution to the renormalization of the $d_{5/2}$ orbital of states containing the $h_{11/2}$ state, shifts the $\tilde{\varepsilon}_{d_{5/2}}$ perturbed energy by -1.508 MeV, while blocking the contribution to $\tilde{\varepsilon}_{h_{11/2}}$ by intermediate states containing the same $h_{11/2}$ state (and thus either the 2^+ or 4^+ phonons), leads to a shift of this state of -0.584 MeV.

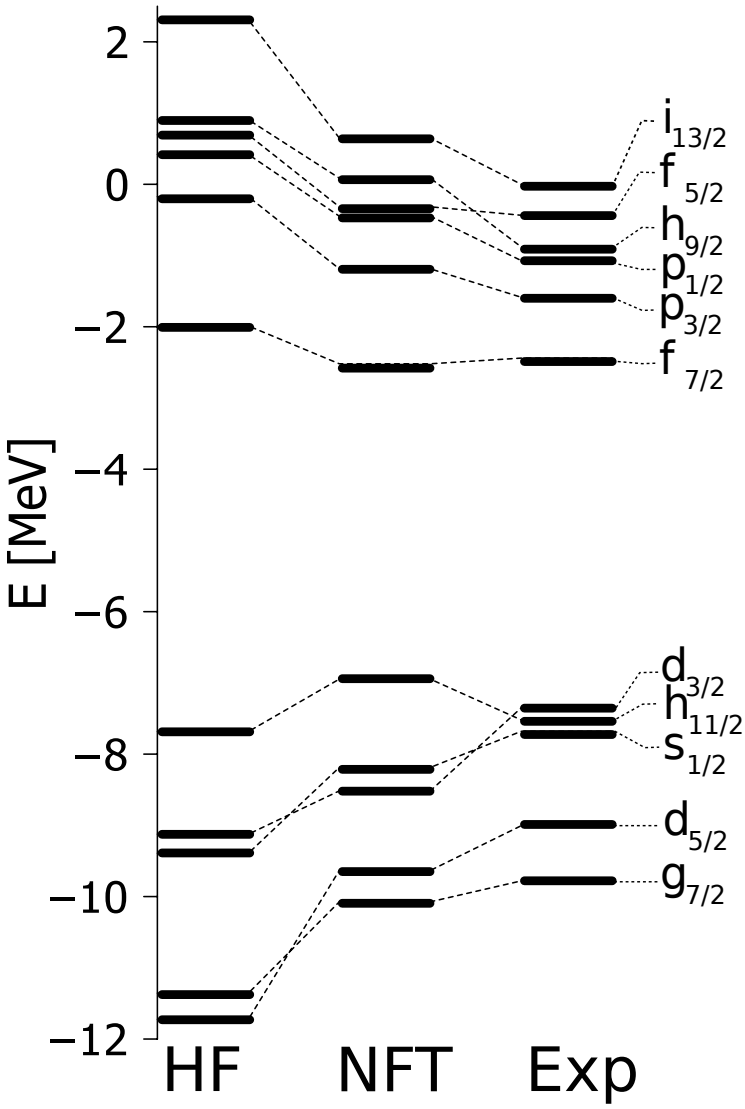

Figure 2.1: Single particle energy spectrum of the valence shells of ^{132}Sn. The Hartree-Fock calculations and renormalized NFT results are displayed together with the experimental data [30, 37].

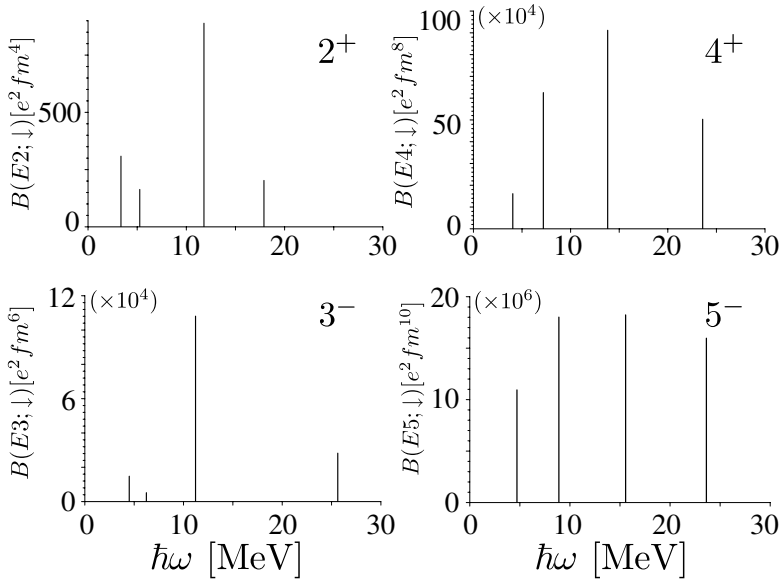

Figure 2.2: Linear response functions of ^{132}Sn associated with density modes of different multipolarities.

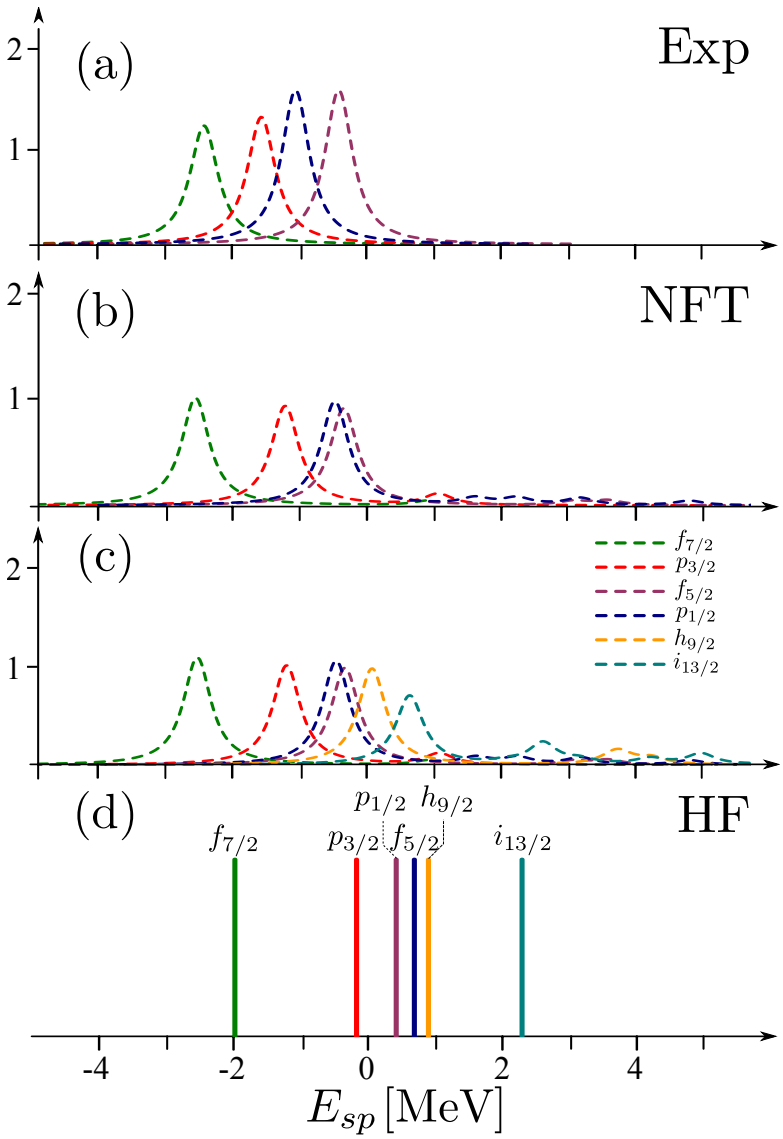

Figure 2.3: Strength functions associated with the single-particle levels of ^{133}Sn displayed in terms of the colour code shown in the upper right inset of panel (c). **(a)** Experimental results corresponding to the Q-value spectrum (spectroscopic factors) of the ^{132}Sn(^{2}H,^{1}H)^{133}Sn inverse kinematic reaction at 54° in the center of mass [30]. Although not shown, a 21% statistical error is to be adscribed to this data. It is of notice that in this experiment the $h_{9/2}$ state was not significantly populated and therefore was not included in the fit. **(b)** Renormalized (NFT) results considering only the four $(f_{5/2}, p_{1/2}, p_{3/2}, f_{7/2})$ single-particle levels included in the experimental data. The different fragments in which the dressed single-particle states divide have been convoluted with the Lorentzian of width 0.5 MeV. It is of notice that for a proper comparison with the data, the corresponding spectroscopic amplitudes should be used to calculate the corresponding absolute differential cross sections and extract the corresponding $\theta = 54^{\circ}$ value. **(c)** The same as in (b), but for all the six valence single-particle orbitals i.e. including also the results associated with the NFT $h_{9/2}$ and $i_{13/2}$ results. **(d)** Independent-particle, sharp HF strengths ($S = 1$ by definition). In the cases (a), (b) and (c) the integral over the different single peaks lead to the spectroscopic factors reported in Table 2.2.

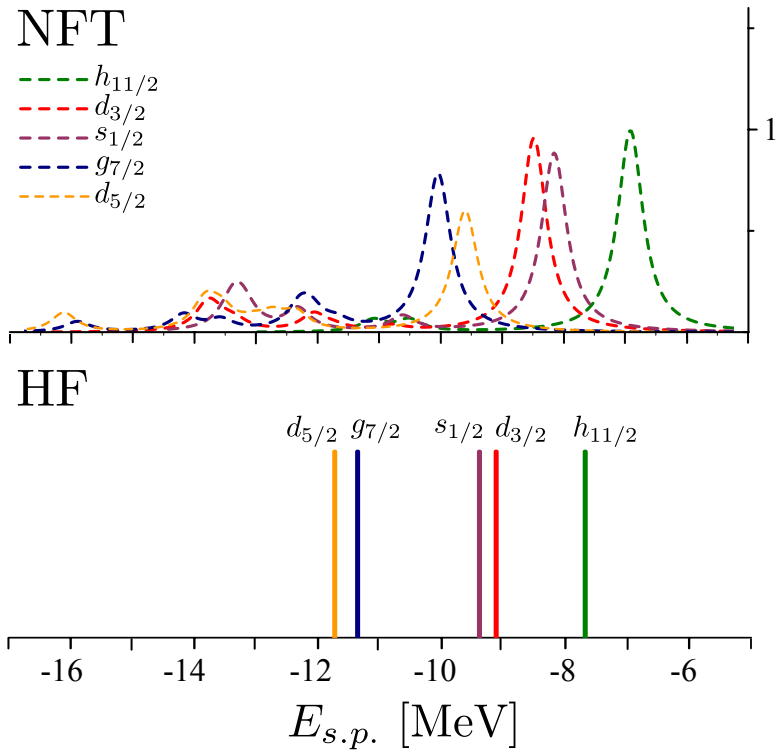

Figure 2.4: Strength function associated with the valence levels lying below the ^{132}Sn Fermi energy (holes), displayed making use of the color code shown in the upper left inset.

CHAPTER 3

Conclusions

Nuclear field theory (NFT) within the framework of the Hartree-Fock and QRPA, and of the Nambu-Gor′kov equation, provides a powerful and economic scheme to implement renormalization effects in both superfluid and normal nuclei, leading to dressed quasiparticles and to induced interactions.

In the case of a typical superfluid nucleus like ^{120}Sn, NFT including polarization and correlation diagrams, as well as phonon induced pairing taking into account both density and spin modes, and allowing for vertex corrections, leads to highly accurate two-nucleon spectroscopic amplitudes for the reaction $^{122}\mathrm{Sn}(p,t)^{120}\mathrm{Sn}(gs)$. In fact, used in conjuction with a state of the art reaction software that takes into account successive and simultaneous contributions, properly corrected by non-orthogonality processes, the caulculated (NFT) spectroscopic amplitudes predicts absolute differential cross section which agree with the experimental findings within statistical errors. NFT also predicts quasiparticle strength functions (spectroscopic factors) associated with the system ^{119}Sn and ^{121}Sn which account in detail, for the one-particle stripping and pick-up strength functions.

In the case of the exotic doubly magic nucleus $^{132}_{50}\mathrm{Sn}_{82}$, NFT accounts for the observed density of levels and for the empirical spectroscopic factors, within experimental errors. While the Q-value spectrum observed in the $^{132}\mathrm{Sn}(^2\mathrm{H},^1\mathrm{H})^{133}\mathrm{Sn}$ inverse kinematic experiment is consistent with spectroscopic factors of value $1(\pm 0.3)$, NFT predicts a value of 0.74 when the calculated spectroscopic factors are averaged over the observed ($j = f_{7/2}, f_{5/2}, p_{3/2}, p_{1/2}$) valence single-particle states of $^{133}\mathrm{Sn}(j)$, and of ≈ 0.67 when they are averaged over the (hole) valence orbitals ($j^{-1} = d^{-1}_{3/2}, d^{-1}_{5/2}, h^{-1}_{11/2}, s^{-1}_{1/2}, g^{-1}_{7/2}$) of $^{131}\mathrm{Sn}(j^{-1})$. In other words, NFT predicts that ^{132}Sn magicity hardly exceeds 60%, thus pointing to this system as a likely important laboratory where to test many-body nuclear theories. Within this context, consistent deviations from experiment found in the energy of individual single-particle levels, may indicate the need to search for degrees of freedom not considered in the present calculations.

Appendices

APPENDIX A

Quasiparticle Green's function renormalization and HFB

"What we call the beginning is often the end.
And to make an end is to make a beginning.
The end is where we start from."
- T.S. Eliot

As discussed in Sect. 1.1, the self-energy include the processes considered by the NFT, that renormalize the quasiparticles through the basic scattering vertices. In this Appendix, we will be dealing with the general case in which the self-energy processes connect single-particle states having the same angular momentum but in general different energies, that is different number of nodes in their radial wavefunctions, both below and above the Fermi energy, lying even at positive energy (unbound levels). In this way, the self-energy acquires a matricial form. This treatment of the self-energy can account for modifications in the radial wavefunctions of the renormalized single-particles, and can incorporate the self-energy into a selfconsistent calculation of the mean field properties, on the same footing with the HFB equation. We start this Appendix by reformulating the HFB equations to this purpose and then show the general form of the self-energy matrix, including both normal and anomalous components following ref. [38], but allowing for the mentioned non-diagonal processes.

The calculations discussed in the main text, however, are limited to the simpler single mode (BCS) case, and the relevant equations will be also presented.

A.1 HFB

The HFB Hamiltonian for a spherical nucleus is given by

$$\hat{H}_{HFB} = \begin{pmatrix} (\hat{T} + \hat{V} - \varepsilon_F) & \hat{\Delta} \\ \hat{\Delta}^t & -(\hat{T} + \hat{V} - \varepsilon_F) \end{pmatrix}. \tag{A.1.1}$$

The matrix elements of $\hat{H}_{HFB}$ will be expressed in a single-particle basis composed of the vectors $|a_k\rangle$, where a denotes the angular momentum quantum numbers $\{l, j\}$. The basis could coincide with that obtained solving the corresponding HF problem neglecting the pairing field, or could be obtained with a similar mean field potential. We shall consider the general case, in which the single-particle basis contains states with the same a but with different number of nodes, labelled by the index k. For each state a_k, there is a time reversal state indicated by $|\bar{a}_k\rangle$: they are coupled by the pairing field Δ. It will be convenient in the following to distinguish between hole and particle states, lying respectively below and above the Fermi energy ε_F: they will be labelled p_k and h_k respectively. We shall assume that the basis contains N_h hole states and N_p particle states.

The $\pm\hat{T}+\hat{V}-\varepsilon_F$ sectors of $\hat{H}_{HFB}$ (the "normal" part) can then be written more explicitly as

$$\hat{T}+\hat{V}-\varepsilon_F = \left(\begin{array}{ccc|ccc} T_{h_1}+V_{h_1,h_1} & \cdots & V_{h_1,h_{N_h}} & V_{h_1,p_1} & \cdots & V_{h_1,p_{N_p}} \\ \vdots & \ddots & \vdots & \vdots & \ddots & \vdots \\ V_{h_{N_h},h_1} & \cdots & T_{h_{N_h}}+V_{h_{N_h},h_{N_h}} & V_{h_{N_h},p_1} & \cdots & V_{h_{N_h},p_{N_p}} \\ \hline V_{p_1,h_1} & \cdots & V_{p_1,h_{N_h}} & T_{p_1}+V_{p_1,p_1} & \cdots & V_{p_1,p_{N_p}} \\ \vdots & \ddots & \vdots & \vdots & \ddots & \vdots \\ V_{p_{N_p},h_1} & \cdots & V_{p_{N_p},h_{N_h}} & V_{p_{N_p},p_1} & \cdots & T_{p_{N_p}}+V_{p_{N_p},p_{N_p}} \end{array}\right) - \hat{1}\varepsilon_F, \tag{A.1.2}$$

The pairing ("abnormal") part of $\hat{H}_{HFB}$ can be written

$$\hat{\Delta} = \left(\begin{array}{ccc|ccc} \Delta_{h_1,\bar{h}_1} & \cdots & & \cdots & \Delta_{p_{N_p},\bar{h}_1} \\ \vdots & \ddots & & \ddots & \vdots \\ \Delta_{h_1,\bar{h}_{N_h}} & \cdots & & \cdots & \Delta_{p_{N_p},\bar{h}_{N_h}} \\ \hline \Delta_{h_1,\bar{p}_1} & \cdots & & \cdots & \Delta_{p_{N_p},\bar{p}_1} \\ \vdots & \ddots & & \ddots & \vdots \\ \Delta_{h_1,\bar{p}_{N_p}} & \cdots & & \cdots & \Delta_{p_{N_p},\bar{p}_{N_p}} \end{array}\right). \tag{A.1.3}$$

The eigenvalue problem to be solved is then given by

$$\hat{H}_{HFB}\left(\begin{array}{c} u_{a^\mu,h_1} \\ \vdots \\ \hline u_{a^\mu,h_{N_h}} \\ u_{a^\mu,p_1} \\ \vdots \\ \hline\hline u_{a^\mu,p_{N_p}} \\ v_{a^\mu,h_1} \\ \vdots \\ \hline v_{a^\mu,h_{N_h}} \\ v_{a^\mu,p_1} \\ \vdots \\ v_{a^\mu,p_{N_p}} \end{array}\right) = E_{a^\mu}\left(\begin{array}{c} u_{a^\mu,h_1} \\ \vdots \\ \hline u_{a^\mu,h_{N_h}} \\ u_{a^\mu,p_1} \\ \vdots \\ \hline\hline u_{a^\mu,p_{N_p}} \\ v_{a^\mu,h_1} \\ \vdots \\ \hline v_{a^\mu,h_{N_h}} \\ v_{a^\mu,p_1} \\ \vdots \\ v_{a^\mu,p_{N_p}} \end{array}\right). \tag{A.1.4}$$

The HFB Hamiltonian can be diagonalized using the Bogoliubov-Valatin transformation,

$$|a^{\mu\,(+)}\rangle = \sum_{k=1}^{N}[u_{a^\mu,k}|a_k\rangle + v_{a^\mu,k}|\bar{a_k}\rangle] \tag{A.1.5}$$

$$|a^{\mu\,(-)}\rangle = \sum_{k=1}^{N}[-v_{a^\mu,k}|a_k\rangle + u_{a^\mu,k}|\bar{a_k}\rangle], \tag{A.1.6}$$

leading to quasiparticle states a^μ which are linear combinations of single-particle states weighted with the amplitudes $u_{a^\mu,k}, v_{a^\mu,k}$, where the index k runs over the N_p particle and the N_h states ($N \equiv N_p + N_h$). The HFB matrix admits pairs of eigenvalues

$E_{a^\mu}, -E_{a^\mu}$ which are associated with the eigenvectors $|a^{\mu\,(+)}\rangle$ and $|a^{\mu\,(-)}\rangle$ respectively. Even if usually only the solutions with positive quasiparticle energy E_{a^μ} are explicitely considered, because they contain all the needed information, in order to have a complete orthonormal set of vectors of the basis both solutions must be taken into account. The transformation (A.1.5)-(A.1.6) can be rewritten as

$$\begin{pmatrix} |a^{1\,(+)}\rangle \\ \vdots \\ |a^{N\,(+)}\rangle \\ |a^{1\,(-)}\rangle \\ \vdots \\ |a^{N\,(-)}\rangle \end{pmatrix} = \left(\begin{array}{ccc|ccc} u_{a^1,1} & \cdots & u_{a^1,N} & v_{a^1,1} & \cdots & v_{a^1,N} \\ \vdots & \ddots & \vdots & \vdots & \ddots & \vdots \\ u_{a^N,1} & \cdots & u_{a^N,N} & v_{a^N,1} & \cdots & v_{a^N,N} \\ \hline -v_{a^1,1} & \cdots & -v_{a^1,N} & u_{a^1,1} & \cdots & u_{a^1,N} \\ \vdots & \ddots & \vdots & \vdots & \ddots & \vdots \\ -v_{a^N,1} & \cdots & -v_{a^N,N} & u_{a^N,1} & \cdots & u_{a^N,N} \end{array}\right) \begin{pmatrix} |a_1\rangle \\ \vdots \\ |a_N\rangle \\ |\bar{a}_1\rangle \\ \vdots \\ |\bar{a}_N\rangle \end{pmatrix}. \quad \text{(A.1.7)}$$

In order to diagonalize the complete Hamiltonian $\hat{H}_{HFB} + \Sigma$ (cf. the next Section), it will be convenient to use a particular quasiparticle basis, defined as

$$|a^{(+)}_{p_k}\rangle = |a_{p_k}\rangle \quad \text{(A.1.8)}$$

$$|a^{(-)}_{p_k}\rangle = |\bar{a}_{p_k}\rangle \quad \text{(A.1.9)}$$

for particle ($\varepsilon_{a_{p_k}} - \varepsilon_F > 0$) states, and

$$|a^{(+)}_{h_k}\rangle = |\bar{a}_{h_k}\rangle \quad \text{(A.1.10)}$$

$$|a^{(-)}_{h_k}\rangle = -|a_{h_k}\rangle \quad \text{(A.1.11)}$$

for hole ($\varepsilon_{a_{h_k}} - \varepsilon_F < 0$) states.

The change of basis matrix from the single-particle to this basis is then given by

$$\hat{M}_1 = \left(\begin{array}{c|c||c|c} \hat{0} & \hat{0} & \hat{1} & \hat{0} \\ \hline \hat{0} & \hat{1} & \hat{0} & \hat{0} \\ \hline\hline -\hat{1} & \hat{0} & \hat{0} & \hat{0} \\ \hline \hat{0} & \hat{0} & \hat{0} & \hat{1} \end{array}\right), \quad \text{(A.1.12)}$$

and in the new basis the HFB Hamiltonian takes the form

$$\hat{M}_1 \hat{H}_{HFB} \hat{M}_1^t = \left(\begin{array}{c|c||c|c} -(\hat{T}+\hat{V}-\lambda)_{hh} & \hat{\Delta}^t_{ph} & -\Delta_{hh} & -(\hat{T}+\hat{V}-\lambda)_{hp} \\ \hline \hat{\Delta}_{ph} & (\hat{T}+\hat{V}-\lambda)_{pp} & -(\hat{T}+\hat{V}-\lambda)_{ph} & \hat{\Delta}_{pp} \\ \hline\hline -\hat{\Delta}_{hh} & -(\hat{T}+\hat{V}-\lambda)_{hp} & (\hat{T}+\hat{V}-\lambda)_{hh} & -\hat{\Delta}_{hp} \\ \hline -(\hat{T}+\hat{V}-\lambda)_{ph} & \hat{\Delta}^t_{pp} & -\Delta^t_{hp} & -(\hat{T}+\hat{V}-\lambda)_{pp} \end{array}\right). \quad \text{(A.1.13)}$$

The quasiparticle amplitudes obtained diagonalizing the HFB Hamiltonian in this basis will be indicated as x, y; the associated transformation is given by

$$|a^{\mu\,(+)}\rangle = \sum_k x_{a^\mu,k}|a^{(+)}_k\rangle + y_{a^\mu,k}|a^{(-)}_k\rangle \quad \text{(A.1.14)}$$

$$|a^{\mu\,(-)}\rangle = \sum_k -y_{a^\mu,k}|a^{(+)}_k\rangle + x_{a^\mu,k}|a^{(-)}_k\rangle \quad \text{(A.1.15)}$$

This transformation is associated with the matrix

$$\left(\begin{array}{ccc|ccc} x_{a^1,1} & \cdots & x_{a^1,N} & y_{a^1,1} & \cdots & y_{a^1,N} \\ \vdots & \ddots & \vdots & \vdots & \ddots & \vdots \\ x_{a^N,1} & \cdots & x_{a^N,N} & y_{a^N,1} & \cdots & y_{a^N,N} \\ \hline -y_{a^1,1} & \cdots & -y_{a^1,N} & x_{a^1,1} & \cdots & x_{a^1,N} \\ \vdots & \ddots & \vdots & \vdots & \ddots & \vdots \\ -y_{a^N,1} & \cdots & -y_{a^N,N} & x_{a^N,1} & \cdots & x_{a^N,N} \end{array}\right). \tag{A.1.16}$$

The relation between x, y and u, v is obtained considering the transformation (A.1.8)-(A.1.11):

$$|a^{\mu\,(+)}\rangle = \sum_{k=1}^{N_p} x_{a^\mu,k}|a_{p_k}\rangle + y_{a^\mu,k}|\bar{a}_{p_k}\rangle + \sum_{k=1}^{N_h} x_{a^\mu,k}|\bar{a}_{h_k}\rangle - y_{a^\mu,k}|a_{h_k}\rangle, \tag{A.1.17}$$

$$|a^{\mu\,(-)}\rangle = \sum_{k=1}^{N_p} -y_{a^\mu,k}|a_{p_k}\rangle + x_{a^\mu,k}|\bar{a}_{p_k}\rangle + \sum_{k=1}^{N_h} -y_{a^\mu,k}|\bar{a}_{h_k}\rangle - x_{a^\mu,k}|a_{h_k}\rangle, \tag{A.1.18}$$

leading to

$$u_{a^\mu,k} = x_{a^\mu,k} \quad ; \quad v_{a^\mu,k} = y_{a^\mu,k} \quad \text{for the particle case,} \quad \varepsilon_{a_k} > \varepsilon_F, \tag{A.1.19}$$

$$u_{a^\mu,k} = -y_{a^\mu,k} \quad ; \quad v_{a^\mu,k} = x_{a^\mu,k} \quad \text{for the hole case,} \quad \varepsilon_{a_k} < \varepsilon_F, . \tag{A.1.20}$$

The matrix (A.1.16) can then be rewritten as

$$\left(\begin{array}{ccccc|ccccc} v_{a^1,h_1} & \cdots & v_{a^1,h_{N_h}} & u_{a^1,p_1} & \cdots & u_{a^1,p_{N_p}} & -u_{a^1,h_1} & \cdots & -u_{a^1,h_{N_h}} & v_{a^1,p_1} & \cdots & v_{a^1,p_{N_p}} \\ \vdots & \ddots & \vdots & \vdots & \ddots & \vdots & \vdots & \ddots & \vdots & \vdots & \ddots & \vdots \\ v_{a^N,h_1} & \cdots & v_{a^N,h_{N_h}} & u_{a^N,p_1} & \cdots & u_{a^N,p_{N_p}} & -u_{a^N,h_1} & \cdots & -u_{a^N,h_{N_h}} & v_{a^N,p_1} & \cdots & v_{a^N,p_{N_p}} \\ \hline u_{a^1,h_1} & \cdots & u_{a^1,h_{N_h}} & -v_{a^1,p_1} & \cdots & -v_{a^1,p_{N_p}} & v_{a^1,h_1} & \cdots & v_{a^1,h_{N_h}} & u_{a^1,p_1} & \cdots & u_{a^1,p_{N_p}} \\ \vdots & \ddots & \vdots & \vdots & \ddots & \vdots & \vdots & \ddots & \vdots & \vdots & \ddots & \vdots \\ u_{a^N,h_1} & \cdots & u_{a^N,h_{N_h}} & -v_{a^N,p_1} & \cdots & -v_{a^N,p_{N_p}} & v_{a^N,h_1} & \cdots & v_{a^N,h_{N_h}} & u_{a^N,p_1} & \cdots & u_{a^N,p_{N_p}} \end{array}\right). \tag{A.1.21}$$

Notice that we adopted a particular ordering of the single-particle levels, which will be useful to write the expression for the self-energy in the next Section.

A.2 Green's functions and Self Energy

The energy-dependent self-energy associated with a given quantum number $a = \{l, j\}$ for the pairing hamiltonian has the structure (cf. Appendix D)

$$\hat{\Sigma}(a,\omega) = \left(\begin{array}{cc} \Sigma^{11}(a,\omega) & \Sigma^{12}(a,\omega) \\ \Sigma^{21}(a,\omega) & \Sigma^{22}(a,\omega) \end{array}\right). \tag{A.2.1}$$

The eigenvalue problem associated with the total hamiltonian $\hat{H}_{HFB} + \hat{\Sigma}$ takes then the form

$$\left(\hat{H}_{HFB} + \hat{\Sigma}(a, \widetilde{E}_{a^\mu})\right)_{a^\mu} \left(\begin{array}{c} x \\ y \end{array}\right)_{a^\mu} = \widetilde{E}_{a^\mu} \left(\begin{array}{c} x \\ y \end{array}\right)_{a^\mu}, \tag{A.2.2}$$

that, besides the solutions of the HFB problem, has as many solutions as the number of poles of $\hat{\Sigma}(a,\omega)$. These, in turn, are given by the number of couplings between the single-particle states and the possible intermediate states (cf. Eqs. (A.2.8)-(A.2.11) below). This

leads to the fragmentation of the single-particle strength which in the mean field picture is collected in the N_a orbitals carrying the quantum number a. As a consequence, the normalization of the eigenvectors $\{x, y\}$ associated with a specific quasiparticle is such as

$$\sum_{k=1}^{N_a}[x^2_{a^\mu,k} + y^2_{a^\mu,k}] < 1; \tag{A.2.3}$$

on the other hand, summing over all the quasiparticles one finds

$$\sum_{k=1}^{N_a}\sum_{\mu}[x^2_{a^\mu,k} + y^2_{a^\mu,k}] = N_a. \tag{A.2.4}$$

A self-consistent solution of the energy-dependent problem implies an iteration procedure, until the values of the $\{x, y\}$ amplitudes obtained from Eq. (A.2.1) coincide with those used to compute the self-energy. At each iteration step, new intermediate states are produced, and the number of poles increases exponentially. It is then necessary to adopt some sort of numerical approximation. To this purpose we shall make use of a continuous description and of strength functions (cf. Appendix D), which will be recasted below.

The matrix elements of the self-energy will be computed in the $a^{(+)}$,$a^{(-)}$ basis. In this basis, the self-energy takes the block form, analogous to that presented in Eq. (A.1.21) for $\hat{H}_{HFB}$:

$$\left(\begin{array}{c|c||c|c} \Sigma^{11}_{hh} & \Sigma^{11}_{hp} & \Sigma^{12}_{hh} & \Sigma^{12}_{hp} \\ \hline \Sigma^{11}_{ph} & \Sigma^{11}_{pp} & \Sigma^{12}_{ph} & \Sigma^{12}_{pp} \\ \hline\hline \Sigma^{21}_{hh} & \Sigma^{21}_{hp} & \Sigma^{22}_{hh} & \Sigma^{22}_{hp} \\ \hline \Sigma^{21}_{ph} & \Sigma^{21}_{pp} & \Sigma^{22}_{ph} & \Sigma^{22}_{pp} \end{array}\right) \tag{A.2.5}$$

The amplitudes of the quasiparticles obtained diagonalizing Eq. (A.2.1) can then be expressed in the same way as in the HFB case (cf. Eqs. (A.1.14)-(A.1.15)). To indicate that the quasiparticle energy has been obtained diagonalizing the energy-dependent problem, we shall label the 'dressed' quasiparticle energy with a tilde, and we shall introduce the quantities

$$\widetilde{u}_{b^\mu,l} = x_{b^\mu,l} \quad ; \quad \widetilde{u}_{b^\mu,l} = y_{b^\mu,l} \quad \text{if } \epsilon_{b_l} > \epsilon_F \tag{A.2.6}$$

$$\widetilde{u}_{b^{\mu,l}} = -y_{b^\mu,l} \quad ; \quad \widetilde{u}_{b^{\mu,l}} = x_{b^\mu,l} \quad \text{if } \epsilon_{b_l} < \epsilon_F. \tag{A.2.7}$$

The matrix elements of $\hat{\Sigma}$ are associated with processes connecting states belonging to the same $(+)$ (normal self-energy, Σ^{11}) or $(-)$ sector (normal self-energy, Σ^{22}) or belonging to different sectors (abnormal self-energy, Σ^{12}).

These processes in turn involve scattering of the initial or final state with intermediate 1qp-1phonon state (cf. Fig. A.2). The associated vertex has a different character, depending on whether the initial (or final) state belongs to the same sector as the intermediate quasiparticle or to the other one. In the following, we give the relevant expressions for each case. Let us first consider in more detail the case, in which the initial state is a particle state, and the intermediate quasiparticles belongs to the same sector:

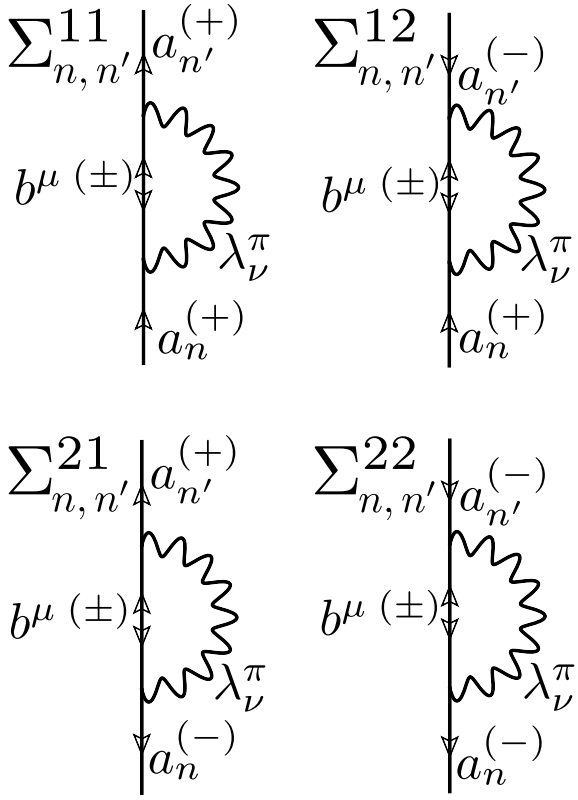

Figure A.1: Feynman representation of the components of self energy matrix (A.2.5). The Green's functions lines with the empty arrow represent respectively the positive and negative quasiparticle eigenvalue $^{(\pm)}$ of the basis (A.1.14)-(A.1.15).

$$
\begin{aligned}
V(p^{(+)}_k, b^{\mu(+)}, \lambda^{\pi}_{\nu}) \equiv & \langle p^{(+)}_k | \hat{V_{res}} | b^{\mu(+)} \lambda^{\pi}_{\nu} \rangle = -\langle p^{(-)}_k | \hat{V_{res}} | b^{\mu(-)} \lambda^{\pi}_{\nu} \rangle \\
= & \langle 0 | a_{p_k} \hat{V_{res}} \alpha^{\dagger}_{b^{\mu}} \Gamma_{\lambda^{\pi}_{\nu}} | 0 \rangle = \langle 0 | a_{p_k} \hat{V} (\sum_{l} \widetilde{u}_{b^{\mu},l} a^{\dagger}_{b_l} + \widetilde{v}_{b^{\mu},l} a_{b_l}) \Gamma_{\lambda^{\pi}_{\nu}} | 0 \rangle \\
= & \sum_{l} (f+g)(p_k, b_l, \lambda^{\pi}_{\nu}) \widetilde{u}_{b^{\mu},l} \qquad \text{cf. Fig. A.2(a)} \qquad \text{(A.2.8)}
\end{aligned}
$$

where the phonon entering the intermediate state is labeled by its multipolarity λ and parity π; phonons of different energies are labeled by the quantum number ν. The other

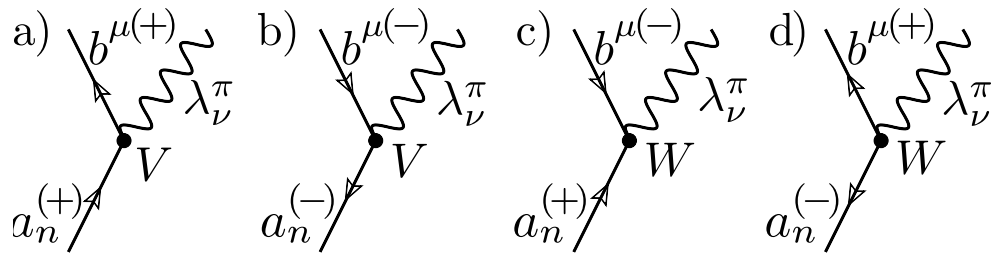

Figure A.2: Feynman representation of V and W vertices (A.2.8)-(A.2.11) for the case of particle a represented in the quasiparticle basis (A.1.14)-(A.1.15) $^{(\pm)}$ scattering into quasiparticle $b^{(\pm)}_{\mu}$ and a phonon λ^{π}_{ν}.

expressions for the quasiparticle-phonon vertices are given by,

$$\begin{aligned} V(h_k^{(+)}, b^{\mu(+)}, \lambda^{\pi}_{\nu}) \equiv & \langle h_k^{(+)} | \hat{V_{res}} | b^{\mu(+)} \lambda^{\pi}_{\nu} \rangle = -\langle h_k^{(-)} | \hat{V_{res}} | b^{\mu^{(-)}} \lambda^{\pi}_{\nu} \rangle \\ = & \sum_l -\widetilde{v}_{b^{\mu},l}(f-g)(h_k, b_l, \lambda^{\pi}_{\nu}) \qquad \text{cf. Fig. A.2(b),} \end{aligned} \tag{A.2.9}$$

$$\begin{aligned} W(p_k^{(+)}, b^{\mu(-)}, \lambda^{\pi}_{\nu}) \equiv & \langle p_k^{(+)} | \hat{V_{res}} | b^{\mu^{(-)}} \lambda^{\pi}_{\nu} \rangle = \langle p_k^{(-)} | \hat{V_{res}} | b^{\mu^{(+)}} \lambda^{\pi}_{\nu} \rangle \\ = & \sum_l \widetilde{v}_{b^{\mu},l}(f-g)(p_k, b_l, \lambda^{\pi}_{\nu}) \qquad \text{cf. Fig. A.2(c),} \end{aligned} \tag{A.2.10}$$

$$\begin{aligned} W(h_k^{(+)}, b^{\mu(-)}, \lambda^{\pi}_{\nu}) \equiv & \langle h_k^{(+)} | \hat{V_{res}} | b^{\mu^{(-)}} \lambda^{\pi}_{n} \rangle = \langle h_k^{(-)} | \hat{V_{res}} | b^{\mu^{(+)}} \lambda^{\pi}_{n} \rangle \\ = & \sum_l \widetilde{u}_{b^{\mu},l}(f+g)(h_k, b_l, \lambda^{\pi}_{\nu}) \qquad \text{cf. Fig. A.2(d).} \end{aligned} \tag{A.2.11}$$

Having spelled out the expressions for the various quasiparticle-phonon matrix elements, one can now compute the different terms of the self-energy.

- $\Sigma^{11}_{n,n'}(a,\omega)$ involves two vertices of the V kind for the forward part, and two vertices of the W kind for the backward one; its expression is thus given by

$$\begin{aligned} \Sigma^{11}_{n,n'}(a,\omega) = \sum_{b,\lambda^{\pi}_{\nu}} \sum_{\mu} & \frac{V(a_n^{(+)}; b^{\mu(+)}\lambda^{\pi}_{\nu}) V(a_{n'}^{(+)}; b^{\mu(+)}\lambda^{\pi}_{\nu})}{\omega - E_{b^{\mu}} - \hbar\omega_{\lambda^{\pi}_{\nu}}} + \\ & \frac{W(a_n^{(+)}; b^{\mu(-)}\lambda^{\pi}_{\nu}) W(a_{n'}^{(+)}; b^{\mu(-)}\lambda^{\pi}_{\nu})}{\omega + E_{b^{\mu}} + \hbar\omega_{\lambda^{\pi}_{\nu}}}, \end{aligned} \tag{A.2.12}$$

- $\Sigma^{22}_{n,n'}(a,\omega)$ involves two vertices of the V (W) kind for the forward (backward) part:

$$\begin{aligned} \Sigma^{22}_{n,n'}(a,\omega) = \sum_{b,\lambda^{\pi}_{\nu}} \sum_{\mu} & \frac{W(a_n^{(-)}; b^{\mu(+)}\lambda^{\pi}_{\nu}) W(a_{n'}^{(-)}; b^{\mu(+)}\lambda^{\pi}_{\nu})}{\omega - E_{b^{\mu}} - \hbar\omega_{\lambda^{\pi}_{\nu}}} + \\ & \frac{V(a_n^{(-)}; b^{\mu(-)}\lambda^{\pi}_{\nu}) V(a_{n'}^{(-)}; b^{\mu(-)}\lambda^{\pi}_{\nu})}{\omega + E_{b^{\mu}} + \hbar\omega_{\lambda^{\pi}_{\nu}}}; \end{aligned} \tag{A.2.13}$$

  one then obtains the relation

$$\Sigma^{22}_{n,n'}(a,\omega) = -\Sigma^{11}_{n,n'}(a,-\omega). \tag{A.2.14}$$

- $\Sigma^{12}_{n,n'}(a,\omega)$ involves both kind of vertices:

$$\Sigma^{12}_{n,n'}(a,\omega) = -\sum_{b,\lambda^\pi_\nu}\sum_{\mu}\frac{V(a^{(+)}_n;b^{\mu(+)}\lambda^\pi_\nu)W(a^{(-)}_{n'};b^{\mu(+)}\lambda^\pi_\nu)}{\omega - E_{b^\mu} - \hbar\omega_{\lambda^\pi_\nu}} - \frac{W(a^{(+)}_n;b^{\mu(-)}\lambda^\pi_\nu)V(a^{(-)}_{n'};b^{\mu(-)}\lambda^\pi_\nu)}{\omega + E_{b^\mu} + \hbar\omega_{\lambda^\pi_\nu}}, \tag{A.2.15}$$

and similarly

$$\Sigma^{21}_{n,n'}(a,\omega) = -\sum_{b,\lambda^\pi_\nu}\sum_{\mu}\frac{W(a^{(-)}_n;b^{\mu(+)}\lambda^\pi_\nu)V(a^{(+)}_{n'};b^{\mu(+)}\lambda^\pi_\nu)}{\omega - E_{b^\mu} - \hbar\omega_{\lambda^\pi_\nu}} - \frac{V(a^{(+)}_n;b^{\mu(-)}\lambda^\pi_\nu)W(a^{(+)}_{n'};b^{\mu(-)}\lambda^\pi_\nu)}{\omega + E_{b^\mu} + \hbar\omega_{\lambda^\pi_\nu}}, \tag{A.2.16}$$

leading to

$$\Sigma^{12}_{n,n'}(a,\omega) = \Sigma^{21}_{n',n}(a,\omega). \tag{A.2.17}$$

Numerically it can be very convenient to use a continuous representation of the self-energies. In this case, the properties of the discrete quasiparticles $\widetilde{u}_{b^\mu,l}, \widetilde{v}_{b^\mu,l}$ and E_{b_μ} are substituted by continuous strength functions and variables, so that the sum over μ is substituted by an integral over a dummy variable ω':

$$\sum_{\mu}\widetilde{u}_{b^\mu,l}\widetilde{u}_{b^\mu,l'} \rightarrow \int_0^{+\infty} S^+_{l,l'}(b,\omega')\mathrm{d}\omega, \tag{A.2.18}$$

$$\sum_{\mu}\widetilde{v}_{b^\mu,l}\widetilde{v}_{b^\mu,l'} \rightarrow \int_0^{+\infty} S^-_{l,l'}(b,\omega')\mathrm{d}\omega, \tag{A.2.19}$$

$$\sum_{\mu}\widetilde{u}_{b^\mu,l}\widetilde{v}_{b^\mu,l'} \rightarrow \int_0^{+\infty} \widetilde{S}_{l,l'}(b,\omega'\mathrm{d}\omega), \tag{A.2.20}$$

where the strength functions S and $\widetilde{S}$ are related to the imaginary part of the Green's function (see below). While $S^+_{l,l'}, S^-_{l,l'}$ are symmetric respect to l, l', $\widetilde{S}_{l,l'}$ is not.

These relations determine the continuous Lehmann representation

$$\Sigma^{11}_{n,n'\ (p,p)}(a,\omega) = \sum_{b,\lambda^\pi_\nu}\int_0^{+\infty}\mathrm{d}\omega' \frac{\sum_{l,l'}[(f+g)(a_n,b_l,\lambda^\pi_\nu)][(f+g)(a_{n'},b_{l'},\lambda^\pi_\nu)]S^+_{l,l'}(b,\omega')}{\omega - \omega' - \hbar\omega_{\lambda^\pi_\nu}} + \frac{\sum_{l,l'}[(f-g)(a_n,b_l,\lambda^\pi_\nu)][(f-g)(a_{n'},b_{l'},\lambda^\pi_\nu)]S^-_{l,l'}(b,\omega')}{\omega + \omega' + \hbar\omega_{\lambda^\pi_\nu}}, \tag{A.2.21}$$

$$\Sigma^{11}_{n,n'\ (h,h)}(a,\omega)=\sum_{b,\lambda^{\pi}_{\nu}}\int_0^{+\infty}\mathrm{d}\omega'\frac{\sum_{l,l'}[(f-g)(a_n,b_l,\lambda^{\pi}_{\nu})][(f-g)(a_{n'},b_{l'},\lambda^{\pi}_{\nu})]S^{-}_{l,l'}(b,\omega')}{\omega-E_{b_\mu}-\hbar\omega_{\lambda^{\pi}_{\nu}}}+$$
$$\frac{\sum_{l,l'}[(f+g)(a_n,b_l,\lambda^{\pi}_{\nu})][(f+g)(a_{n'},b_{l'},\lambda^{\pi}_{\nu})]S^{+}_{l,l'}(b,\omega')}{\omega+E_{b_\mu}+\hbar\omega_{\lambda^{\pi}_{\nu}}}. \tag{A.2.22}$$

The off-diagonal blocks are given by

$$\Sigma^{11}_{n,n'\ (p,h)}(a,\omega)=\sum_{b,\lambda^{\pi}_{\nu}}\int_0^{+\infty}\mathrm{d}\omega'-\frac{\sum_{l,l'}(f+g)(a_n,b_l,\lambda^{\pi}_{\nu})(f-g)(a_{n'},b_{l'},\lambda^{\pi}_{\nu})\widetilde{S}_{l,l'}(b,\omega')}{\omega-\omega'-\hbar\omega_{\lambda^{\pi}_{\nu}}}$$
$$+\frac{\sum_{l,l'}(f-g)(a_n,b_l,\lambda^{\pi}_{\nu})(f+g)(a_{n'},b_{l'},\lambda^{\pi}_{\nu})\widetilde{S}_{l',l}(b,\omega')}{\omega+\omega'+\hbar\omega_{\lambda^{\pi}_{\nu}}}, \tag{A.2.23}$$

or vice versa

$$\Sigma^{11}_{n,n'\ (h,p)}(a,\omega)=\sum_{b,\lambda^{\pi}_{\nu}}\int_0^{+\infty}\mathrm{d}\omega'-\frac{\sum_{l,l'}(f-g)(a_n,b_l,\lambda^{\pi}_{\nu})(f+g)(a_{n'},b_{l'},\lambda^{\pi}_{\nu})\widetilde{S}_{l',l}(b,\omega')}{\omega-\omega'-\hbar\omega_{\lambda^{\pi}_{\nu}}}+$$
$$\frac{\sum_{l,l'}(f+g)(a_n,b_l,\lambda^{\pi}_{\nu})(f-g)(a_{n'},b_{l'},\lambda^{\pi}_{\nu})\widetilde{S}_{l,l'}(b,\omega')}{\omega+\omega'+\hbar\omega_{\lambda^{\pi}_{\nu}}}. \tag{A.2.24}$$

In a similar way

$$\Sigma^{12}_{n,n'\ (p,p)}(a,\omega)=-\sum_{b,\lambda^{\pi}_{\nu}}\int_0^{+\infty}\mathrm{d}\omega'\frac{\sum_{l,l'}(f+g)(a_n,b_l,\lambda^{\pi}_{\nu})(f-g)(a_{n'},b_{l'},\lambda^{\pi}_{\nu})\widetilde{S}_{l,l'}(b,\omega')}{\omega-\omega'-\hbar\omega_{\lambda^{\pi}_{\nu}}}-$$
$$-\frac{\sum_{l,l'}(f-g)(a_n,b_l,\lambda^{\pi}_{\nu})(f+g)(a_{n'},b_{l'},\lambda^{\pi}_{\nu})\widetilde{S}_{l,l'}(b,\omega')}{\omega+\omega'+\hbar\omega_{\lambda^{\pi}_{\nu}}}, \tag{A.2.25}$$

$$\Sigma^{12}_{n,n'\ (h,h)}(a,\omega)=\sum_{b,\lambda^{\pi}_{\nu}}\int_0^{+\infty}\mathrm{d}\omega'\frac{\sum_{l,l'}(f-g)(a_n,b_l,\lambda^{\pi}_{\nu})(f+g)(a_{n'},b_{l'},\lambda^{\pi}_{\nu})\widetilde{S}_{l,l'}(b,\omega')}{\omega-\omega'-\hbar\omega_{\lambda^{\pi}_{\nu}}}$$
$$-\frac{\sum_{l,l'}(f+g)(a_n,b_l,\lambda^{\pi}_{\nu})(f-g)(a_{n'},b_{l'},\lambda^{\pi}_{\nu})\widetilde{S}_{l,l'}(b,\omega')}{\omega+\omega'+\hbar\omega_{\lambda^{\pi}_{\nu}}}, \tag{A.2.26}$$

$$\Sigma^{12}_{n,n'\ (p,h)}(a,\omega)=-\sum_{b,\lambda^{\pi}_{\nu}}\int_0^{+\infty}\mathrm{d}\omega'\frac{\sum_{l,l'}(f+g)(a_n,b_l,\lambda^{\pi}_{\nu})(f+g)(a_{n'},b_{l'},\lambda^{\pi}_{\nu})S^{+}_{l,l'}(b,\omega')}{\omega-\omega'-\hbar\omega_{\lambda^{\pi}_{\nu}}}+$$
$$\frac{\sum_{l,l'}(f-g)(a_n,b_l,\lambda^{\pi}_{\nu})(f-g)(a_{n'},b_{l'},\lambda^{\pi}_{\nu})S^{-}_{l,l'}(b,\omega')}{\omega+\omega'+\hbar\omega_{\lambda^{\pi}_{\nu}}}, \tag{A.2.27}$$

or vice versa

$$\Sigma^{12}_{n,n'\ (h,p)}(a,\omega) = \sum_{b,\lambda^\pi_\nu} \int_0^{+\infty} \mathrm{d}\omega' - \frac{\sum_{l,l'}(f-g)(a_n,b_l,\lambda^\pi_\nu)(f-g)(a_{n'},b_{l'},\lambda^\pi_\nu)S^-_{l,l'}(b,\omega')}{\omega-\omega'-\hbar\omega_{\lambda^\pi_\nu}} + \frac{\sum_{l,l'}(f+g)(a_n,b_l,\lambda^\pi_\nu)(f+g)(a_{n'},b_{l'},\lambda^\pi_\nu)S^+_{l,l'}(b,\omega')}{\omega+\omega'+\hbar\omega_{\lambda^\pi_\nu}}. \tag{A.2.28}$$

Following the representation of the Σ we represent the Green's function G in the same quasiparticle basis, as, by definition, the inverse of the running variable - the eigenvalues multiplied by the matrix composed by the eigenvectors of the total hamiltonian,

Once the self-energy has been calculated, the Green's function is obtained following the prescriptions of the Dyson equation (cf. Appendix D.3.3), that are the inversion that define the dressed Green's function,

$$\hat{G}(a,\omega+i\eta) = \left[\omega+i\eta-\hat{H}_{HFB}-\hat{\Sigma}(a,\omega+i\eta)\right]^{-1}. \tag{A.2.29}$$

Equivalently, one can write

$$\hat{G}(a,\omega+i\eta) = \sum_\mu \frac{1}{\omega+i\eta-E_\mu} \begin{pmatrix} x_1 \\ \vdots \\ x_n \\ y_1 \\ \vdots \\ y_n \end{pmatrix}_\mu (x_1 \ \cdots \ x_n \ \ y_1 \ \cdots \ y_n)_\mu, \tag{A.2.30}$$

where μ runs over all positive and negative solutions.

The Green's function is then divided into 4 blocks with terms proportional to $x_n \cdot x_{n'}$, $x_n \cdot y_{n'}$, $y_n \cdot x_{n'}$ and $y_n \cdot y_{n'}$, that will be indicated by $G^{11}_{n,n'}$, $G^{12}_{n,n'}$, $G^{21}_{n,n'}$ and $G^{22}_{n,n'}$ respectively, in analogy with the self-energy, and it's imaginary part is related to the strength function as described in the Lehmann representation, and it reads

$$\Im m\{\hat{G}(a,\omega+i\eta)\} = \sum_{\widetilde{E}_{a_\mu}>0} -\pi\mathcal{L}_\eta(\omega-\widetilde{E}_{a_\mu}) \left(\begin{array}{ccc|ccc} x_1x_1 & \cdots & x_1x_N & x_1y_1 & \cdots & x_1y_N \\ \vdots & \ddots & \vdots & \vdots & \ddots & \vdots \\ x_Nx_1 & \cdots & x_Nx_N & x_Ny_1 & \cdots & x_Ny_N \\ \hline y_1x_1 & \cdots & y_1x_N & y_1y_1 & \cdots & y_1y_N \\ \vdots & \ddots & \vdots & \vdots & \ddots & \vdots \\ y_Nx_1 & \cdots & y_Nx_N & y_Ny_1 & \cdots & y_Ny_N \end{array}\right) - \pi\mathcal{L}_\eta(\omega+\widetilde{E}_{a_\mu}) \left(\begin{array}{ccc|ccc} y_1y_1 & \cdots & y_1y_N & -x_1y_1 & \cdots & -x_1y_N \\ \vdots & \ddots & \vdots & \vdots & \ddots & \vdots \\ y_Ny_1 & \cdots & y_Ny_N & -x_Ny_1 & \cdots & -x_Ny_N \\ \hline -y_1x_1 & \cdots & -y_1x_N & x_1x_1 & \cdots & x_1x_N \\ \vdots & \ddots & \vdots & \vdots & \ddots & \vdots \\ -y_Nx_1 & \cdots & -y_Nx_N & x_Nx_1 & \cdots & x_Nx_N \end{array}\right) \tag{A.2.31}$$

In the adopted basis the strength function $S^{+}_{l,l'}(b,\omega')$ corresponding to $\widetilde{u}_{b^\mu,l}\widetilde{u}_{b^\mu,l'}$ is given by the imaginary part of the corresponding Green's function, depending on the particle or hole character of the orbitals l, l'. If both l, l' corrrespond to particle states, $S^{+}_{l,l'}$ is proportional to $u_l \cdot u_{l'}$ in the single-particle basis and to $x_l \cdot x_{l'}$ in the quasiparticle basis, and is obtained from the imaginary part of the $G^{11}_{l,l'}$. On the other hand, if l is a particle state and l' is a hole state, $S^{+}_{l,l'}$ is porportional to $u_l \cdot u_{l'}$ in the single particle basis and to $x_l \cdot (-y_{l'})$ character in the quasiparticle basis, and consequently is obtained from the imaginary part of $-G^{12}_{l,l'}$. Extending this considerations to all cases we get

$$\widetilde{u}^{\mu}_{l}\widetilde{u}^{\mu}_{l'} \sim S^{+}_{l,l'}(b,\omega) = -\frac{\Im m}{\pi}\begin{cases} G^{11}_{l,l'}(b,\omega) & \text{for } \varepsilon_l, \varepsilon_{l'} > \varepsilon_F \\ -G^{12}_{l,l'}(b,\omega) & \text{for } \varepsilon_l > \varepsilon_F,\ \varepsilon_{l'} < \varepsilon_F \\ -G^{21}_{l,l'}(b,\omega) = -G^{12}_{l',l}(b,\omega) & \text{for } \varepsilon_l < \varepsilon_F,\ \varepsilon_{l'} > \varepsilon_F \\ G^{22}_{l,l'}(b,\omega) & \text{for } \varepsilon_l, \varepsilon_{l'} < \varepsilon_F \end{cases}, \tag{A.2.32}$$

and, extending this consideration to the other strength functions, we get

$$S^{-}_{l,l'}(b,\omega) = -\frac{\Im m}{\pi}\begin{cases} G^{22}_{l,l'}(b,\omega) & \text{for } \varepsilon_l, \varepsilon_{l'} > \varepsilon_F \\ G^{21}_{l,l'}(b,\omega) & \text{for } \varepsilon_l > \varepsilon_F,\ \varepsilon_{l'} < \varepsilon_F \\ G^{12}_{l,l'}(b,\omega) & \text{for } \varepsilon_l < \varepsilon_F,\ \varepsilon_{l'} > \varepsilon_F \\ G^{11}_{l,l'}(b,\omega) & \text{for } \varepsilon_l, \varepsilon_{l'} < \varepsilon_F \end{cases} \tag{A.2.33}$$

$$= S^{+}_{l,l'}(b,-\omega), \tag{A.2.34}$$

and finally

$$\widetilde{S}_{l,l'}(b,\omega) = -\frac{\Im m}{\pi}\begin{cases} G^{12}_{l,l'}(b,\omega) & \text{for } \varepsilon_l, \varepsilon_{l'} > \varepsilon_F \\ G^{11}_{l,l'}(b,\omega) & \text{for } \varepsilon_l > \varepsilon_F,\ \varepsilon_{l'} < \varepsilon_F \\ -G^{22}_{l,l'}(b,\omega) & \text{for } \varepsilon_l < \varepsilon_F,\ \varepsilon_{l'} > \varepsilon_F \\ -G^{21}_{l,l'}(b,\omega) & \text{for } \varepsilon_l, \varepsilon_{l'} < \varepsilon_F \end{cases} \tag{A.2.35}$$

A.3 Two-step diagonalization

The formalism outlined in the previous sections is based on the use of the single-particle basis to solve the mean field pairing problem plus self energy in one step . Depending on the type of the pairing force considered, the particle space needed to obtain convergence in the pairing properties can include states of very high momenta (up to ~ 800 MeV in the case of bare Argonne v_{14} interaction [20]). However, the effects of the coupling between quasiparticle and phonons are particularly important in a restricted energy range close to the Fermi energy, and it can be convenient in practical applications to perform the diaognalization of the energy-dependent problem in two steps. In the first step one solves the HFB equations in a large single-particle basis; one then restricts the basis to a smaller energy range, solving in the second step the energy-dependent problem within the restricted basis.

It has been shown that, in the case of a seniority force, the results obtained with this two-step procedure are very similar to the one-step solution for realistic values of the paring constant [16].

To perform the two step calculation, we first diagonalize $\hat{H}_{HFB}$. We then transform the self energy $\hat{\Sigma}$ in this quasiparticle basis that diagonalizes the HFB, in other words we

apply the change of basis M,

$$\hat{\Sigma}^{HFB} = M\hat{\Sigma}M^t. \tag{A.3.1}$$

The full hamiltonian now reads

$$\left[\left(\begin{array}{cc|cc} E_1 & \hat{0} & & \\ & & \hat{0} & \\ \hat{0} & E_N & & \\ \hline & & -E_1 & \hat{0} \\ & \hat{0} & & \\ & & \hat{0} & -E_N \end{array}\right) + \hat{\Sigma}^{HFB}(a, E_{a^{m,\mu}})\right] \begin{pmatrix} x^m_{\mu=1} \\ \vdots \\ x^m_{\mu=N} \\ y^m_{\mu=1} \\ \cdots \\ y^m_{\mu=N} \end{pmatrix} = E_{a^{\mu,m}} \begin{pmatrix} x^m_{\mu=1} \\ \vdots \\ x^m_{\mu=N} \\ y^m_{\mu=1} \\ \cdots \\ y^m_{\mu=N} \end{pmatrix} \tag{A.3.2}$$

and the associated representation of the dressed quasiparticle is given by

$$|a^m\rangle = \sum_\mu x^m_\mu |a^{\mu\ (+)}\rangle + y^m_\mu |a^{\mu\ (-)}\rangle, \tag{A.3.3}$$

that is the diagonalization making use of x, y amplitudes of the eigenvector of the full hamiltonian over the quasiparticle basis. The label m index the fragmentation coming from the energy dependence of Σ. That can be also represented as a correction to the familiar u, v factors,

$$\tilde{u}^m_l = \sum_\mu x^m_\mu u^{HFB}_{\mu,l} - y^m_\mu v^{HFB}_{\mu,l}, \tag{A.3.4}$$

$$\tilde{v}^m_l = \sum_\mu x^m_\mu v^{HFB}_{\mu,l} + y^m_\mu u^{HFB}_{\mu,l}. \tag{A.3.5}$$

To be noted that the u, v factors used in (A.2.8)-(A.2.11) have to be these corrected $\tilde{u}, \tilde{v}$ in order to consider the dressed quasiparticle following the prescriptions of the Dyson equation, where the intermediate state is the dressed quasiparticle.

In this case, the strength functions of the continuum representation relate with the Green's function matrix considering

$$\begin{aligned} \tilde{u}^m_l \tilde{u}^m_{l'} &= \left(\sum_\mu x^m_\mu u^{HFB}_{\mu,l} - y^m_\mu v^{HFB}_{\mu,l}\right)\left(\sum_{\mu'} x^m_{\mu'} u^{HFB}_{\mu',l'} - y^m_{\mu'} v^{HFB}_{\mu',l'}\right) = \\ &= \sum_{\mu,\mu'} x^m_\mu x^m_{\mu'} u_{\mu,l} u_{\mu',l'} - x^m_\mu y^m_{\mu'} u_{\mu,l} v_{\mu',l'} - y^m_\mu x^m_{\mu'} v_{\mu,l} u_{\mu',l'} + y^m_\mu y^m_{\mu'} v_{\mu,l} v_{\mu',l'} \end{aligned} \tag{A.3.6}$$

which gives,

$$\begin{aligned} \tilde{u}^m_l \tilde{u}^m_{l'} \to S^+_{l,l'} = -\frac{\Im m}{\pi}\{&\sum_{\mu,\mu'} G^{11}_{\mu,\mu'} u_{\mu,l} u_{\mu',l'} - G^{12}_{\mu,\mu'} u_{\mu,l} v_{\mu',l'} \\ &- G^{21}_{\mu,\mu'} v_{\mu,l} u_{\mu',l'} + G^{22}_{\mu,\mu'} v_{\mu,l} v_{\mu',l'}\}, \end{aligned} \tag{A.3.7}$$

and analogously,

$$\begin{aligned} \tilde{v}^m_l \tilde{v}^m_{l'} \to S^-_{l,l'} = -\frac{\Im m}{\pi}\{&\sum_{\mu,\mu'} G^{11}_{\mu,\mu'} v_{\mu,l} v_{\mu',l'} + G^{12}_{\mu,\mu'} v_{\mu,l} u_{\mu',l'} \\ &+ G^{21}_{\mu,\mu'} u_{\mu,l} v_{\mu',l'} + G^{22}_{\mu,\mu'} u_{\mu,l} u_{\mu',l'}\}, \end{aligned} \tag{A.3.8}$$

and

$$\tilde{u}_l^m \tilde{v}_{l'}^m \to \widetilde{S}_{l,l'} = -\frac{\Im m}{\pi}\{\sum_{\mu,\mu'} G^{11}_{\mu,\mu'} u_{\mu,l} v_{\mu',l'} + G^{12}_{\mu,\mu'} u_{\mu,l} u_{\mu',l'} - G^{21}_{\mu,\mu'} v_{\mu,l} v_{\mu',l'} - G^{22}_{\mu,\mu'} v_{\mu,l} u_{\mu',l'}\}, \tag{A.3.9}$$

A.4 BCS approximation

An extreme case of truncation of the basis space is that of describing a single-shell around the Fermi energy. In that case only one quasiparticle and its associated single-particle level of given l, j are retained, the μ with the largest abnormal density $\sum_l u_{\mu l} v_{\mu l}$, that is the one with the smaller quasiparticle energy E_{a^μ}, and that l with the largest contribution to the quasiparticle strength $u^2_{\mu l} + v^2_{\mu l}$ respectively. Since N, number of nodes,$= 1$, so that the node and quasiparticle l, μ are fixed by the above relations, their writing can be implicitly assumed defining, for the chosen l, μ, $u^{HFB}_{\mu l} = u^{BCS}$ or simply u.

The truncated self energy $\hat{\Sigma}$ is now just a 2×2 matrix,

$$\hat{\Sigma}(a,\omega) = \begin{pmatrix} \Sigma^{11}(a,\omega) & \Sigma^{12}(a,\omega) \\ \Sigma^{21}(a,\omega) & \Sigma^{22}(a,\omega) \end{pmatrix} \tag{A.4.1}$$

and its writing in the quasiparticle basis is given by

$$\Sigma^{\hat{BCS}} = \hat{M}\hat{\Sigma}\hat{M}^t, \tag{A.4.2}$$

we will call this the BCS approximation for the self-energy.

Thus, if the chosen strongest node l is particle like ($\varepsilon_a > \varepsilon_F$)

$$\hat{\Sigma}^{BCS} = \begin{pmatrix} u^{BCS} & -v^{BCS} \\ -v^{BCS} & u^{BCS} \end{pmatrix} \hat{\Sigma} \begin{pmatrix} u^{BCS} & -v^{BCS} \\ v^{BCS} & u^{BCS} \end{pmatrix}, \tag{A.4.3}$$

while if have hole character ($\varepsilon_a < \varepsilon_F$)

$$\hat{\Sigma}^{BCS} = \begin{pmatrix} v^{BCS} & -u^{BCS} \\ u^{BCS} & v^{BCS} \end{pmatrix} \hat{\Sigma} \begin{pmatrix} v^{BCS} & u^{BCS} \\ -u^{BCS} & v^{BCS} \end{pmatrix}, \tag{A.4.4}$$

where $\hat{\Sigma}$ has been written with the $|a^{(+)}\rangle; |a^{(-)}\rangle$ basis.

In order that the change of basis remains unitary, u and v must be scaled to have the normalization condition

$$u^2 + v^2 = 1 \tag{A.4.5}$$

Matrix elements are now independent of the node indexes, and so are factorizable giving

$$\Sigma_{11}(a,\omega) = \sum_{b(n),\lambda^\pi_\nu} \frac{(f+g)^2(a,b,\lambda^\pi_\nu)\widetilde{u}_{b(n)}\widetilde{u}_{b(n)}}{\omega - E_{b(n)} - \hbar_{\lambda^\pi_\nu}} + \frac{(f-g)^2(a,b,\lambda^\pi_\nu)\widetilde{v}_{b(n)}\widetilde{v}_{b(n)}}{\omega + E_{b(n)} + \hbar_{\lambda^\pi_\nu}}, \tag{A.4.6}$$

and

$$\Sigma_{12}(a,\omega) = -\sum_{b(n),\lambda^\pi_\nu} (f+g)(f-g)(a,b,\lambda^\pi_\nu)\widetilde{u}_{b(n)}\widetilde{v}_{b(n)} \left(\frac{1}{\omega - E_{b(n)} - \hbar_{\lambda^\pi_\nu}} - \frac{1}{\omega + E_{b(n)} + \hbar_{\lambda^\pi_\nu}} \right), \tag{A.4.7}$$

Then the Self Energy (or the Green's Function) matrix in the BCS basis is explicitely given, following the prescriptions discussed above, by

$$\left(\begin{array}{cc} u & v \\ -v & u \end{array} \right) \left(\begin{array}{cc} \Sigma_{11} & \Sigma_{12} \\ \Sigma_{21} & \Sigma_{22} \end{array} \right) \left(\begin{array}{cc} u & -v \\ v & u \end{array} \right), \tag{A.4.8}$$

multiplying row and columns this gives

$$\begin{array}{l} \left(\begin{array}{cc} u\Sigma_{11} + v\Sigma^{21} & u\Sigma_{12} + v\Sigma_{22} \\ -v\Sigma_{11} + u\Sigma^{21} & -v\Sigma_{12} + u\Sigma_{22} \end{array} \right) \left(\begin{array}{cc} u & -v \\ v & u \end{array} \right) = \\ \left(\begin{array}{c|c} u^2\Sigma_{11} + uv\Sigma_{21} + vu\Sigma_{12} + v^2\Sigma_{22} & -uv\Sigma_{11} - v^2\Sigma_{21} + u^2\Sigma_{12} + uv\Sigma_{22} \\ \hline -uv\Sigma_{11} + u^2\Sigma_{21} - v^2\Sigma_{12} + uv\Sigma_{22} & v^2\Sigma_{11} - uv\Sigma_{21} - vu\Sigma_{12} + u^2\Sigma_{22} \end{array} \right), \end{array} \tag{A.4.9}$$

that is,

$$\begin{aligned} \Sigma_{11}^{BCS}(a,\omega) =& u_a^2\Sigma_{11} + u_a v_a \Sigma_{21} + v_a u_a \Sigma_{12} + v_a^2 \Sigma_{22} = \\ =& u_a^2 \sum_{b(n),\lambda_\nu} \frac{\widetilde{u}^2_{b(n)}(f+g)^2(a,b,\lambda^\pi_\nu)}{\omega - E_{b(n)} - \hbar\omega_{\lambda^\pi_\nu}} + \frac{\widetilde{v}^2_{b(n)}(f-g)^2(a,b,\lambda^\pi_\nu)}{\omega + E_{b(n)} + \hbar\omega_{\lambda^\pi_\nu}} \\ &+ v_a^2 \sum_{b(n),\lambda_\nu} \left(\frac{\widetilde{v}^2_{b(n)}(f-g)^2(a,b,\lambda^\pi_\nu)}{\omega - E_{b(n)} - \hbar\omega_{\lambda^\pi_\nu}} + \frac{\widetilde{u}^2_{b(n)}(f+g)^2(a,b,\lambda^\pi_\nu)}{\omega + E_{b(n)} + \hbar\omega_{\lambda^\pi_\nu}} \right) \\ &+ 2u_a v_a \sum_{b(n),\lambda_\nu} -\widetilde{u}_{b(n)}\widetilde{v}_{b(n)}(f+g)(f-g)(a,b,\lambda^\pi_\nu) \\ &\left(\frac{1}{\omega - E_{b(n)} - \hbar\omega_{\lambda^\pi_\nu}} - \frac{1}{\omega + E_{b(n)} + \hbar\omega_{\lambda^\pi_\nu}} \right). \end{aligned} \tag{A.4.10}$$

Let us now tackle only the the "forward-going" terms (which have the $\omega - E_{b(n)} - \hbar_{\lambda^p i_\nu}$ denominator), that correspond, since we are considering $\Sigma_{11}^{BCS}(a,\omega)$, to the forward vertex V^2 in Fig. A.2 in the case in which also the incoming particle a to be renormalized is a quasiparticle. This gives

$$\begin{aligned} (V^{BCS})^2 &= u_a^2\widetilde{u}^2_{b(n)}(f+g) + v_a^2\widetilde{v}^2_{b(n)}(f-g) - 2u_a v_a \widetilde{u}_{b(n)}\widetilde{v}_{b(n)}(f+g)(f-g) = \\ &= f^2(u_a\widetilde{u}_{b(n)} - v_a\widetilde{v}_{b(n)})^2 + g^2(u_a\widetilde{u}_{b(n)} + v_a\widetilde{v}_{b(n)})^2 + 2fg(u_a^2\widetilde{u}^2_{b(n)} - v_a^2\widetilde{v}^2_{b(n)}) = \\ &= [f(u_a\widetilde{u}_{b(n)} - v_a\widetilde{v}_{b(n)}) + g(u_a\widetilde{u}_{b(n)} + v_a\widetilde{v}_{b(n)})]^2, \end{aligned} \tag{A.4.11}$$

while the backward going term, analogously gives,

$$(W^{BCS})^2 = [f(u_a\widetilde{v}_{b(n)} + v_a\widetilde{u}_{b(n)}) + g(-u_a\widetilde{v}_{b(n)} + v_a\widetilde{u}_{b(n)})]^2 \tag{A.4.12}$$

These vertices between BCS quasiparticles and self-energy-dressed quasiparticle plus phonon, must then be used in (A.2.12)-(A.2.16) to obtain the self energies in the case of two-step diagonalization.

These combination of u^{BCS}, v^{BCS} and $\widetilde{u}, \widetilde{v}$ factors is that found, e.g. in [39] (eq. (6-207) for spin independent and spin-dependent QRPA phonons.)

APPENDIX B

Vertex Correction

The Dyson equation considered in Appendix A, takes into account only the rainbow-type diagrams, as explained in Appendix D.3.3. On the contrary non-intersecting diagrams like the ones in Fig. B.1 are not included in the treatment of the Dyson equation in Section 1.2 and App. A and D. These close of diagrams can be included by considering

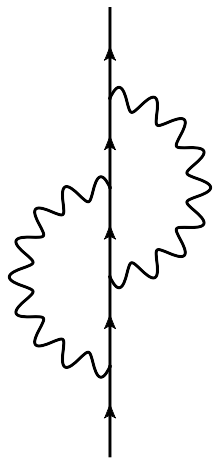

Figure B.1: Feynman diagram representing a perturbation of intersecting phonons lines.

an energy dependent correction to the vertex V (and W), summing to the energy independent elements (cf. Fig. A.2 and Eqs. (A.2.8)-(A.2.11)), which renormalize the vertex taking into account to the exchange of virtual phonons within the scattering processes.

The correction is given by considering all the possible time orderings, or, in other words, all the combination of $^{(+)}$ and $^{(-)}$ character for the quasiparticles in considerations. The vertices can be of type V, coupling two quasiparticles with the same character (both $^{(+)}$ or $^{(-)}$), and W, coupling two quasiparticles with opposite character (one $^{(+)}$, the other $^{(-)}$) (cf. Figs. A.2 and B.2, Eqs. (A.2.8)-(A.2.11). In the following $Vertex$ denote any of the vertices V and W, depending on the case. The correction $\delta Vertex_i$, that is a

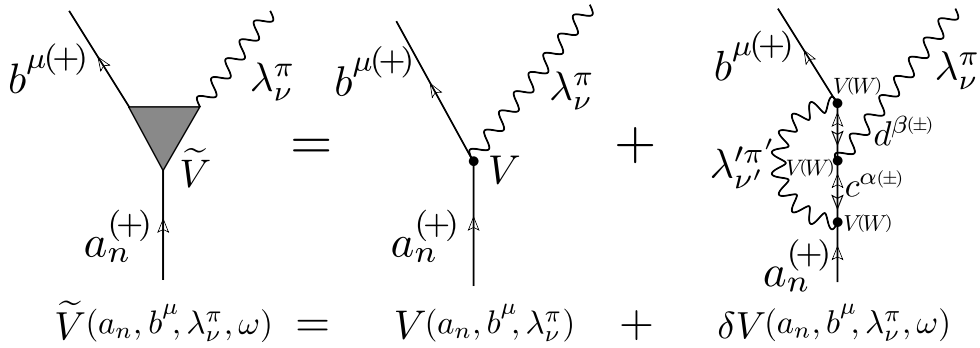

Figure B.2: The renormalized vertex $\widetilde{V}$, that couples $a_n^{(+)}$ with $b^{\mu(+)}$ and the phonon λ^{π}_{ν}, is given by the basic vertex V plus an energy dependent correction δV coming from the exchange of a virtual phonon $\lambda'^{\pi'}_{\nu'}$ scattering with other two virtual quasiparticle states $c^{\alpha(\pm)}$, $d^{\beta(\pm)}$. The energy dependent contribution involves a total of three vertices,that can be of V- or W-type, Depending on the (+) or (-) character of the virtual intermediate quasiparticles, there are 4 possible time orderings for the energy dependent contribution, each one associated with three vertices that may be of V- or W- type. The other 3 vertices to be renormalized are the ones connecting $a_n^{(-)}$ with $b^{\mu(-)}$, that is the other V vertex, and $a_n^{(+)}$ with $b^{\mu(-)}$ and $a_n^{(-)}$ with $b^{\mu(+)}$, that are the two W vertices (cf. Fig. A.2). Each one of them has 4 time orderings, for a total of 16 time orderings to be considered.

single time-ordering i contribution to the total renormalization of vertex, then reads,

$$\begin{aligned}\delta Vertex_i(a_n, b^{\mu}, \lambda^{\pi}_{\nu}, \omega) = & \sum_{c,d,\lambda'^{\pi'}_{\nu'}} \frac{(-1)^{j_c+\lambda'-j_a}(-1)^{j_d+\lambda'-j_b}}{1+\delta_{\lambda^{\pi}_{\nu},\lambda'^{\pi'}_{\nu'}}} \langle (\lambda' j_d) j_b \lambda; j_a | \lambda' (j_d \lambda) j_c; j_a \rangle \\ & \sum_{\alpha,\beta} Vertex(a_n, c^{\alpha}, \lambda'^{\pi'}_{\nu'}) Vertex(c^{\alpha}, d^{\beta}, \lambda^{\pi}_{\nu}) Vertex(d^{\beta}, b^{\mu}, \lambda'^{\pi'}_{\nu'}) \\ & \frac{1}{\omega \mp (E_{c^{\alpha}} + \hbar\omega_{\lambda'^{\pi'}_{\nu'}})} \frac{1}{\omega \mp (E_{d^{\beta}} + \hbar\omega_{\lambda'^{\pi'}_{\nu'}} + \hbar\omega_{\lambda^{\pi}_{\nu}})}\end{aligned} \tag{B.0.1}$$

where $Vertex$, is V or W depending on the correction and time ordering considered and the denominators adjust accordingly,

- if $Vertex(a_n, c^{\alpha}, \lambda'^{\pi'}_{\nu'}) = V(a_n, c^{\alpha}, \lambda'^{\pi'}_{\nu'})$ the denominator reads $\omega - (E_{c^{\alpha}} + \hbar\omega_{\lambda'^{\pi'}_{\nu'}})$, else if $Vertex(a_n, c^{\alpha}, \lambda'^{\pi'}_{\nu'}) = W(a_n, c^{\alpha}, \lambda'^{\pi'}_{\nu'})$ the denominator reads $\omega + (E_{c^{\alpha}} + \hbar\omega_{\lambda'^{\pi'}_{\nu'}})$.

- if $Vertex(c^{\alpha}, d^{\beta}, \lambda^{\pi}_{\nu}) = V(c^{\alpha}, d^{\beta}, \lambda^{\pi}_{\nu})$ the denominator reads $\omega - (E_{d^{\beta}} + \hbar\omega_{\lambda'^{\pi'}_{\nu'}} + \hbar\omega_{\lambda^{\pi}_{\nu}})$ else if $Vertex(c^{\alpha}, d^{\beta}, \lambda^{\pi}_{\nu}) = W(c^{\alpha}, d^{\beta}, \lambda^{\pi}_{\nu})$ the denominator reads $\omega + (E_{d^{\beta}} + \hbar\omega_{\lambda'^{\pi'}_{\nu'}} + \hbar\omega_{\lambda^{\pi}_{\nu}})$.

- the last $Vertex(d^{\beta}, b^{\mu}, \lambda'^{\pi'}_{\nu'})$ is then set V or W depending on the character of d^{β}. E.g. if considering the vertex correction $\delta V_i(a_n^{(+)}, b^{\mu(+)}, \lambda^{\pi}_{\nu}, \omega)$, $Vertex(d^{\beta}, b^{\mu}, \lambda'^{\pi'}_{\nu'})$ can be $V(d^{\beta(+)}, b^{\mu(+)}, \lambda'^{\pi'}_{\nu'})$ or $W(d^{\beta(-)}, b^{\mu(+)}, \lambda'^{\pi'}_{\nu'})$. In other words, to calculate δV there are an odd number of V-type vertices, instead to calculate δW there are an

p	$[\langle a_n\|V\|c_m\lambda'\rangle]$	$[\langle c_{m'}\|V\|d_q\lambda\rangle]$	$[\langle d_{q'}\lambda'\|V\|b_l\rangle]$	$S_{m,m'}(c^\alpha)$	$S_{q,q'}(d^\beta)$	$A(b_l^\mu)$	$A(a_m)$
$(-1)^0$	$(f+g)$	$(f+g)$	$(f+g)$	$u_m u_{m'}$	$u_q u_{q'}$	u	u
$(-1)^1$	$(f+g)$	$(f+g)$	$(f-g)$	$u_m u_{m'}$	$u_q v_{q'}$	u	v
$(-1)^1$	$(f+g)$	$(f-g)$	$(f+g)$	$u_m v_{m'}$	$v_q u_{q'}$	u	u
$(-1)^1$	$(f-g)$	$(f+g)$	$(f+g)$	$v_m u_{m'}$	$u_q u_{q'}$	u	v
$(-1)^2$	$(f-g)$	$(f-g)$	$(f+g)$	$v_m v_{m'}$	$v_q u_{q'}$	u	v
$(-1)^2$	$(f-g)$	$(f+g)$	$(f-g)$	$v_m u_{m'}$	$u_q v_{q'}$	v	v
$(-1)^2$	$(f+g)$	$(f-g)$	$(f-g)$	$u_m v_{m'}$	$v_q v_{q'}$	v	u
$(-1)^3$	$(f-g)$	$(f-g)$	$(f-g)$	$v_m v_{m'}$	$v_q v_{q'}$	v	v

Table B.1: Every row represents the factors entering in each one of the eight contributions to the energy-dependent vertex correction δV, in the particular case in which the intermediate quasiparticles c^α, d^β have (+) character (cf. Fig. B.2). The column p is given by the minus sign of the $(f-g)$ factor, the eight rows represent the possible combinations of $(f+g)$ and $(f-g)$ and the corresponding u, v factors. The elements of each row have to be used in Eq. (B.0.4).

odd number of W-type ones, the type of $Vertex(d^\beta, b^\mu, \lambda'^{\pi'}_{\nu'})$ is then stated accordingly.

The total correction $\delta Vertex$ is then given by the sum over all the possible time orderings $\delta Vertex_i$.

The various V and W vertices must be then calculated making use of the Eqs. (A.2.8)-(A.2.11) as shown in the following example (B.0.4). This gets complicated configurations of u, v factors and $(f+g), (f-g)$ matrix elements that, in order to iterate and use the strength functions formalism of Eqs. (A.2.18)-(A.2.20), have to be explicitated. We recast the matrix elements equations for the general case of two quasiparticles (A.4.11)-(A.4.12),

$$\begin{aligned} V(c^{\alpha(+)}, d^{\beta(+)}, \lambda^\pi_\nu) &= -V(c^{\alpha(-)}, d^{\beta(-)}, \lambda^\pi_\nu) \\ &= \sum_{m,q} (f+g)(c_m, d_q, \lambda^\pi_\nu) u_{c^\alpha,m} u_{d^\beta,q} - (f-g)(c_m, d_q, \lambda^\pi_\nu) v_{c^\alpha,m} v_{d^\beta,q}, \end{aligned} \tag{B.0.2}$$

$$\begin{aligned} W(c^{\alpha(+)}, d^{\beta(-)}, \lambda^\pi_\nu) &= W(c^{\alpha(-)}, d^{\beta(+)}, \lambda^\pi_\nu) \\ &= \sum_{m,q} (f+g)(c_m, d_q, \lambda^\pi_\nu) u_{c^\alpha,m} v_{d^\beta,q} + (f-g)(c_m, d_q, \lambda^\pi_\nu) v_{c^\alpha,m} u_{d^\beta,q}. \end{aligned} \tag{B.0.3}$$

As an example we consider explicitly the correction $\delta V_1(a_n^{(+)}, b^{\mu(+)}, \lambda^\pi_\nu, \omega)$, that is composed by all V-type elements connecting quasiparticles with character $^{(+)}$. For convenience we put the components to all the contributions to this time ordering in Table B.1. The explicit equation of the vertex correction is obtained from the sum over all the $rows$ of the Table B.1, where its elements have to be used as components of the following

vertex correction equation,

$$\delta V_1(a_n^{(+)}, b^{\mu(+)}, \lambda_\nu^\pi, \omega) = \sum_{c,d,\lambda'^{\pi'}_{\nu'}} \frac{1}{1+\delta_{\lambda^\pi_\nu,\lambda'^{\pi'}_{\nu'}}} (-1)^{j_c+\lambda'-j_a}(-1)^{j_d+\lambda'-j_b}\langle(\lambda' j_d)j_b\lambda; j_a|\lambda'(j_d\lambda)j_c; j_a\rangle$$
$$\sum_{\alpha,\beta}\sum_{rows}\sum_{m,m';q,q'} p[\langle a_n|V|c_m\lambda'\rangle][\langle c_{m'}|V|d_q\lambda\rangle][\langle d_{q'}\lambda'|V|b_l\rangle]$$
$$\frac{S_{m,m'}(c^\alpha)}{\omega - E_{c^\alpha} - \hbar\omega_{\lambda'^{\pi'}_{\nu'}}} \frac{S_{q,q'}(d^\beta)}{\omega - E_{d^\beta} - \hbar\omega_{\lambda'^{\pi'}_{\nu'}} - \hbar\omega_{\lambda^\pi_\nu}} A(b_l^\mu)A(a_m) \quad \text{(B.0.4)}$$

eventually $S(\cdot)$ can be substituted following the prescriptions of (A.2.18)-(A.2.20), consequently substituting the $\sum_{\alpha\ \beta}$ with an integral over two running variables to be substituted with E_{c^α} and E_{d^β}.

The vertex correction can be finally used to calculate the perturbation on the Self Energy, which finally reads,

$$\delta\Sigma^{11}_{nn'}(a,\omega) = \sum_{\lambda^\pi_\nu}\sum_{b^\mu} \frac{\delta V(a_n, b^\mu, \lambda^\pi_\nu, \omega)V(a_{n'}, b^\mu, \lambda^\pi_\nu) + V(a_n, b^\mu, \lambda^\pi_\nu)\delta V(a_{n'}, b^\mu, \lambda^\pi_\nu, \omega)}{\omega - \widetilde{E}_{b^\mu} - \hbar\omega_{\lambda^\pi_\nu}} +$$
$$+ \frac{\delta W(a_n, b^\mu, \lambda^\pi_\nu, \omega)W(a_{n'}, b^\mu, \lambda^\pi_\nu) + W(a_n, b^\mu, \lambda^\pi_\nu)\delta W(a_{n'}, b^\mu, \lambda^\pi_\nu, \omega)}{\omega + \widetilde{E}_{b^\mu} + \hbar\omega_{\lambda^\pi_\nu}}, \quad \text{(B.0.5)}$$

where the vertex corrections δV and δW are the sum of all time orderings, and must be applied on both matrix elements regarding nodes n and n'.

APPENDIX C

More detailed results

"...a unified field theory had been found, only the technical details are missing"
- W. Heisenberg
"I can paint like Tiziano...
...Only technical details are missing"
- W. Pauli

C.1 Calculation with SkM* potential

In Ch. 1 we have studied the renormalization of quasiparticle properties of ^{120}Sn making use of the SLy4 effective interaction to compute the mean field as well as the particle vibration matrix elements. In this appendix we present the results of a parallel calculation, performed with a different effective force, namely the SkM* interaction, which is also of the Skyrme type, but is associated with a larger effective mass and a different spatial dependence of the Landau parameters, implying different effects of the coupling to spin and density modes.

In the following we first consider the properties of the dressed quasiparticles (cf. Sect. C.1.1). Then the matrix elements of the particle vibration coupling (cf. Sect. C.1.2) are used to computer the various components of the Nambu-Gorkov equation, such as $\Sigma(a,\omega)$, $G(a,\omega)$, $Z(a,\omega)$ and $\Delta(a,\omega)$ (cf. Sect. C.1.3), and the resulting Strength Functions (Sect. C.1.4) and pairing gaps (Sect. C.1.5). In Fig. C.17 the present results will be compared with those obtained with a first order induced interaction (Sect. C.1.7), neglecting the effects associated with quasiparticle renormalization, similar to the one used in [17] to study the contribution to the pairing gap coming from the spin modes.

C.1.1 Mean Field and QRPA

The first step in the calculation is the solution of the HF equations using the SkM* interaction. The energies of the five single-particle levels lying closest to the Fermi energy are shown in Fig. C.1.

We then perform a BCS calculation with a monopole force. The pairing constant G_0 is adjusted so as to obtain a pairing gap equal to $\Delta = 1$ MeV that corresponds to the result obtained by the bare Argonne v_{14} force in this mean field [18]. Based on these HF+BCS results, collective excitations are calculated in form of phonons of the various multipolarities of natural and not natural parity using Quasi Random Phase Approximation (QRPA). The associated electromagnetic transition probabilities $B(E\lambda)$ and $B(M\lambda)$ are shown in Fig. C.2.

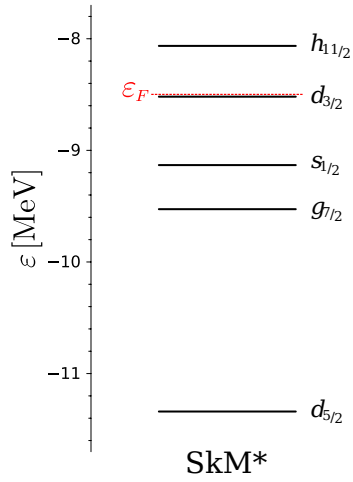

Figure C.1: Energies of single-particle levels in ^{120}Sn obtained in a HF calculation using the SkM* interaction. The output of HF calculation (single particle levels) represent the independent-particle degrees of freedom. The BCS Fermi Energy is Also shown.

C.1.2 Quasiparticle-phonon matrix elements

Matrix elements are then of two main categories, spin indepedent matrix elements f and depedent matrix elements g. As a rule, these couplings have attractive and repulsive effect respectively, determining a positive or negative contribution to the pairing gap when considering the contribution of the induced interaction (cf. Fig. C.3 left panel and [17])

The main contribution to the spin-independent matrix elements comes from phonons with 2^+ multipolarity, expecially from the low-lying collective vibration (cf. Fig. C.4).

C.1.3 Renormalization: self-energies and occupation factors

The main quantities obtained from the solution of (Dyson) Nambu-Gor'kov equation in the present framework (cf. Appendix A, D and Sect. 1.2), are shown in the next figures: the diagonal (Σ^{11} cf. Fig. C.5) and anomalous (Σ^{12} cf. Fig. C.6) self energy, Green's functions ($\Im m\{G^{11}\}$ and $\Im m\{G^{12}\}$, cf. Figs. C.7 and C.8 respectively), and the renormalization factor Z (cf. Fig. C.9).

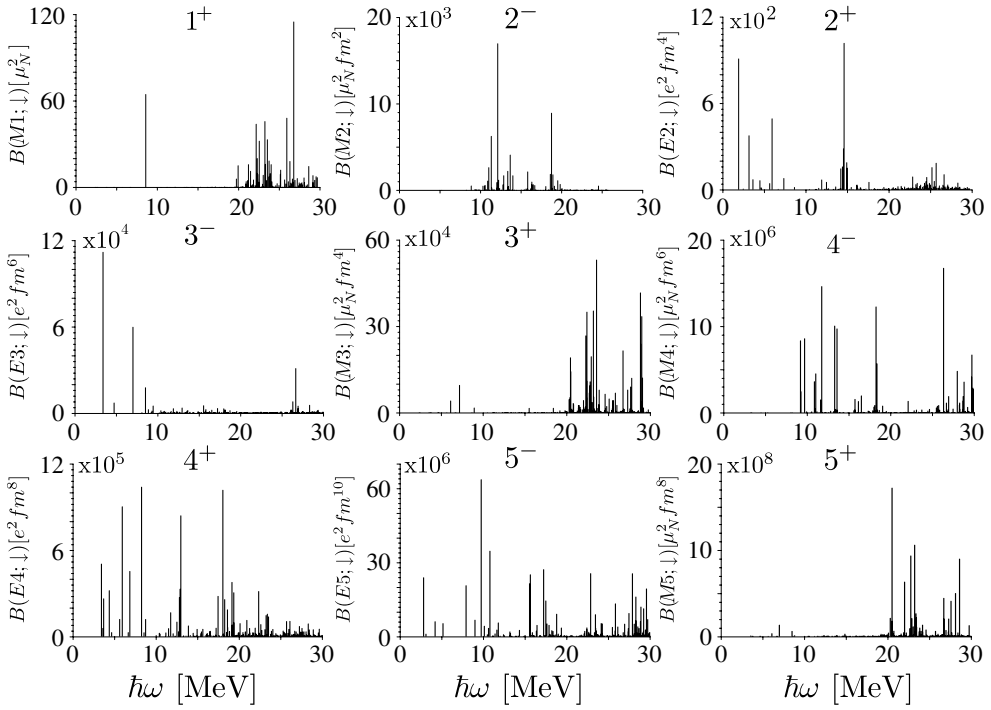

Figure C.2: Phonon spectra for different multipolarities calculated making use of the QRPA based on a Skyrme SkM* interaction. The output of QRPA calculation (phonon spectra and associated transition densities) represent the collective degrees of freedom.

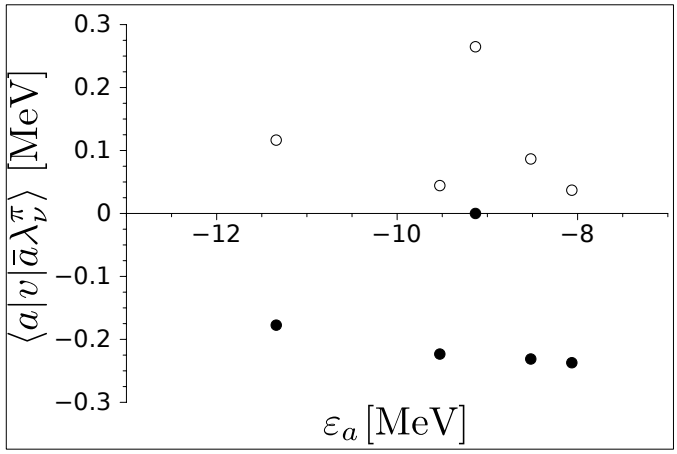

Figure C.3: Sum of diagonal particle vibration coupling matrix elements contributing to induced pairing interaction, $\sum_{\lambda^\pi_\nu} f(a,\bar{a},\lambda^\pi_\nu)$ (black dots) and $\sum_{\lambda^\pi_\nu L} g(a,\bar{a},\lambda^\pi_\nu L)$ (empty circles).

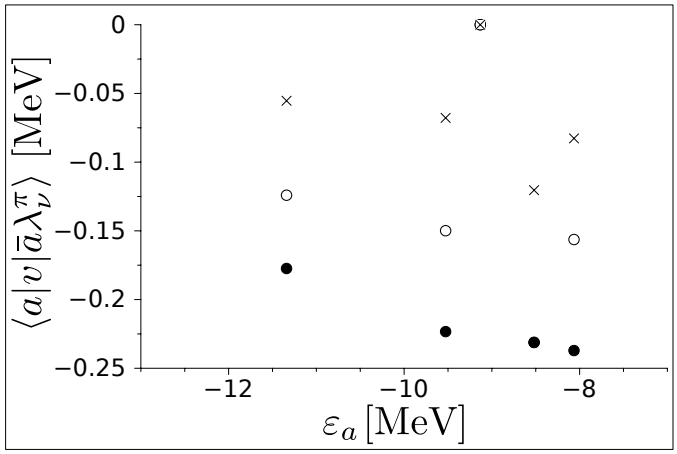

Figure C.4: The sum of the diagonal, spin-independent particle vibration coupling matrix elements $\sum_{\lambda_\nu^\pi} f(a,\bar{a},\lambda_\nu^\pi)$ over all multipolarities (black dots) for the various levels a is compared to the sum of 2^+ phonons (empty circles) and to the contribution of the lowest 2^+ phonon (black crosses). To be noticed the 2^+ phonon is the only one that can be coupled to the $s_{1/2}$ state.

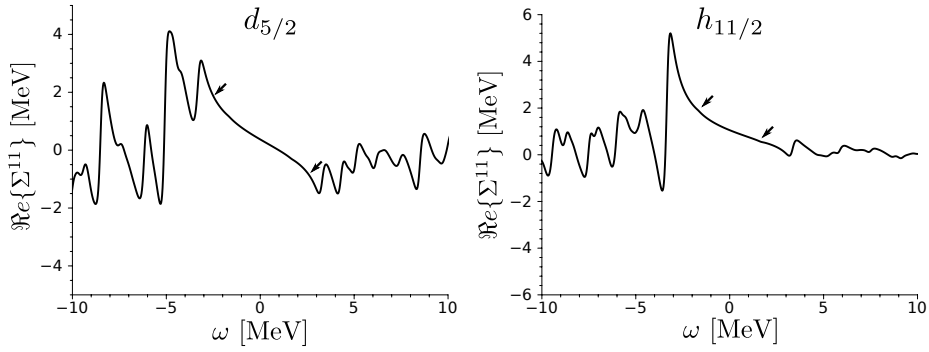

Figure C.5: Real part of the self-energy $\Sigma_{11}(a,\omega)$ for the $d_{5/2}$ (left panel) and $h_{11/2}$ (right panel) levels. The arrow indicates the centroid energy of the strongest quasiparticle peak for the orbital under consideration.

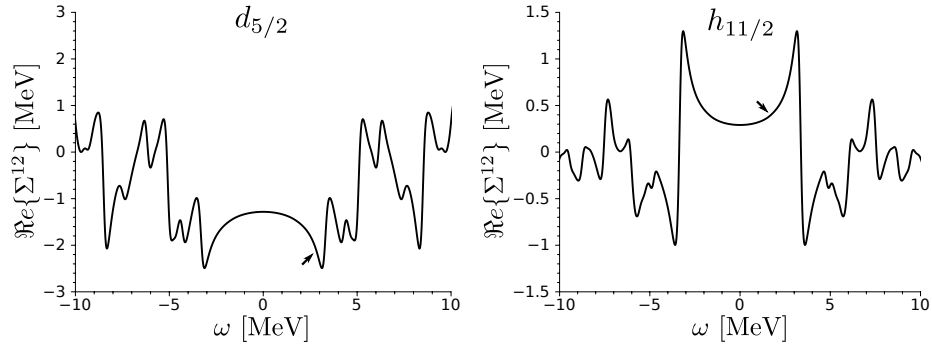

Figure C.6: Real part of the anomalous self-energy $\Sigma_{12}(\omega)$ for the $d_{5/2}$ (left panel) and $h_{11/2}$ (right panel) levels. The arrow indicates the centroid energy of the strongest quasiparticle peak for the orbital under consideration.

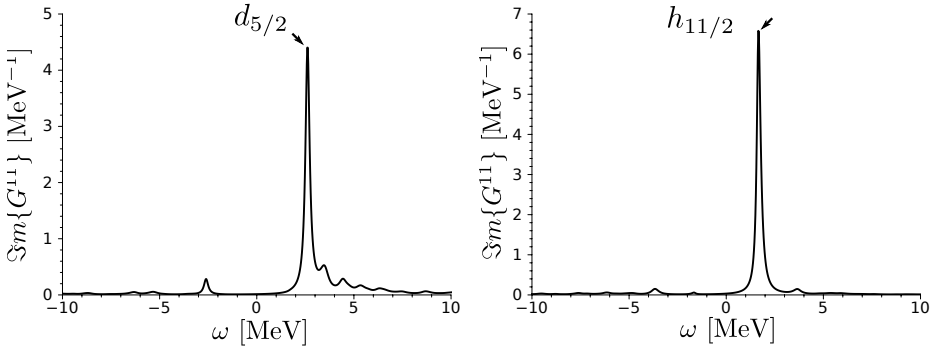

Figure C.7: Imaginary part of the Green's function $G_{11}(\omega)$ for the $d_{5/2}$ (left panel) and $h_{11/2}$ (right panel) levels. The arrow indicates the centroid energy of the strongest quasiparticle peak for the orbital under consideration.

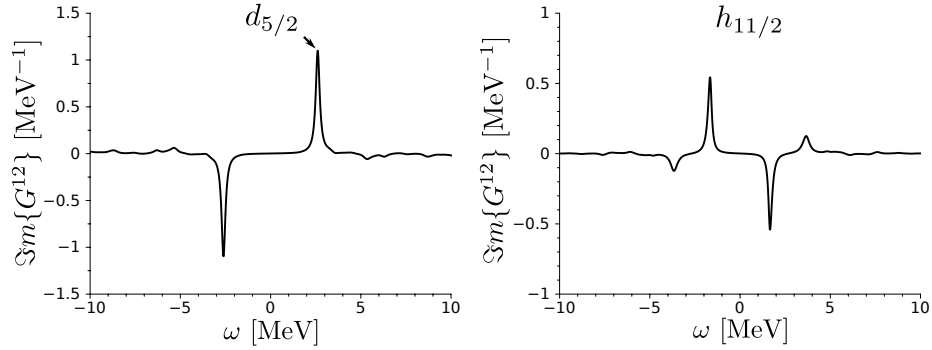

Figure C.8: Imaginary part of the Green's function $G_{12}(\omega)$ for the $d_{5/2}$ (left panel) and $h_{11/2}$ (right panel) levels. The arrow indicates the centroid energy of the strongest quasiparticle peak for the orbital under consideration.

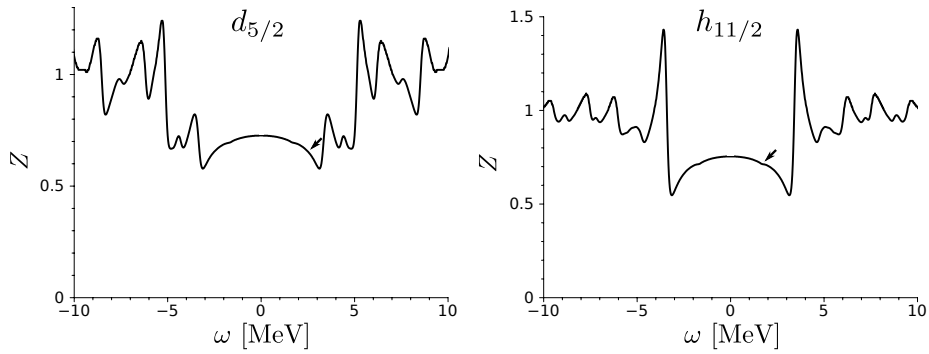

Figure C.9: ω dependent Z coefficient (1.23) for the $d_{5/2}$ (left panel) and $h_{11/2}$ (right panel) levels. The arrow indicates the centroid energy of the strongest quasiparticle peak for the orbital under consideration.

C.1.4 Renormalization:strength functions

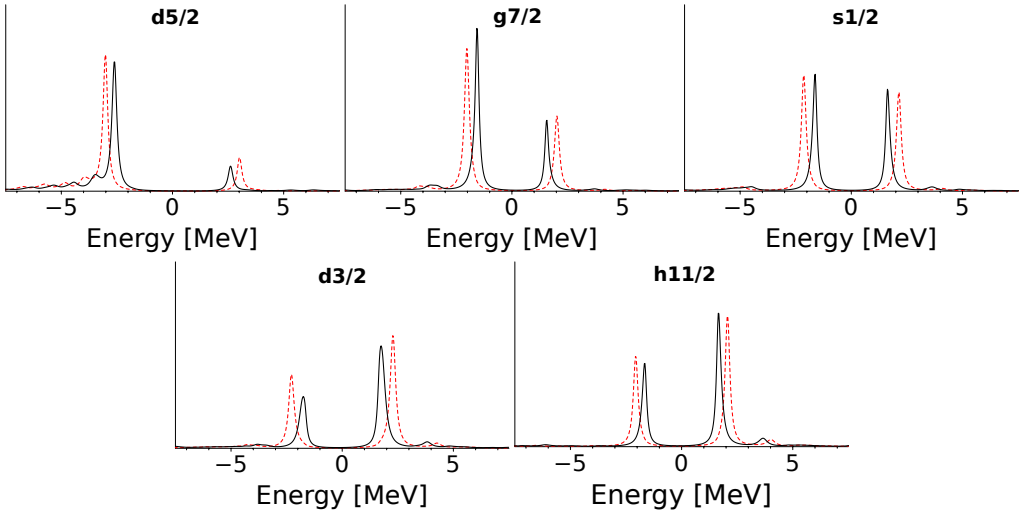

Figure C.10: Strength profile for the valence shell levels, for the density (dashed red line) and spin+density modes (black solid line). Spin modes contribution tend to reduce the pairing gap lowering the (BCS) energies of Green's functions peaks.

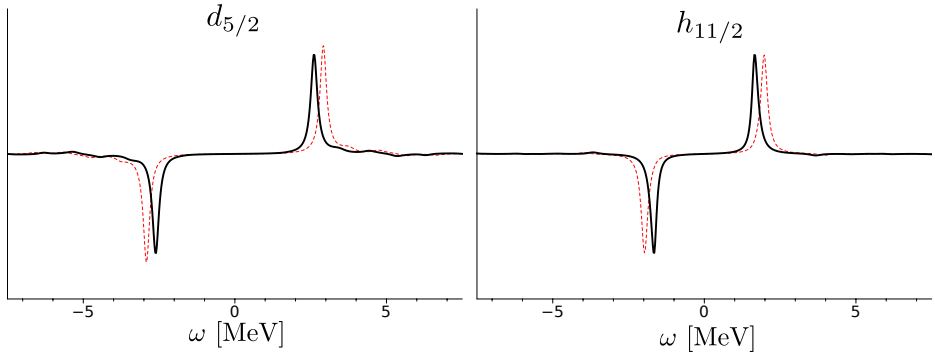

Figure C.11: Strength function $\widetilde{S}(\omega)$ for the $d_{5/2}$ (left panel) and $h_{11/2}$ (right panel) states, for the density (dashed red line) and spin+density modes (solid black line).

C.1.5 Renormalization: pairing gap

The state-dependent pairing gap is shown in Fig. C.12; its average value is about $\tilde{\Delta} = 1.7$ MeV. The calculation starts from the initial value $\Delta^{BCS} = 1$ MeV. This value is reduced by the spectroscopic factor $Z(a, \tilde{E}_a)$, leading to $\tilde{\Delta}^{bare} = Z(a, \tilde{E}_a)\Delta^{BCS} \approx 0.5 - 0.7$ MeV: this contribution account for about 40% of the total gap. The remaining 60% is given by the other contribution, $\tilde{\Delta}^{ind} = Z(a, \tilde{E}_a)\Sigma^{12}(a, \tilde{E}_a) \approx 0.8 - 1.2$, which is associated with the pairing induced interaction.

The effect of the repulsive interaction associated with the coupling with spin modes can be clearly observed in Fig. C.13. Including only the spin-independent contribution, in fact, the average value of the total gap increases from 1.7 MeV to 2.1 MeV.

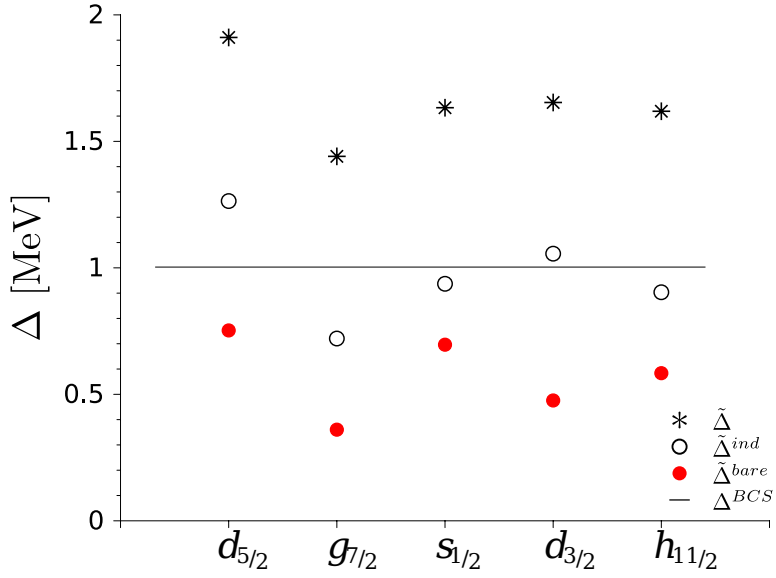

Figure C.12: State-dependent pairing gap (stars) calculated solving the Nambu-Gor'kov equation equation, including both spin-dependent and -independent matrix elements for every multipolarity. The initial pairing gap obtained in the BCS calculation, $\Delta^{BCS} = 1$ MeV (black line), is renormalized by the Z-factor, leading to $\tilde{\Delta}^{bare}$ (full dots); the contribution of the induced pairing gap $\tilde{\Delta}^{ind} = Z\Sigma^{12}$ (empty circles) accounts for about 60% of the total gap $\tilde{\Delta} = \tilde{\Delta}^{bare} + \Delta^{ind}$ (stars) (cf. Eq. (1.19)). To be noticed that in the case of the $g_{7/2}$ state, $\Delta^{ind} \simeq \Delta^{bare}$.

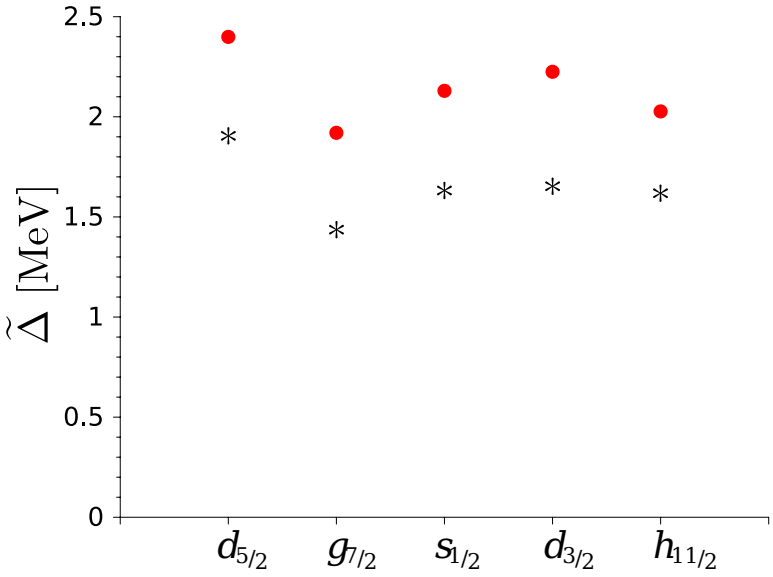

Figure C.13: Pairing gap Δ calculated making use of the the Dyson equation including only the spin-independent vertices (full dots) or including both spin-independent and spin-dependent contributions (stars).

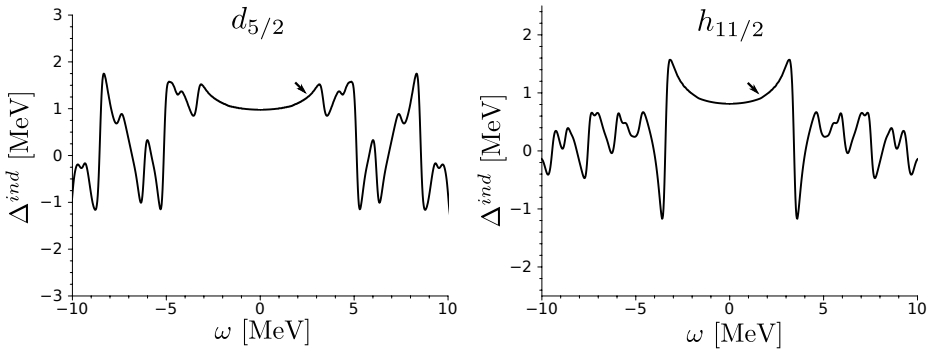

Figure C.14: ω-dependent pairing gap $\Delta(\omega) = Z(\omega)\widetilde{\Sigma}_{12}(\omega)$ (cf. Sect. 1.2.1) for the $d_{5/2}$ (left panel) and $h_{11/2}$ (right panel) states.

C.1.6 Contribution of low-energy collective modes

The most important contribution to the induced interaction is provided by the coupling to the lowest collective states of natural parity. In Fig. C.15 we compare the values of $\tilde{\Delta}^{ind}$ obtained including the coupling to all phonons of natural parity with those obtained including only the strongest phonon of each multipolarity. It can be seen that the latter account for 50% of the gap. This ratio can be compared to that of 75% obtained in [16], making use of a a separable interaction and of a collective form factor [39]. Also shown in the right panel of Fig. C.15 is the effect on the $d_{5/2}$ strength function. In Fig. C.16 we also include the coupling to the strongest spin mode of each multipolarity, selecting the phonons ν carrying the largest value of $\sum_{i,j} g^2(i,j,\lambda^{\pi}_{\nu})/\hbar\omega$. The effect of the latter is almost negligible (less than 50 keV on the gap).

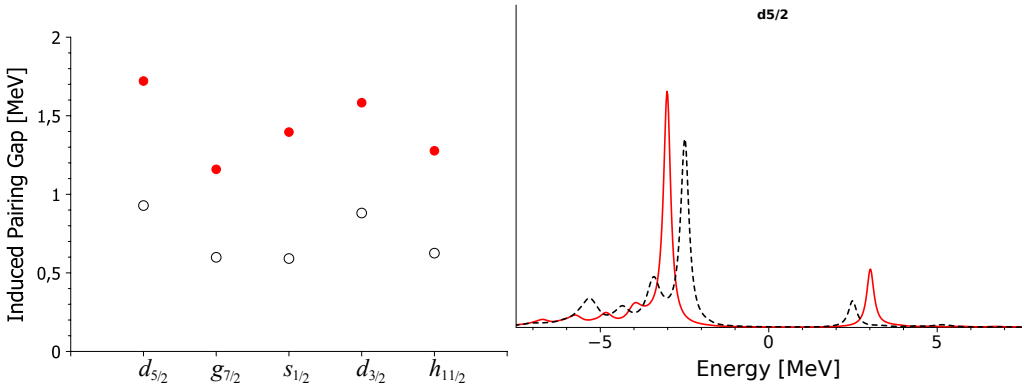

Figure C.15: Comparison of the pairing gap (left panel) and of the $d_{5/2}$ strength function (right panel) calculated including the coupling with density modes, including only the contributions from the low-lying collective vibrations (empty black circles, dotted black line) or with the full phonon spectrum up to 30 MeV (full red dots, continuous red line).

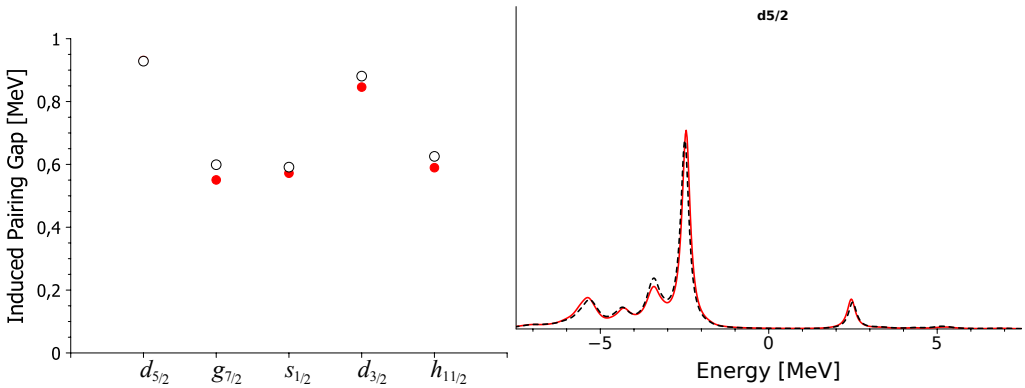

Figure C.16: Comparison of the induced pairing gap (left panel) and of the $d_{5/2}$ strength function (right panel) calculated with a single phonon for every multipolarity (low-lying, for the natural-parity multipolarities) taking into account both spin-dependent and -independent (full red dots, continuous red line) or only spin-independent (empty black circles, dotted black line) matrix elements. Contributions coming from the spin-dependent matrix elements are negligible in this case, since spin modes are scarcely collective.

C.1.7 First order induced interaction

We can compare the previous results with those obtained making use of a simple estimate of the interaction induced by phonon exchange [17], obtained through Bloch-Horowitz perturbation theory and given by

$$v_{ind}(a,b) = \sum_{\lambda_n^\pi} \frac{4}{2j_a+1} \frac{[(f+g)(f-g)](a,b,\lambda_n^\pi)}{E_0 - E_a - E_b - \hbar\omega_{\lambda_n^\pi}}, \tag{C.1.1}$$

where f and g denote the particle-vibration coupling matrix elements described in Sect. C.1.2. Using this induced interaction one can then solve the BCS gap equation

$$\Delta_a = \sum_b \frac{2j_a+1}{2} \frac{\Delta_a}{2\sqrt{(\varepsilon_b - \varepsilon_F)^2 + \Delta_b^2}} v_{ind}(a,b), \tag{C.1.2}$$

where E_0 a parameter of the order of $2\overline{\Delta}$ (in the following calculations we have used $E_0 = 3$ MeV). We remark that the single-particle energies appearing in the denominators are the 'bare' values obtained in the HF calculations, without renormalization.

The resulting pairing gaps are shown in Fig. C.17 and in Fig. C.18), respectively including the coupling to all modes or only to density modes. The values of the total gaps $\tilde{\Delta} = \tilde{\Delta}^{ind} + \tilde{\Delta}^{bare}$ are remarkably close to those obtained in the full calculation. However, the contribution of $\tilde{\Delta}^{ind}$ is smaller, while that of $\tilde{\Delta}^{bare}$ is larger, being equal to $\tilde{\Delta}^{BCS} = 1$ MeV since $Z = 1$.

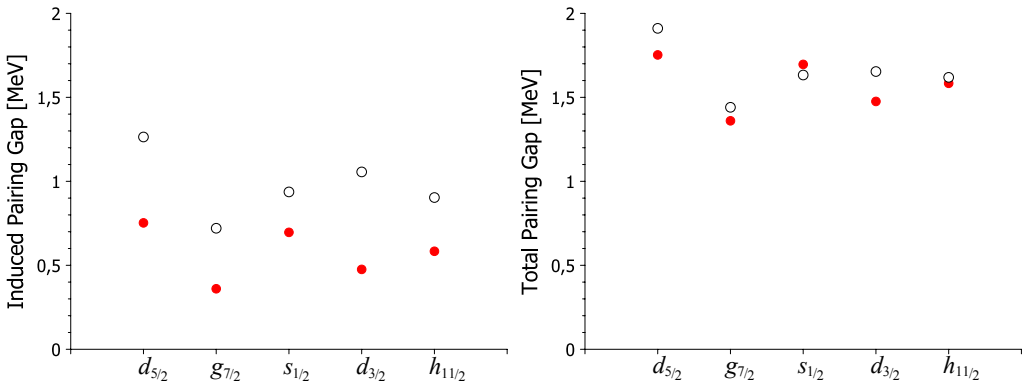

Figure C.17: Total pairing gap $\tilde{\Delta}$ (right panel) and induced pairing gap $\tilde{\Delta}^{ind}$ (left panel) calculated by solving the BCS Gap equation (C.1.2) using the first order induced interaction (C.1.1) with the Hartree-Fock single particle spectrum (full dots), compared with the corresponding gaps calculated making use of the Dyson equation (empty circles). Both spin-dependent and -independent couplings are included.

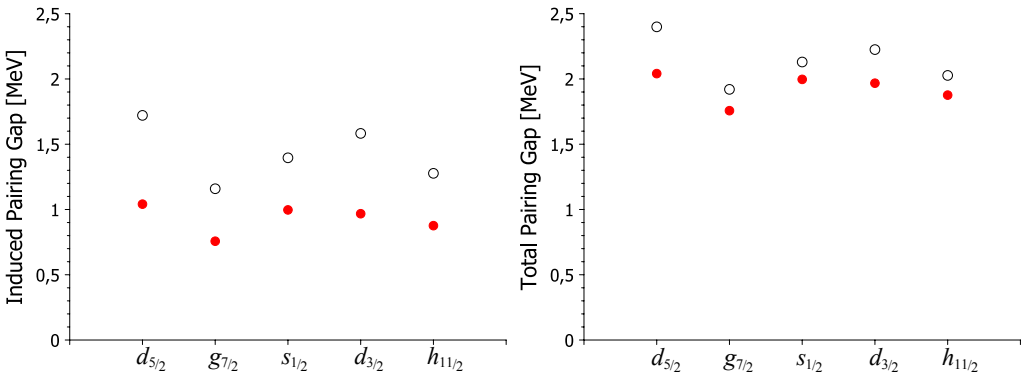

Figure C.18: The same as Fig. C.17, including only spn-independent couplings.

C.2 Numerical Approximations

C.2.1 Convergence in the number of iterations

In Fig. C.19 the results obtained for a different number of iterations of the Dyson equation are compared, so that one can assess the contributions at different orders of perturbation in the rainbow series. In practice, 4 or 5 iterations of the Dyson equation in the Green's function continuous representation, grant a satisfactory convergence of the results in the valence space. The third iteration is already quite close to the converged result, both regarding the position of the peak of the $d_{5/2}$ quasiparticle (within 100 keV), and the profile of the induced pairing gap profile (within 10 keV near the Fermi energy).

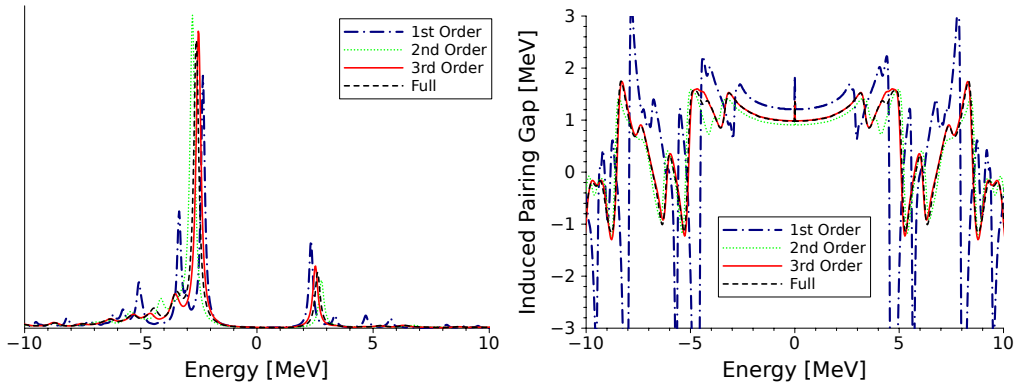

Figure C.19: Strength profile (left panel) and induced pairing gap contribution $Z(E, 1d_{5/2})\Sigma_{12}^{pho}(E, 1d_{5/2})$ (right panel) for the $1d_{5/2}$ state, for different number of iterations of the Dyson equation: one (dash-dotted blue line), two (dotted green line), three (red line) and ten (dashed black line).

C.2.2 Convergence in the imaginary parameter

The imaginary parameter η is a component of the Green's function, coming from the Fourier transform of the time ordering function $\theta(t' - t)$, and is essential to smooth out the poles corresponding to the eigenvalues of the Dyson equation (and of the perturbed Hamiltonian). While analytically this constant should go to zero, numerically it must be kept to a value that makes the calculations feasible. Using a smaller value of η allows more precise calculations (with a smaller discretization of the continuum mesh), but requires a longer computation time. So one can study the dependence of the physical quantities from the parameter η in order to verify the correctness of the calculation and tune the program. From Fig. C.20 and C.21 one concludes that a convenient value for the parameter is $\eta = 0.1$ MeV, that leads to pairing gaps differing by less than 5% compared to the values obtained with $\eta = 0.02$ MeV. The value $\eta = 0.1$ MeV is used in the calculations reported in the thesis, if a different value is not specified.

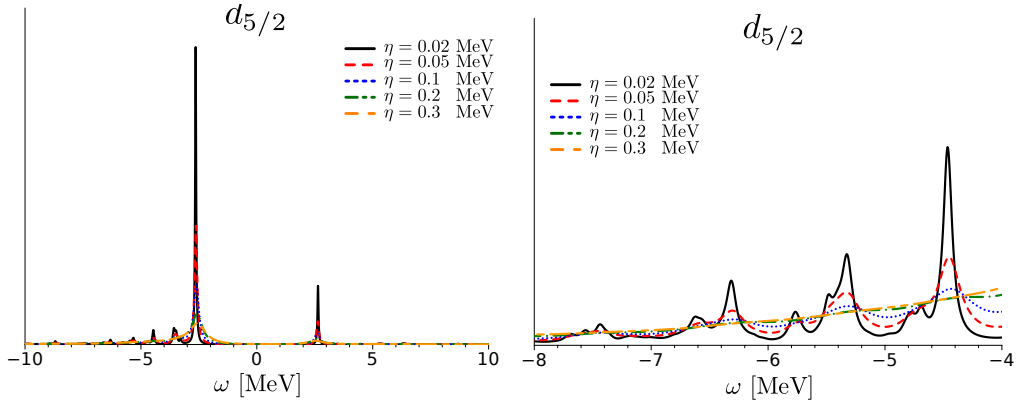

Figure C.20: Strength profile of the $d_{5/2}$ state for different values of the parameter η in the range -10 MeV $\leq \omega \leq$ 10 MeV (left panel). The corresponding values of η for different curves are displayed in the legend. In the right panel be seen that for values of $\eta \gtrsim 0.2$ MeV the information of the structure in the range -8 MeV $\leq \omega \leq -4$ MeV is overwhelmed by the width of the main quasiparticle peak at 2.6 MeV, thus neglecting some contribution from that region for high values of η, that imply a reduction of the value of the pairing gap for increasing value of η (cf. Fig. C.21).

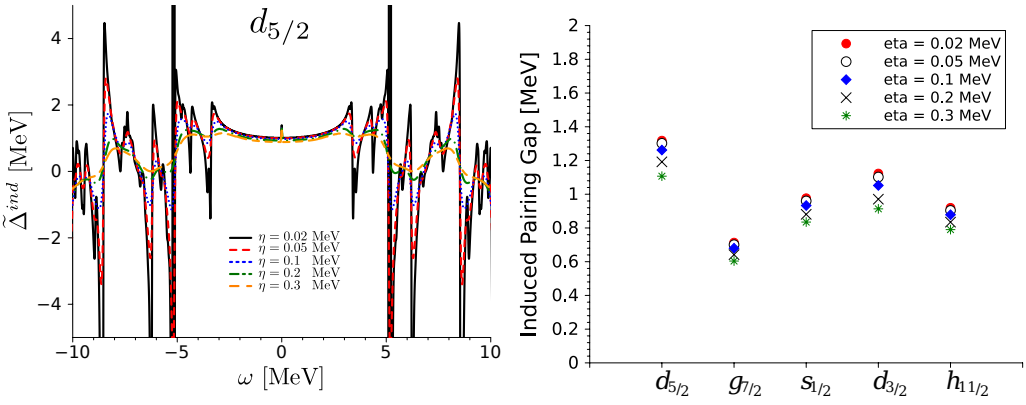

Figure C.21: Energy dependence of the pairing gap associated with the $d_{5/2}$ orbital, ($\Delta(d_{5/2},\omega) = Z(d_{5/2},\omega)\widetilde{\Sigma}_{12}(d_{5/2},\omega)$) for different values of the parameter η (left panel) and values of $\Delta(a,\omega_{a_1})$ calculated at the energy of the lowest quasiparticle peak for the various valence orbitals (right panel). The corresponding values of parameter η for different curves are displayed in the legend.

C.2.3 Dependence on the phonon cutoff

The required computational effort depends linearly on the number of phonons included in the QRPA calculation. In turn, the number of phonons in the QRPA spectrum increases roughly quadratically function of the phonon cutoff for a given multipolarity. For example, in a SkM* calculation in a 20 fm box the 2^+ spectrum up to 15 MeV is described by 41 phonons, while 281 are needed for reaching 30 MeV and 768 phonons must be considered for a description of the spectrum up to 60 MeV. The calculations below are done with the imaginary parameter $\eta = 0.2$ MeV. Due to the competitive effects of density and spin modes it is important for the present study to consider results obtained with and without the contribution of spin-dependent matrix elements. The dependence of the pairing gaps and of the $d_{5/2}$ strength function on the phonon cutoff is shown in Figs. C.22 and C.23. Both quantities display a weak dependence on the cutoff. A more extended study on the cutoff dependence is ongoing.

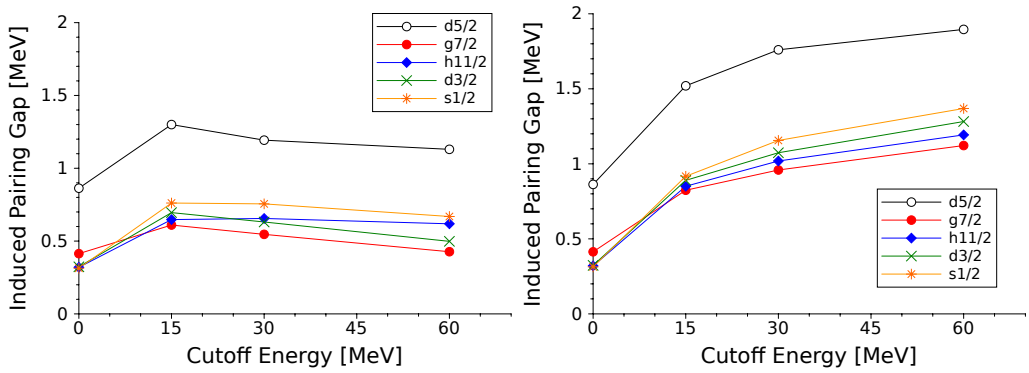

Figure C.22: Value of the pairing gap $\Delta^{ind}(a, \omega_{a_1})$ for the 5 different levels in the valence shell as a function of the phonon energy cutoff $\hbar\omega_{cutoff}$ considering all the matrix elements (left panel) or including only spin-independent matrix elements (right panel). Both mean field and phonons are calculated with the SkM* effective interaction.

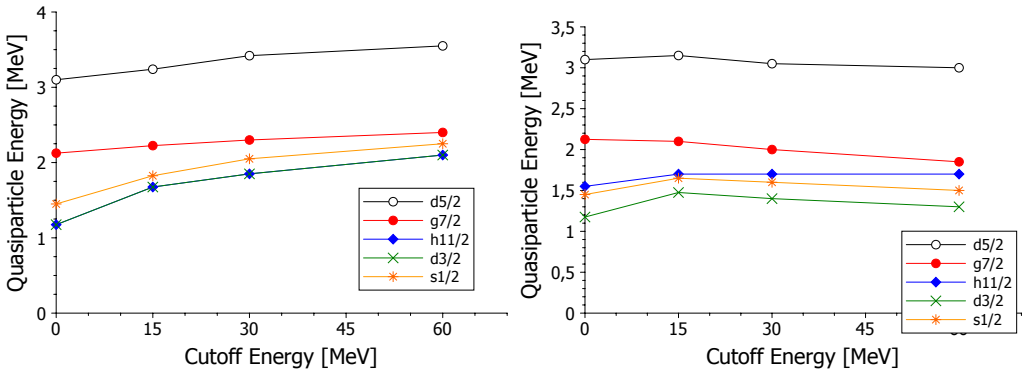

Figure C.23: Value of the Energy ω_{a_1} of the maximum of the lowest energy peak in the strength function $S(a,\omega)$ for the five different levels in the valence shell as a function of the phonon energy cutoff $\hbar\omega_{cutoff}$, considering all the matrix elements (left panel) or including only spin-independent matrix elements (right panel). Both mean field and phonons are calculated with the SkM* effective interaction.

C.2.4 Comparison between valence space and full space

While the calculations in [17] used a single-particle space including all the orbitals from $0s_{1/2}$ to a discretized continuum up to 30 MeV in a 15 fm box, the calculations in the present thesis are performed in a much smaller valence space composed by the five orbitals nearest to the Fermi energy for the sake of computational effort. However, this small space should keep almost all the relevant information about the induced interaction, as can be seen in Fig. C.24. In this figure, the total and induced pairing gaps obtained calculating the induced interaction (C.1.1) and solving the BCS equation (C.1.2) including only the same five valence levels or all the single-particle levels up to 30 MeV are compared. The results are essentially the same, in keeping with the fact that the induced interaction acts preferably in a relatively small energy range around the Fermi energy.

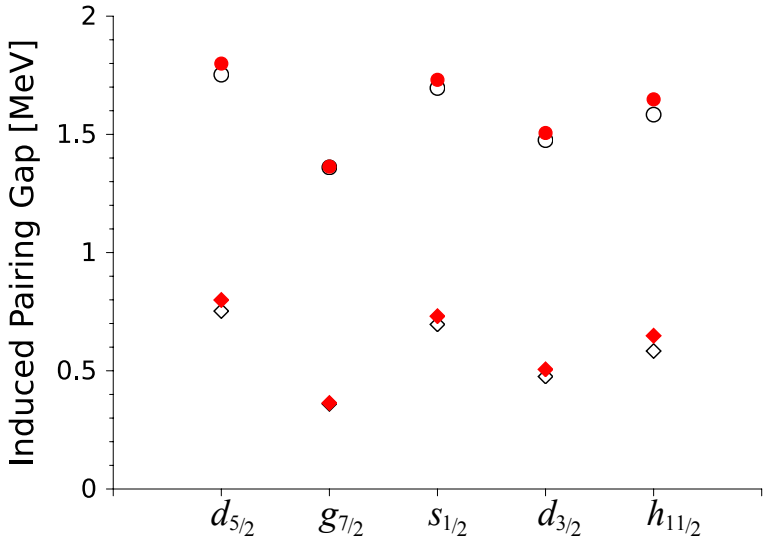

Figure C.24: Pairing gaps $\tilde{\Delta}$ (circles) and $\tilde{\Delta}^{ind}$ (diamonds) associated with the valence orbitals. Comparison of the results of the calculation performed including only the single particles in the valence shell (empty symbols) and up to 30 MeV (full symbols).

APPENDIX D

Green's Functions formalism for renormalization

D.1 Green function formalism

In this Appendix I recall some parts of Green's function formalism, which constitute a useful background material for this thesis. First I summarize the definitions and the basic properties of Green's function for a uniform system of fermions. I then provide the rules to evaluate Feynman's diagrams describing the renormalization processes of quasiparticles due to their coupling with phonons, and outline a derivation of Dyson's equation, giving the expressions for the self-energy. Finally, I introduce the quasiparticle approximation.

Green's functions are a useful tool for a systematic perturbative treatment of many-psrticle systems (in principle up to infinite order). In order to conveniently build over a (vacuum) ground state, are derived starting from the formalism of second-quantization (cf. [40, 15] and refs. therein, and also App. A of [41]) and so the concept of creation (and annihilation) operators, that act over a quantum state creating (and annihilating) a sub-state describing a particle in $\mathcal{H}_{\pm}(N)$ (or $\mathcal{F}_{\pm}$) Hilbert (or Fock) (anti-)symmetrized spaces, and thus is well-suited for many-particle systems. In the case of a system composed by N fermions ($\mathcal{H}_{-}(N)$), obeying the Pauli principle (there cannot be two fermions in the same quantum state),

$$\begin{aligned}
&\widehat{c}_i|0\rangle_F = |i^{-1}\rangle && \text{if } i \in |0\rangle_F,\\
&\widehat{c}_i^{\dagger}|0\rangle_F = 0 && \text{if } i \in |0\rangle_F,\\
&\widehat{c}_k|0\rangle_F = 0 && \text{if } k \notin |0\rangle_F,\\
&\widehat{c}_k^{\dagger}|0\rangle_F = |k\rangle && \text{if } k \notin |0\rangle_F,
\end{aligned} \tag{D.1.1}$$

where

$$\langle r|a\rangle = \phi_a(r) \qquad \left(\langle r|i^{-1}\rangle = \phi_i(r)\right), \tag{D.1.2}$$

is a single particle (hole) wavefunction. So, in other terms, the operators are defined in order to create a non-existing particle (or annihilate an existing particle thus creating an hole) over the Fermi vacuum that defines the ground state.

Field operators $\widehat{\psi}_m(\mathbf{x}, t)$ are a set of creation (and annihilation) operators weighted over the possible single-particle wavefunctions of the described system making a change of basis that diagonalizes the Hamiltonian of the system, diagonal in the field operator basis,

$$\widehat{\psi}_m(\mathbf{x}, t) = \sum_a \psi_{m,a}(\mathbf{x}, t)\widehat{c}_a. \tag{D.1.3}$$

In other words in a system described in the $\mathcal{H}_{\pm}(N)$ (or $\mathcal{F}_{\pm}$) space, with an Hamiltionan H and ground state $|\psi_0\rangle$, the field operator (that is eventually a vector field of m

components, e.g. the spin $\pm$ of fermions) create (and annihilate) particles. That is the description of the Hamiltonian itself, in the second quantization representation.

In such (general) system, the Green's function is defined as

$$iG_{m,m'}(\mathbf{x}t,\mathbf{x}'t') = \langle\psi_0|\mathcal{T}[\widehat{\psi}_{Hm}(\mathbf{x},t)\widehat{\psi}^{\dagger}_{Hm'}(\mathbf{x}',t')]|\psi_0\rangle, \tag{D.1.4}$$

where the subscript H stands for Heisenberg representation and $\mathcal{T}[...]$ is the time ordering product that is essential in order to treat the Green's functions in the perturbation theory and so within the framework of Feynman's propagators.

The Green's function description comes useful in many ways. Considering the properties of the second-quantization representation the expectation value of any single-particle operator is bracketed over a creation and an annihilation field operators and so the Green's function becomes the natural way to consider the expectation value of any single-particle operator in the ground state of the system.

The one particle Green's function has all the information of the ground state of a single-particle Hamiltonian; being the expectation value of the field in the ground state for a given $\mathbf{x}t, \mathbf{x}'t'$ it makes it possible to calculate the expectation value of every single-particle operator that is, in II^{nd} quantization, a linear combination of one-creator and one-annihilator operators. Green's functions are like field-testing on a given spacetime interval during which they perturb the "vacuum" of the ground state.

Expliciting the time ordering it becomes

$$\begin{aligned} iG_{m,m'}(\mathbf{x}t,\mathbf{x}'t') = &\langle\psi_0|\widehat{\psi}_{Hm}(\mathbf{x},t)\widehat{\psi}^{\dagger}_{Hm'}(\mathbf{x}',t')|\psi_0\rangle\Theta(t-t') \\ &\pm\langle\psi_0|\widehat{\psi}^{\dagger}_{Hm'}(\mathbf{x}',t')\widehat{\psi}_{Hm}(\mathbf{x},t)|\psi_0\rangle\Theta(t'-t), \end{aligned} \tag{D.1.5}$$

where the $\pm$ sign is consequence of the Hilbert (Fock) space chosen to be symmetrical or anti-symmetrical, in order to describe bosons or fermions. Time dependence can be written explicitly in the Heisenberg representation

$$\widehat{\psi}_{Hm}(\mathbf{x},t)\widehat{\psi}^{\dagger}_{Hm'}(\mathbf{x}',t') = e^{\frac{i}{\hbar}Ht}\widehat{\psi}_{m}(\mathbf{x})e^{-\frac{i}{\hbar}H(t-t')}\widehat{\psi}^{\dagger}_{m'}(\mathbf{x}')e^{-\frac{i}{\hbar}Ht'}, \tag{D.1.6}$$

and so remembering that $|\psi_0\rangle$ is an eigenstate of the Hamiltonian it follows that $e^{-\frac{i}{\hbar}Ht'}|\psi_0\rangle = e^{-\frac{i}{\hbar}\omega_0 t'}|\psi_0\rangle$ with $\hbar\omega_0$ eigenvalue energy of the ground state, and can be carried out of the the bracket since is a number.

$$\begin{aligned} iG_{m,m'}(\mathbf{x}t,\mathbf{x}'t') = &e^{i\omega_0(t-t')}\langle\psi_0|\widehat{\psi}_{m}(\mathbf{x})e^{-\frac{i}{\hbar}H(t-t')}\widehat{\psi}^{\dagger}_{m'}(\mathbf{x}')|\psi_0\rangle\Theta(t-t')\pm \\ &e^{i\omega_0(t'-t)}\langle\psi_0|\widehat{\psi}^{\dagger}_{m'}(\mathbf{x}')e^{-\frac{i}{\hbar}H(t'-t)}\widehat{\psi}_{m}(\mathbf{x})|\psi_0\rangle\Theta(t'-t), \end{aligned} \tag{D.1.7}$$

introducing a resolution of identity summing over all the possible excited states, $\sum_n |\psi_n\rangle\langle\psi_n|$,

$$\begin{aligned} iG_{m,m'}(\mathbf{x}t,\mathbf{x}'t') = &\sum_n e^{i\omega_0(t-t')}\langle\psi_0|\widehat{\psi}_{m}(\mathbf{x})e^{-\frac{i}{\hbar}H(t-t')}|\psi_n\rangle\langle\psi_n|\widehat{\psi}^{\dagger}_{m'}(\mathbf{x}')|\psi_0\rangle\Theta(t-t')\pm \\ &\sum_n e^{i\omega_0(t'-t)}\langle\psi_0|\widehat{\psi}^{\dagger}_{m'}(\mathbf{x}')e^{-\frac{i}{\hbar}H(t'-t)}|\psi_n\rangle\langle\psi_n|\widehat{\psi}_{m}(\mathbf{x})|\psi_0\rangle\Theta(t'-t) = \\ = &\sum_n e^{i\omega_0(t-t')}e^{-i\omega_n(t-t')}\langle\psi_0|\widehat{\psi}_{m}(\mathbf{x})|\psi_n\rangle\langle\psi_n|\widehat{\psi}^{\dagger}_{m'}(\mathbf{x}')|\psi_0\rangle\Theta(t-t')\pm \\ &\sum_n e^{i\omega_0(t'-t)}e^{-i\omega_n(t'-t)}\langle\psi_0|\widehat{\psi}^{\dagger}_{m'}(\mathbf{x}')|\psi_n\rangle\langle\psi_n|\widehat{\psi}_{m}(\mathbf{x})|\psi_0\rangle\Theta(t'-t), \end{aligned} \tag{D.1.8}$$

which yields,

$$iG_{m,m'}(\mathbf{x}t,\mathbf{x}'t') = \sum_n e^{i(\omega_0-\omega_n)(t-t')}\langle\psi_0|\widehat{\psi}_m(\mathbf{x})|\psi_n\rangle\langle\psi_n|\widehat{\psi}^\dagger_{m'}(\mathbf{x}')|\psi_0\rangle\Theta(t-t')\pm \sum_n e^{i(\omega_0-\omega_n)(t'-t)}\langle\psi_0|\widehat{\psi}^\dagger_{m'}(\mathbf{x}')|\psi_n\rangle\langle\psi_n|\widehat{\psi}_m(\mathbf{x})|\psi_0\rangle\Theta(t'-t), \quad \text{(D.1.9)}$$

that contains explicitly the $t-t'$ exponential. The same considerations can be made for the dependence on $\mathbf{x}$ and its conjugate variable $\mathbf{p}$,

$$\widehat{\psi}_m(\mathbf{x}) = e^{-\frac{i}{\hbar}\mathbf{p}\cdot\mathbf{x}}\widehat{\psi}_m(0)e^{\frac{i}{\hbar}\mathbf{p}\cdot\mathbf{x}}, \quad \text{(D.1.10)}$$

and so Green's function can be written as

$$iG_{m,m'}(\mathbf{x}t,\mathbf{x}'t') = \sum_n e^{i(\omega_0-\omega_n)(t-t')}e^{\frac{i}{\hbar}\mathbf{p_n}\cdot(\mathbf{x}-\mathbf{x}')}\langle\psi_0|\widehat{\psi}_m|\psi_n\rangle\langle\psi_n|\widehat{\psi}^\dagger_{m'}|\psi_0\rangle\Theta(t-t')\pm \sum_n e^{i(\omega_0-\omega_n)(t'-t)}e^{\frac{i}{\hbar}\mathbf{p_n}\cdot(\mathbf{x}'-\mathbf{x})}\langle\psi_0|\widehat{\psi}^\dagger_{m'}|\psi_n\rangle\langle\psi_n|\widehat{\psi}_m|\psi_0\rangle\Theta(t'-t), \quad \text{(D.1.11)}$$

with the explicit dependence from exponentials in $t-t'$ and $\mathbf{x}-\mathbf{x}'$. Consequently, the corresponding Fourier transform is

$$G_{m,m'}(\mathbf{k},\omega) = V\sum_n \frac{\langle\psi_0|\widehat{\psi}_m|n,\mathbf{k}\rangle\langle n,\mathbf{k}|\widehat{\psi}^\dagger_{m'}|\psi_0\rangle}{\omega-(\omega_n-\omega_0)+i\eta}\pm \frac{\langle\psi_0|\widehat{\psi}^\dagger_{m'}|n,-\mathbf{k}\rangle\langle n,-\mathbf{k}|\widehat{\psi}_m|\psi_0\rangle}{\omega+(\omega_n-\omega_0)-i\eta}, \quad \text{(D.1.12)}$$

obtained by introducing the Fourier transform of $\Theta(t'-t)$. In the denominator ω_0 represents the energy frequency of the ground state with N particles, while ω_n represent the energy frequency of the intermediate state $|\psi_n\rangle$. Since $\langle\psi_0|\widehat{\psi}_m|\psi_n\rangle$ must be non-zero for the first term, $|\psi_n\rangle$ is the system with $N+1$ particles due to the destructor operator between the ground state and the intermediate state. The same happens for the second term, where $|\psi_n\rangle$ must represent the system with $N-1$ particles in order to have the matrix element $\langle\psi_0|\widehat{\psi}^\dagger_{m'}|n\mathbf{k}\rangle$ non-zero. Keeping into account this distinction the denominator can be rewritten considering $\omega_n(N+1)-\omega_0(N) = \omega_n(N+1)-\omega_0(N+1)+\omega_0(N+1)-\omega_0(N)$, that becomes $\epsilon_n+\epsilon_F$ being $\omega_n(N+1)-\omega_0(N+1)$ the excitation energy of the $N+1$ particle system, and $\omega_0(N+1)-\omega_0(N)$ the minimum energy required to add a particle to the N particle system, known as Fermi energy (ϵ_F) or chemical potential (μ). Doing this substitutions also for the denominator of the second term of the representation of $G_{m,m'}(\mathbf{k},\omega)$ one obtains the so-called **Lehmann representation** of Green's functions,

$$G_{m,m'}(\mathbf{k},\omega) = V\sum_n \frac{\langle\psi_0|\widehat{\psi}_m|n,\mathbf{k}\rangle\langle n,\mathbf{k}|\widehat{\psi}^\dagger_{m'}|\psi_0\rangle}{\omega-\epsilon_F-\epsilon_{n,\mathbf{k}}+i\eta} + \frac{\langle\psi_0|\widehat{\psi}^\dagger_{m'}|n,-\mathbf{k}\rangle\langle n,-\mathbf{k}|\widehat{\psi}_m|\psi_0\rangle}{\omega-\epsilon_F+\epsilon_{n,-\mathbf{k}}-i\eta}, \quad \text{(D.1.13)}$$

where the intermediate states have the same $|\mathbf{k}|$ due to properties of Fourier transform.

If we consider the limit of a system with a very high level density we get that,

$$\sum_n \langle\psi_0|\widehat{\psi}_m|n,\mathbf{k}\rangle\langle n,\mathbf{k}|\widehat{\psi}^\dagger_{m'}|\psi_0\rangle \to \int \mathrm{d}n \langle\psi_0|\widehat{\psi}_m|n,\mathbf{k}\rangle\langle n,\mathbf{k}|\widehat{\psi}^\dagger_{m'}|\psi_0\rangle$$
$$= \int \mathrm{d}\epsilon \langle\psi_0|\widehat{\psi}_m|n,\mathbf{k}\rangle\langle n,\mathbf{k}|\widehat{\psi}^\dagger_{m'}|\psi_0\rangle \frac{\mathrm{d}n}{\mathrm{d}\epsilon} \tag{D.1.14}$$

with $\frac{\mathrm{d}n}{\mathrm{d}\epsilon}$ the level density, and then we can define

$$\langle\psi_0|\widehat{\psi}_m|n,\mathbf{k}\rangle\langle n,\mathbf{k}|\widehat{\psi}^\dagger_{m'}|\psi_0\rangle \frac{\mathrm{d}n}{\mathrm{d}\epsilon} \equiv A(\mathbf{k},\omega), \tag{D.1.15}$$

giving the definition of strength function

$$\sum_n \langle\psi_0|\widehat{\psi}_m|n,\mathbf{k}\rangle\langle n,\mathbf{k}|\widehat{\psi}^\dagger_{m'}|\psi_0\rangle \to \int \mathrm{d}\epsilon A_{m,m'}(\mathbf{k},\epsilon), \tag{D.1.16}$$

where the diagonal part $A_{m,m}(\mathbf{k},\epsilon)$, since $\langle\psi_0|\widehat{\psi}_m|n,\mathbf{k}\rangle\langle n,\mathbf{k}|\widehat{\psi}^\dagger_m|\psi_0\rangle = |\langle\psi_0|\widehat{\psi}_m|n,\mathbf{k}\rangle|^2$, is real and definite positive. The same happens for the other term in (D.1.13), where we define

$$\langle\psi_0|\widehat{\psi}^\dagger_{m'}|n,-\mathbf{k}\rangle\langle n,-\mathbf{k}|\widehat{\psi}_m|\psi_0\rangle \frac{\mathrm{d}n}{\mathrm{d}\epsilon} \equiv B(\mathbf{k},\epsilon). \tag{D.1.17}$$

These definitions give rise to the integral form of the Lehmann representation

$$G_{m,m'}(\mathbf{k},\omega) = \int_0^{+\infty} \mathrm{d}\omega' \frac{A_{m,m'}(\mathbf{k},\omega')}{\omega - \epsilon_F - \omega' + i\eta} + \frac{B_{m,m'}(\mathbf{k},\omega')}{\omega - \epsilon_F + \omega' - i\eta}$$
$$= \int_{-\infty}^{+\infty} \mathrm{d}\omega' \frac{\widetilde{S}_{m,m'}(\mathbf{k},\omega')}{\omega - \epsilon_F - \omega' + i\eta\mathrm{sign}(\omega')}, \tag{D.1.18}$$

with,

$$S_{m,m'}(\mu,\omega') \equiv A_{m,m'}(\mu,\omega'), \qquad S_{m,m'}(\mu,-\omega') \equiv B_{m,m'}(\mu,\omega'),$$
$$\widetilde{S}_{m,m'}(\mu,\omega') = \begin{cases} \widetilde{S}^+_{m,m'}(\mu,\omega') & \text{if } \omega' > 0, \\ \widetilde{S}^-_{m,m'}(\mu,\omega') & \text{if } \omega' < 0, \end{cases} \tag{D.1.19}$$

considering that,

$$\int_0^{+\infty} A_{m,m'}(\mathbf{k},\omega') + B_{m,m'}(\mathbf{k},\omega')\mathrm{d}\omega' = \int_{-\infty}^{+\infty} \widetilde{S}_{m,m'}(\mathbf{k},\omega')\mathrm{d}\omega' = 1 \tag{D.1.20}$$

due to the normalization and completeness of the set $|n\rangle$.

Considering then the Cauchy principal value of a complex denominator (Sokhotski-Plemelj formula)

$$\frac{1}{\omega \pm i\eta} = \mathcal{P}\frac{1}{\omega} \mp i\pi\delta(\omega), \tag{D.1.21}$$

with $\delta(\omega)$ the Dirac's delta, valid in the limit $\eta \to 0$, one can rewrite (D.1.18) as

$$G_{m,m'}(\mathbf{k},\omega+\epsilon_F) = \int_{-\infty}^{+\infty} \mathrm{d}\omega' \frac{\widetilde{S}_{m,m'}(\mathbf{k},\omega')}{\omega - \omega' + i\eta\mathrm{sign}(\omega')}$$
$$= \mathcal{P}\int_{-\infty}^{+\infty} \mathrm{d}\omega' \frac{\widetilde{S}_{m,m'}(\mathbf{k},\omega')}{\omega - \omega'} + i\pi\widetilde{S}_{m,m'}(\mathbf{k},\omega). \tag{D.1.22}$$

Considering that $\widetilde{S}_{m,m'}$ is a real number, one concludes that the first term is real and the second one is imaginary. That brings to

$$\pi\widetilde{S}_{m,m'}(\mathbf{k},\omega) = \begin{cases} - & \Im m\{G_{m,m'}(\mathbf{k},\omega+\epsilon_F)\}, \quad \text{if } \omega > 0 \\ & \Im m\{G_{m,m'}(\mathbf{k},\omega+\epsilon_F)\}, \quad \text{if } \omega < 0 \end{cases} \tag{D.1.23}$$

which is the equation to calculate the strength function from the Green's function.

The Green's functions are conveniently represented in the Lehmann representations also because they can be associated to particle lines in Feynman diagrams, allowing to think diagrammatically, thus representing perturbation processes and interactions in an intuitive and graphical way.

D.2 Green's function and Feynman diagrams

For a comprehensive treatment of Feynman diagrams in many-body physics cf. [42, 40]. For what concerns us, in order to familiarize with the Feynman diagrams representations and prescriptions, we can consider the "dressing" of the "bare" Green's Functions G^0, representing free particles when we turn on a two-body interaction v. In other words the perturbative representation and renormalization of the properties of a particle implied by the interaction with itself and possibly other ones. The result of the renormalization of a free particle implied by an (effective) two-particle interaction are the Hartree-Fock equations.

Let us consider the Green's function of a free-fermion in a system without interaction, in other words the Green's function G^0 corresponding to the hamiltonian

$$H_0 = \sum_\nu \frac{p_\nu^2}{2m} \equiv \sum_\nu \epsilon_\nu^0 a_\nu^\dagger a_\nu, \tag{D.2.1}$$

with $\epsilon_\nu^0 = \frac{k_\nu^2}{2m}$, This is given by, in the Lehmann representation (D.1.13),

$$G^0(\nu,\omega) = \sum_\mu \frac{1}{\omega - \epsilon_\mu^0 + i\eta} + \frac{1}{\omega + \epsilon_\mu^0 - i\eta}. \tag{D.2.2}$$

Turning on an interaction makes it possible for the "bare" particle G^0 to interact with other particles, and with itself, by the so called self energy process.

Introducing an interaction between the described particles, that can be a "bare" one (like the force between electrons in a metal, often considered in the first order of perturbation as the Coulomb force between charges in vacuum) or an "effective" one (like Skyrme interaction that tries to parametrize, as functions of the density, some lower order normalization processes), one obtain contributions that, in the lowest order, are:

1)

$$\begin{array}{ccccccc} iG^0(k) & (-i) & (-1) & \displaystyle\sum_{spin}\int \frac{d_4k'}{(2\pi)^4}\langle k,k'|v|k,k'\rangle & iG^0(k') & iG^0(k) \\ \text{I particle line} & \text{I interaction line} & \text{I loop} & \text{interaction I part. lines w loop} & \text{loop part line} & \text{II part line} \end{array} \tag{D.2.3}$$

2)

This is the lowest order exchange contribution coming from the bare interaction and is intimately related to the Pauli principle. This relation can be seen noticing that the

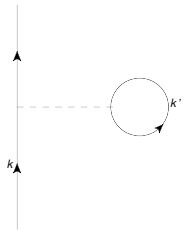

Figure D.1: This diagram represents the interaction of the bare particle $G^0(k)$ with an average distribution of the other particles, that, in this language, is represented by the loop of $G^0(k')$.

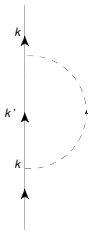

Figure D.2: This diagram represents the bare particle, that is in a state k and virtually jumps in a state k' returning to k in a second moment.

diagram above (Fig. D.2)is equivalent topologically with Fig. D.3(a). That is the Pauli exchange between the antisymmetrized state of a particle k and another one in the same state k coming from a virtual particle-hole excitation of the vacuum (Fig. D.3(b)).

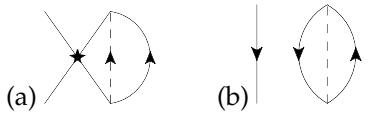

Figure D.3: Topological equivalent of Fig. D.2 (left) that comes from the exchange of hole line k with anothe one in the vacuum excitation (right).

The corresponding contribution is then given by

$$iG^0(k)(-1)\sum_{spin}\int\frac{d_4k'}{(2\pi)^4}\langle k',k|v|k,k'\rangle iG^0(k')iG^0(k), \tag{D.2.4}$$

the difference with 1) is that the interaction v brings $k \to k'$ and vice versa.

3) Instead of the interaction with another particle-line in Fig. D.4 is represented the interaction with a given field $\widetilde{U}$, so instead of integrating along the dummy variable k' there is a definite matrix element, so the equation is

$$iG^0(k)\langle k|\widetilde{U}|k\rangle iG^0(k). \tag{D.2.5}$$

These three contributions are taken into account in the Hartree Fock approximation: the first one, that average the contributions from all the particles k', is called Hartree term. The second one that considers the Pauli exchange principle and the antisimmetrization of the wavefunctions, is the Fock term. The third one is an (eventual)

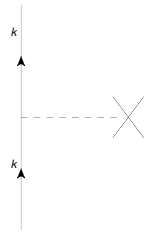

Figure D.4: This diagram represent the interaction with a one body (external) mean field.

external one body correction (eg. background of Jellium). This approach, making use of the one body Green's functions, approximate the two body interaction v with a one body mean field, in a way equivalent to other Hartree-Fock (plus eventually external field) formulations.

D.3 Dressed Green's function and Dyson equation

Direct nucleon-nucleon interaction, in the form of "bare" (same as vacuum) or "effective" (fitted to reproduce experimental results in finite nuclei) force, is not the only mean for a particle to interact with another one, or itself. A nucleon can interact not only via an interaction but also making use of other degrees of freedom of the system, namely collective states. In other words building block of the coupling in Feynman diagrams are vertexes, there can be particle-interaction vertexes, linking nucleons with the corresponding interaction, but also particle-vibration ones where nucleons scatters exciting or reabsorbing a vibration of the system.

The collective excitations of the system can be calculated with various methods, one of the most used in nuclear structure theory is (Quasiparticle) Random Phase Approximation, (Q)RPA. This framework consider all the correlated particle-hole excitations in order to represents the dynamical deformation of the system. This can be perturbatevly represented with Feynman diagrams as in Fig. D.5. The treatment of QRPA is out of the aim of the present work, but many comprehensive studies can be found in literature [43] as well as state-of-the-art considerations and calculations [44, 45].

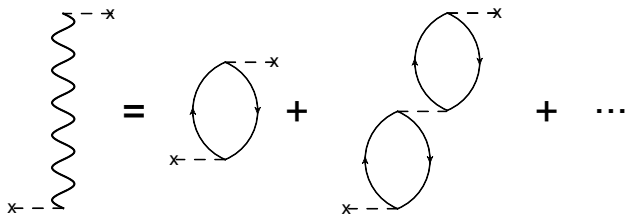

Figure D.5: Phonons arise from correlated particle-hole excitations in the RPA framework here represented diagrammatically.

In other words, for a given multipolarity λ, parity π (e.g. a 2^+ state, representing the quadrupolar isoscalar vibration of the system), the phonons spectrum $\omega_{\lambda^\pi_\nu}$ is calculated within (Q)RPA framework. The spectrum is then used to determine the "bare" phonon's

Green's function that, considering its boson nature, is

$$D^0_{\lambda^\pi}(\omega) = \sum_n \frac{1}{\omega - \omega_{\lambda^\pi\ n} + i\delta} - \frac{1}{\omega + \omega_{\lambda^\pi\ n} - i\delta}, \tag{D.3.1}$$

that is symmetric respect to ω ($D^0_{\lambda^\pi}(\omega) = D^0_{\lambda^\pi}(-\omega)$).

D.3.1 Pairing Hamiltonian and quasiparticles

Green's functions representation are particularly useful for treating perturbation to a known solution. Hartree-Fock can be represented diagrammatically and deduced directly as a perturbation of the free fermion problem, working out the two body interaction between nucleons as the one-body interaction of a particle with an averaging over the density of the system (Hartree-term), plus a term coming from the Pauli exclusion principle D.2. In this way the system can be represented as independent single particles in a self-consistent potential, moving in a medium dressing the particle inducing an effective mass m_k (usually $m_k \approx 0.7$). If the system is not a closed shell nucleus, and so there is no clear distinction between occupied and unoccupied states being the energy coming from coupling interaction between particles greater than the level density near the Fermi energy, the pairing interaction must be included explicitly. This can be done while (Hartree-Fock-Bogoliubov) or after (Bardeen-Cooper-Schrieffer) calculating the self-consistent Hartree-Fock field. Even if HFB is a better approximation respect to BCS, especially for a system with a very high level-density (usually slightly bound system in which the continuum plays a relevant part), the difference is small in the case of well-bound nuclei (e.g. ^{120}Sn), and is some cases [46, 16] we use the latter for simplicity.

The starting point of this perturbative approach is writing the Green's Function corresponding to the HFB pairing hamiltonian (considered solved) H_0, that in the second quantization is written as

$$H_{pair} = \sum_\mu \epsilon_\mu N_\mu + \sum_{\mu,\mu'} v_{\mu,\mu'} P^\dagger_\mu P_{\mu'}, \tag{D.3.2}$$

with

$$N_\mu = a^\dagger_\mu a_\mu \tag{D.3.3}$$

$$P^\dagger_\mu = a^\dagger_\mu a^\dagger_{\bar\mu}, \qquad P_\mu = a_{\bar\mu} a_\mu \tag{D.3.4}$$

where $a^\dagger$ represent the creation of a particle in the discrete state with quantum number μ or in its time reversal state $\bar\mu$. The coupling between particles and phonons is given perturbatly by the hamiltonian H' will be relevant in the following, and the total hamiltonian is given by the sum

$$H = H_{pair} + H_{coupl}. \tag{D.3.5}$$

The field operators that diagonalize the pairing hamiltonian are given by two dimensional spinor-like operator,

$$\psi_\mu = \begin{pmatrix} c_\mu \\ c^\dagger_{\bar\mu} \end{pmatrix}, \qquad \psi^\dagger_\mu = \begin{pmatrix} c^\dagger_\mu & c_{\bar\mu} \end{pmatrix}, \tag{D.3.6}$$

that will be used in the following as the field operators of the Green's functions.

D.3.2 Particle-phonon coupling vertex and Feynman rule

The vertex coupling the phonon to the particle is a scattering vertex as represented in Fig. D.6 (and in Fig. A.2). We have to consider the coupling in the Nambu-Gor'kov scheme, to define the eventual additional Feynman rules to use in the case of a BCS quasiparticle coupling to the vibration.

Figure D.6: Particle-Vibration scattering vertex, the building block of the renormalization.

The coupling hamiltonian will have the following operational structure:

$$H_{coupl} = \sum_{\lambda^\pi m} \kappa_\lambda b^\dagger_{\lambda^\pi m} \sum_{\mu\mu'} \langle \mu | F^\dagger_{\lambda^\pi m} | \mu' \rangle c^\dagger_\mu c_{\mu'} \tag{D.3.7}$$

Where $\kappa_{\lambda^\pi} b^\dagger_{\lambda^\pi m}$ is the creation of a phonon m of multipolarity λ, parity π; while $\langle \mu | F^\dagger_{\lambda m} | \mu' \rangle c^\dagger_\mu c_{\mu'}$ is the operator bringing single particle state μ in the state μ' coupled to λm.

One could introduce the common harmonic approximation:

$$a^\dagger_{\lambda m} = \sqrt{\frac{\hbar\omega_{\lambda m}}{2C_{\lambda m}}} \left(\Gamma^\dagger_{\lambda m} + \Gamma_{\lambda m} \right) \tag{D.3.8}$$

but this is not necessary at this point of the calculation and the coupling Hamiltonian can be kept more general.

In the Nambu Gorkov notation [15] $c^\dagger_\mu$, $c_{\mu'}$ are given by:

$$\frac{1}{2}\psi^\dagger_\mu \tau_3 \psi_{\mu'} = \frac{1}{2} \begin{pmatrix} c^\dagger_\mu & c_{\bar\mu} \end{pmatrix} \begin{pmatrix} 1 & 0 \\ 0 & -1 \end{pmatrix} \begin{pmatrix} c_{\mu'} \\ c^\dagger_{\bar\mu} \end{pmatrix} = \begin{pmatrix} c^\dagger_\mu & -c_{\bar\mu} \end{pmatrix} \begin{pmatrix} c_{\mu'} \\ c^\dagger_{\bar\mu} \end{pmatrix} = c^\dagger_\mu c_{\mu'} - c_{\bar\mu} c^\dagger_{\bar\mu'} \tag{D.3.9}$$

(where $\bar\mu$ is the time reversal state of μ). $c^\dagger_\mu c_{\mu'}$ is symmetric by time reversal, giving the equivalence

$$\langle \mu | F^\dagger_{\lambda m} | \mu' \rangle = \langle \bar\mu | F^\dagger_{\lambda m} | \bar\mu' \rangle \Rightarrow$$

$$\begin{aligned} \langle \mu | F^\dagger_{\lambda m} | \mu' \rangle \psi^\dagger_\mu \tau_3 \psi_{\mu'} =& \langle \mu | F^\dagger_{\lambda m} | \mu' \rangle \left(c^\dagger_\mu c_{\mu'} - c_{\bar\mu} c^\dagger_{\bar\mu'} \right) = \\ =& \langle \mu | F^\dagger_{\lambda m} | \mu' \rangle c^\dagger_\mu c_{\mu'} + \langle \bar\mu | F^\dagger_{\lambda m} | \bar\mu' \rangle c^\dagger_{\bar\mu'} c_{\bar\mu} + const = \\ =& 2 \langle \mu | F^\dagger_{\lambda m} | \mu' \rangle c^\dagger_\mu c_{\mu'} + const. \end{aligned} \tag{D.3.10}$$

The matrix elements of particle-phonon coupling, in the Nambu-Gorkov notation, are proportional to $\psi^\dagger_\mu \tau_3 \psi_{\mu'}$. This introduces another Feynman rule when considering this particle-vibration coupling vertex:

- insert for every particle-phonon coupling vertex a product by τ_3.

D.3.3 Dyson equation

After having illustrated the particle-phonon coupling matrix-element/vertex we have to consider its contributions to the renormalization of particle properties. The only process that can give contribution combining particle and phonon Green's functions G and D^0, from whose treated in section D.2, is the rainbow type, similar to the one in Fig. D.2. The equivalent to the process in Fig. D.1 cannot take place because, in order to have momentum conservation, the loop vertex need a $q = 0$ phonon that is a zero-energy phonon (dispersion relation for acustic phonons $\omega(k) \sim 2\omega_0 \sin(ka)$).

A very convenient way to go beyond the first order in perturbation theory, in order to take into account many type of processes, is grouping similar type of contribution, for example in Fig. D.7 the "dressed" Green's function G receives contributions from the

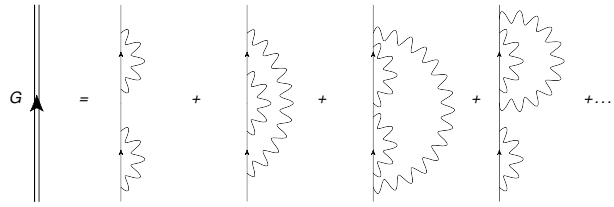

Figure D.7: Dressed Green's Function G is given by the unperturbed G^0 perturbed by the sum of self energy processes. The self energy processes considered in the Dyson equation are the ones of the so-called "rainbow series", so the ones involving Σ- (self-interaction)-type of diagrams.

"rainbow type" diagrams at the first (first contribution), second (from the second to the fourth contribution) and the latter is one of the third order in perturbation theory. In the diagrams in Fig. D.7 there are not all the possible second order diagrams: e.g. the diagram in Fig. D.8 is missing and these types of crossing-lines diagrams at all orders

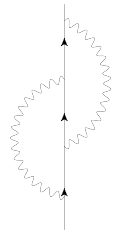

Figure D.8: This type of diagrams are not included in the Dyson equation treatment. Eventually can be added as vertex correction (Cf. Appendix B).

are neglected in this approximation.

The renormalization processes considered in Fig. D.7 can be represented making use of the dressed Green's function itself: if G is as represented in Fig. D.7, one can see that the second order of perturbation is given by the first order rainbow applied over (or after) itself, the third order is given by the first order rainbow applied over (or after) the second order contributions, and so on. This suggests that the series can be written making use of the building block in Fig. D.9, defined to be the "proper Self-Energy" Σ^* ($D^0(\omega - \omega')$ is chosen to have ω as the total energy of the self energy process).

This finally leads to the Dyson equation (cf. Fig. D.10), which reads

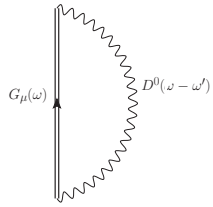

Figure D.9: Feynman representation of the proper self energy considered, building block of the Dyson equation (Fig. D.10), made by the dressed Green's function G and the unpertubed phonon D^0.

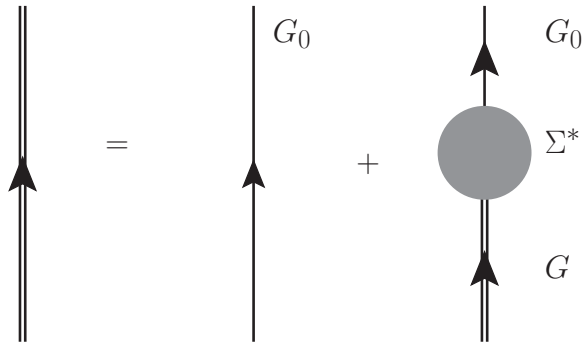

Figure D.10: Representation of the Dyson equation, that, considering as the proper Self Energy Σ^* the one in Fig. D.9, is a compact and efficient way to write the expansion D.7.

$$G = G^0 + G^0\Sigma^* G, \tag{D.3.11}$$

making use of a self-consistency of dressed G in order to take into account infinite order of perturbation. Dyson equation in the form (D.3.11) can be multiplied on the right by G^{-1} giving

$$1 = G^{-1}G^0 + G^0\Sigma^*, \tag{D.3.12}$$

and then multiplied on the left by $(G^0)^{-1}$ giving the more compact writing

$$G^{-1} = (G^0)^{-1} - \Sigma^*. \tag{D.3.13}$$

D.3.4 Self energy calculation

We proceed with the calculation of the proper self energy (cf. Fig. D.9), from now on referred simply with Σ, as it is the building block of the Dyson equation. So following the prescriptions of sect. D.2, we calculate

$$\hbar\Sigma(a,\omega) = -i\int_{-\infty}^{\infty}\frac{d\omega}{2\pi}\sum_{b\lambda_\nu^\pi}\langle\lambda_\nu^\pi|k_{\lambda^\pi}a^\dagger_{\lambda_\nu^\pi}|0\rangle\langle b|F^\dagger_{\lambda_\nu^\pi}|a\rangle\tau_3$$
$$iG(b,\omega')iD^0_{\lambda_\nu^\pi}(\omega-\omega')\langle 0|k^*_{\lambda^\pi}a_{\lambda_\nu^\pi}|\lambda_\nu^\pi\rangle\langle a|F^\dagger_{\lambda_\nu^\pi}|b\rangle\tau_3, \tag{D.3.14}$$

that, commuting c-numbers and c-functions, leads to

$$\hbar\Sigma(a,\omega) = \int_{-\infty}^{\infty}\frac{d\omega}{2\pi}\sum_{b\lambda_\nu^\pi}|\langle\lambda_\nu^\pi|k_{\lambda^\pi}a^\dagger_{\lambda_\nu^\pi}|0\rangle|^2|\langle b|F^\dagger_{\lambda_\nu^\pi}|a\rangle|^2\tau_3G(b,\omega')\tau_3iD^0_{\lambda_\nu^\pi}(\omega-\omega'), \tag{D.3.15}$$

and defining the vertex $|\langle\lambda_\nu^\pi|k_{\lambda^\pi}a^\dagger_{\lambda_\nu^\pi}|0\rangle|^2|\langle b|F^\dagger_{\lambda_\nu^\pi}|a\rangle|^2$ generally as the matrix element $h^2(a,b,\lambda_\nu^\pi)$,

$$\hbar\Sigma(a,\omega) = \int_{-\infty}^{\infty}\frac{d\omega}{2\pi}\sum_{b\lambda_\nu^\pi}\tau_3G(b,\omega')\tau_3iD^0_{\lambda_\nu^\pi}(\omega-\omega')h^2(a,b,\lambda_\nu^\pi) \tag{D.3.16}$$

where τ_3, as in eq. (D.3.9) is a Pauli matrix, that implies a transformation of the Green's Function in the Nambu-Gorkov spinor representation

$$\tau_3G(b,\omega)\tau_3 = \begin{pmatrix}1&0\\0&-1\end{pmatrix}\begin{pmatrix}G^{11}&G^{12}\\G^{21}&G^{22}\end{pmatrix}\begin{pmatrix}1&0\\0&-1\end{pmatrix} = \begin{pmatrix}G^{11}&-G^{12}\\-G^{21}&G^{22}\end{pmatrix}. \tag{D.3.17}$$

This gives the result for the components of the self-energy. E.g. the diagonal part is then given by

$$\hbar\Sigma^{11}(a,\omega) = \int_{-\infty}^{\infty}\frac{d\omega}{2\pi}\sum_{b\lambda_\nu^\pi}\tau_3G^{11}(b,\omega')\tau_3iD^0_{\lambda_\nu^\pi}(\omega-\omega')h^2(a,b,\lambda_\nu^\pi). \tag{D.3.18}$$

If we want to account perturbatively for the coupling of the HFB quasiparticles with the phonons, it is very convenient to recall the definition of the Lehmann representation in eq. (D.1.18), that, due to its the integral nature based on the definition of strength function is very suited for iterating in a perturbative fashion. The symmetry properties reflect on the strength (weight) functions $S_{m,m'}(a,\omega')$ of $G_{m,m'}(a,\omega')$, and even in $\Sigma_{m,m'}(a,\omega)$ as you can see in the following.

A diagonal element $\{a,a\}$ of the Self-Energy matrix (2×2 in the Nambu-Gorkov spinor representation) is given by

$$\Sigma_{m,m}(a,\omega) = \sum_{b\lambda_\nu^\pi}h^2(a,b,\lambda^\pi)\int_{-\infty}^{\infty}\frac{d\omega'}{2\pi}\int_0^\infty d\omega''\left[\frac{A_{m,m}(b,\omega'')}{\omega'-\omega''+i\eta}+\frac{B_{m,m}(b,\omega'')}{\omega'+\omega''-i\eta}\right]$$
$$i\left[\frac{1}{\omega-\omega'-\omega_{\lambda_\nu^\pi}+i\delta}+\frac{1}{\omega'-\omega-\omega_{\lambda_\nu^\pi}+i\delta}\right]. \tag{D.3.19}$$

To compute this integral in the complex plane, we have to consider the ω' variable as complex, then use the prescriptions of the Cauchy integral formula integrating over a closed path like the one in Fig. D.11 and then subtracting the arc contribution,

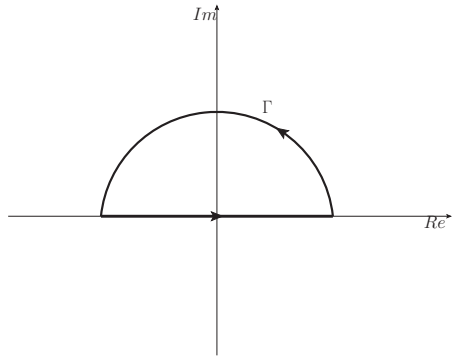

Figure D.11:

$$\int_{-\infty}^{+\infty} = \oint_C - \int_{arc}, \tag{D.3.20}$$

where in our case we can safely assume that we don't have singularity at infinity (for their physical meaning, the strength functions A and B, and the Green's function itself, go to zero at high energy) since the integrand ($G_{a,a} \cdot D^0$) goes to zero as $1/\omega'^2$ and so the upper bound of $\int_{arc}$ is the length of the arc itself (that goes as $\pi\omega'$), its contribution is $\leq \frac{\pi\omega'}{\omega'^2} \xrightarrow[\omega' \to \inf]{} 0$. So the integration over $\int_{-\infty}^{+\infty}$ can be replaced by the contour integration in the upper half plane, so the results will be the sum of the residues of the poles in the upper half plane.

There are four components of the functions in the integral:

- $\frac{A_{m,m}(b,\omega'')}{\omega'-\omega''+i\eta} \equiv G^-$, which has first order poles $\omega' = \omega'' - i\eta$, so only in the lower-half plane (fourth quadrant).

- $\frac{B_{m,m}(b,\omega'')}{\omega'+\omega''-i\eta} \equiv G^+$, which has first order poles $\omega' = -\omega'' + i\eta$, so only in the upper-half plane (second quadrant).

- $\frac{1}{\omega'-\omega-\omega_{\lambda_\nu^\pi}+i\delta} \equiv D^-$, which has first order poles $\omega' = \omega + \omega_{\lambda_\nu^\pi} - i\delta$, so only in the lower-half plane.

- $\frac{1}{\omega-\omega'-\omega_{\lambda_\nu^\pi}+i\delta} \equiv D^+$, which has first order poles $\omega' = \omega - \omega_{\lambda_\nu^\pi} + i\delta$, so only in the upper-half plane.

The contribution given by G^-D^- vanishes, because it has no poles in the upper-half

plane, thus no residues. The contribution of G^+D^+ also vanishes,

$$\begin{aligned}
&\oint_C G^+D^+ih^2(\cdot) = \\
&= \oint_C \frac{d\omega'}{2\pi} \sum_{n\lambda_\nu^\pi} \int_0^\infty d\omega'' ih^2(a,b,\lambda_\nu^\pi) \frac{B_{m,m}(b,\omega'')}{\omega'+\omega''-i\eta} \frac{1}{\omega-\omega'-\omega_{\lambda_\nu^\pi}+i\delta} = \\
&= \text{cost} 2\pi i \text{Res}\{G^+D^+\} = \\
&= \text{cost} \left\{ \left[\frac{\partial}{\partial\omega'}(\omega'+\omega''-i\eta)(\omega-\omega'-\omega_{\lambda_\nu^\pi}+i\delta)\Big|_{\omega'=-\omega''+i\eta} \right]^{-1} + \right. \\
&\quad \left. + \left[\frac{\partial}{\partial\omega'}(\omega'+\omega''-i\eta)(\omega-\omega'-\omega_{\lambda_\nu^\pi}+i\delta)\Big|_{\omega'=\omega-\omega'-\omega_{\lambda_\nu^\pi}+i\delta} \right]^{-1} \right\} = \\
&= \text{cost} \left[\frac{1}{\omega-\omega''-2\omega'-\omega_{\lambda_\nu^\pi}+i\delta+i\eta}\Big|_{\omega'=-\omega''+i\eta} + \right. \\
&\quad \left. + \frac{1}{\omega-\omega''-2\omega'-\omega_{\lambda_\nu^\pi}+i\delta+i\eta}\Big|_{\omega'=\omega-\omega_{\lambda_\nu^\pi}+i\delta} \right] = \\
&= \text{cost} \left[\frac{1}{\omega+\omega''-\omega_{\lambda_\nu^\pi}+i\delta-i\eta} + \frac{1}{-\omega-\omega''+\omega_{\lambda_\nu^\pi}-i\delta+i\eta} \right] = \\
&= 0,
\end{aligned} \tag{D.3.21}$$

because the two residues are opposite and cancel each other. The residues that give contribution in that contour are the ones from G^+D^-,

$$\begin{aligned}
&\oint_C G^+D^-ih^2(\cdot) = \\
&= \oint_C \frac{d\omega'}{2\pi} \sum_{b\lambda_\nu^\pi} \int_0^\infty d\omega'' ih^2(a,b,\lambda_\nu^\pi) \frac{B_{m,m}(b,\omega'')}{\omega'+\omega''-i\eta} \frac{1}{\omega'-\omega-\omega_{\lambda_\nu^\pi}+i\delta} = \\
&= \text{cost} 2\pi i \text{Res}\{G^+D^-\} = \\
&= 2\pi i \sum_{n\lambda_\nu^\pi} \frac{ih^2(a,b,\lambda_\nu^\pi)}{2\pi} \int_0^\infty d\omega'' B_{m,m}(b,\omega'') \left[\frac{\partial}{\partial\omega'}(\omega'+\omega''-i\eta)(\omega'-\omega-\omega_{\lambda_\nu^\pi}+i\delta)\Big|_{\omega'=-\omega''+i\eta} \right]^{-1} = \\
&= -\sum_{b\lambda_\nu^\pi} h^2(\mu,n,\lambda_\nu^\pi) \int_0^\infty d\omega'' \frac{B_{m,m}(b,\omega'')}{2\omega'+\omega''-\omega-\omega_{\lambda_\nu^\pi}+i\delta-i\eta}\Big|_{\omega'=-\omega''+i\eta} = \\
&= \sum_{b\lambda_\nu^\pi} h^2(a,b,\lambda_\nu^\pi) \int_0^\infty d\omega'' \frac{B_{m,m}(b,\omega'')}{\omega+\omega''+\omega_{\lambda_\nu^\pi}-i\delta-i\eta},
\end{aligned} \tag{D.3.22}$$

and the other one from G^-D^+ that, following the same prescriptions used above, gives

$$\oint_C G^+D^-ih^2(\cdot) = \sum_{b\lambda_\nu^\pi} h^2(a,b,\lambda_\nu^\pi) \int_0^\infty d\omega'' \frac{A_{m,m}(b,\omega'')}{\omega-\omega''-\omega_{\lambda_\nu^\pi}+i\delta+i\eta}, \tag{D.3.23}$$

leading finally to the result for the $\{a,a\}$ diagonal component of the proper self-energy

function,

$$\Sigma_{m,m}(a,\omega) = \sum_{b\lambda_\nu^\pi} h^2(a,b,\lambda_\nu^\pi) \int_0^\infty d\omega'' \frac{A_{m,m}(n,\omega'')}{\omega - \omega'' - \omega_{\lambda_\nu^\pi} + i\delta + i\eta} + \frac{B_{m,m}(b,\omega'')}{\omega + \omega'' + \omega_{\lambda_\nu^\pi} - i\delta - i\eta}. \tag{D.3.24}$$

For the off-diagonal part there is a minus sign induced by the $\tau_3 G \tau_3$ transformation as shown in eq. (D.3.17), giving

$$\Sigma_{m,m'}(a,\omega) = -\sum_{b\lambda_\nu^\pi} h^2(a,b,\lambda_\nu^\pi) \int_0^\infty d\omega'' \frac{A_{m,m'}(b,\omega'')}{\omega - \omega'' - \omega_{\lambda_\nu^\pi} + i\delta + i\eta} + \frac{B_{m,m'}(b,\omega'')}{\omega + \omega'' + \omega_{\lambda_\nu^\pi} - i\delta - i\eta}, \tag{D.3.25}$$

with $m \neq m'$, keeping in mind that, in this case, $A_{m,m'}$ and $B_{m,m'}$ are not definite-positive.

D.3.5 Symmetry properties

For the purpose of identifying symmetry properties useful in the calculation, and defining more clearly the structure of A and B strength functions one has to consider the particle-phonon coupling as a perturbation over the pairing hamiltonian, that does not modify the diagonalization implied by the Nambu-Gorkov spinor fields operators illustrated in sect. D.3.1. In other words H_{coupl} as a perturbation of H_{pair}. Keeping this in mind, Green's functions of hamiltonian H_{pair} (and in general 2×2 dimensional) in the Lehmann representation (D.1.13) have many useful symmetry properties.

Eq. (D.1.13) (that, for convenience, I report in the following, using the particle-notation)

$$G_{m,m'}(\mu,\omega) = \sum_n \frac{\langle\psi_0|\widehat{\psi}_\mu^m|n\rangle\langle n|\widehat{\psi}_{\mu\ m'}^\dagger|\psi_0\rangle}{\omega - \epsilon_n + i\eta} + \frac{\langle\psi_0|\widehat{\psi}_{\mu\ m}^\dagger|n\rangle\langle n|\widehat{\psi}_\mu^{m'}|\psi_0\rangle}{\omega + \epsilon_n - i\eta},$$

gives, for diagonal elements:

$$G_{m,m}(\mu,\omega) = \sum_n \frac{|\langle\psi_0|\widehat{\psi}_\mu^m|n\rangle|^2}{\omega - \epsilon_n + i\eta} + \frac{|\langle\psi_0|\widehat{\psi}_{\mu\ m}^\dagger|n\rangle|^2}{\omega + \epsilon_n - i\eta}, \tag{D.3.26}$$

that in our case is

$$G_{11}(\mu,\omega) = \sum_n \frac{|\langle\psi_0|\hat{c}_\mu|n\rangle|^2}{\omega - \epsilon_n + i\eta} + \frac{|\langle\psi_0|\hat{c}_\mu^\dagger|n\rangle|^2}{\omega + \epsilon_n - i\eta}, \tag{D.3.27}$$

$$G_{22}(\mu,\omega) = \sum_n \frac{|\langle\psi_0|\hat{c}_{\bar{\mu}}^\dagger|n\rangle|^2}{\omega - \epsilon_n + i\eta} + \frac{|\langle\psi_0|\hat{c}_{\bar{\mu}}|n\rangle|^2}{\omega + \epsilon_n - i\eta}. \tag{D.3.28}$$

Time reversal symmetry is a physical property that can be, in principle, assumed for physical observables (and thus Green's functions, as connection between observables), in any case in the following we will try to deduce it from the general properties of the complex HFB transformation. Given eq. (A.1.5) and (A.1.6) the square modulus of the matrix element $\hat{c}_\mu$ (that is the quasiparticle creator operator) is symmetrical respect to time reversal transformation since the difference between $\hat{c}_\mu$ and $\hat{c}_{\bar{\mu}}$ is in a gauge space phase change, so

$$|\langle\psi_0|\hat{c}_{\bar{\mu}}^\dagger|n\rangle|^2 = |\langle\psi_0|\hat{c}_\mu^\dagger|n\rangle|^2, \tag{D.3.29}$$

obtaining

$$G_{22}(\mu,\omega)=\sum_n \frac{|\langle\psi_0|\hat{c}^\dagger_\mu|n\rangle|^2}{\omega-\epsilon_n+i\eta}+\frac{|\langle\psi_0|\hat{c}_\mu|n\rangle|^2}{\omega+\epsilon_n-i\eta}=-G_{11}(\mu,-\omega). \tag{D.3.30}$$

The off diagonal elements, that in our case are G_{12} and G_{21}, have not the convenience of the square modulus that make the values real and positive independently from the complex phase,

$$\begin{aligned} G_{12}(\mu,\omega)&=\sum_n \frac{\langle\psi_0|\hat{c}_\mu|n\rangle\langle n|\hat{c}_{\bar{\mu}}|\psi_0\rangle}{\omega-\epsilon_n+i\eta}-\frac{\langle\psi_0|\hat{c}^\dagger_\mu|n\rangle\langle n|\hat{c}^\dagger_{\bar{\mu}}|\psi_0\rangle}{\omega+\epsilon_n-i\eta}\\ &=\sum_n \frac{\langle\psi_0|\hat{c}_\mu|n\rangle\langle n|\hat{c}_{\bar{\mu}}|\psi_0\rangle}{\omega-\epsilon_n+i\eta}-\frac{(\langle\psi_0|\hat{c}_{\bar{\mu}}|n\rangle\langle n|\hat{c}_\mu|\psi_0\rangle)^*}{\omega+\epsilon_n-i\eta} \end{aligned} \tag{D.3.31}$$

$$\begin{aligned} G_{21}(\mu,\omega)&=\sum_n \frac{\langle\psi_0|\hat{c}^\dagger_{\bar{\mu}}|n\rangle\langle n|\hat{c}^\dagger_\mu|\psi_0\rangle}{\omega-\epsilon_n+i\eta}-\frac{\langle\psi_0|\hat{c}_{\bar{\mu}}|n\rangle\langle n|\hat{c}_\mu|\psi_0\rangle}{\omega+\epsilon_n-i\eta}\\ &=\sum_n \frac{(\langle\psi_0|\hat{c}_\mu|n\rangle\langle n|\hat{c}_{\bar{\mu}}|\psi_0\rangle)^*}{\omega-\epsilon_n+i\eta}-\frac{\langle\psi_0|\hat{c}_{\bar{\mu}}|n\rangle\langle n|\hat{c}_\mu|\psi_0\rangle}{\omega+\epsilon_n-i\eta} \end{aligned} \tag{D.3.32}$$

that gives

$$G_{12}(\mu,\omega)=G_{21}(\bar{\mu},-\omega). \tag{D.3.33}$$

Considering again eq. (A.1.5) and (A.1.6) if the matrix element $\langle\psi_0|\hat{c}_\mu|n\rangle\langle n|\hat{c}_{\bar{\mu}}|\psi_0\rangle$ is real ($\propto U'V'$) and so equal to its complex conjugate $\langle n|\hat{c}^\dagger_\mu|\psi_0\rangle\langle\psi_0|\hat{c}^\dagger_{\bar{\mu}}|n\rangle$, giving $G^{HFB}_{12}(\mu,\omega)=G^{HFB}_{12}(\mu,-\omega)=G^{HFB}_{21}(\mu,\omega)$

Recalling the integral representation in eq. (D.1.18) where

$$\begin{aligned} G_{m,m'}(\mu,\omega+\epsilon_F)&=\int_0^{+\infty}\mathrm{d}\omega'\frac{A_{m,m'}(\mu,\omega')}{\omega-\omega'+i\eta}+\frac{B_{m,m'}(\mu,\omega')}{\omega+\omega'-i\eta}\\ &=\int_{-\infty}^{+\infty}\mathrm{d}\omega'\frac{\widetilde{S}_{m,m'}(\mu,\omega')}{\omega-\omega'+i\eta\mathrm{sign}(\omega')} \end{aligned}$$

individuating the properties of strength functions we can deduce the symmetry properties of Green's and Self-Energy functions. Considering G_{11} and G_{22} (respectively eqs. (D.3.27) and (D.3.28)) and the time reversal symmetry of eq. (D.3.29) it can be easily seen that

$$A_{11}(\mu,\omega)=B_{22}(\mu,\omega),\qquad B_{11}(\mu,\omega)=A_{22}(\mu,\omega), \tag{D.3.34}$$

in other terms,

$$S_{11}(\mu,\omega)=S_{22}(\mu,-\omega), \tag{D.3.35}$$

that gives for the Green's functions G_{11} and G_{22},

$$G_{11}(\mu,\omega)=\int_{-\infty}^{+\infty}\mathrm{d}\omega'\frac{S_{11}(\mu,\omega')}{\omega-\omega'+i\eta\mathrm{sign}(\omega')}, \tag{D.3.36}$$

$$G_{22}(\mu,-\omega)=\int_{-\infty}^{+\infty}\mathrm{d}\omega'\frac{S_{22}(\mu,\omega')}{-\omega-\omega''+i\eta\mathrm{sign}(\omega')}=-\int_{-\infty}^{+\infty}\mathrm{d}\omega''\frac{S_{22}(\mu,-\omega'')}{\omega-\omega''+i\eta\mathrm{sign}(\omega'')}, \tag{D.3.37}$$

obtained by changing $\omega'\to\omega''$, which satisfy then the symmetry property (D.3.30) in the case with $S_{11}(\mu,\omega)=S_{22}(\mu,-\omega)$.

D.3.6 Dressed Green's function

The exact form G and the value of the total solution of eigenvector and eigenvalues are then given by the solution of the Dyson equation explained in section D.3.3, which is,

$$G(a,\omega+i\eta) = \left[(G^0(a,\omega))^{-1} - \Sigma^*(a,\omega+i\eta)\right]^{-1} \tag{D.3.38}$$

where G^0 is the Green's function of the unperturbed system, thus giving

$$G^0(a,\omega) = \sum_n \frac{|p_n\rangle\langle p_n|}{\omega-\lambda-\varepsilon_{\hat{T}_n}+i\eta} + \sum_{n'} \frac{|h_{n'}\rangle\langle h_{n'}|}{\omega-\lambda+\varepsilon_{\hat{T}_{n'}}-i\eta} \tag{D.3.39}$$

where $\varepsilon_{\hat{T}_n}$ represent, by definition (D.1.13), the eigenvalue of the hamiltonian of the system the Green's function is describing, and since G^0 is the unperturbed Green's function of the free particle, the hamiltonian under consideration is the kinetic term $\hat{T}_n$. λ is the energy needed to add or remove a single particle on the system, and is the so-called chemical potential, or the Fermi energy $\lambda = -\varepsilon_F$. Were the terms with momenta $|k|$ or $-|k|$ in Eq. (D.1.13) in the nuclear case are particles p_n and holes $h_{n'}$ respectively. $|p_n\rangle\langle p_n|$ and $|h_{n'}\rangle\langle h_{n'}|$ are the matrix of eigenvectors of $\hat{T}$, which is diagonal being the two-body, of diagonal, contributions forbidden. Thus the inverse of G^0 is

$$\begin{aligned}(G^0(a,\omega))^{-1} &= \sum_n |p_n\rangle\langle p_n|(\omega-\lambda-\varepsilon_{\hat{T}_n}+i\eta) + \sum_{n'}|h_{n'}\rangle\langle h_{n'}|(\omega-\lambda+(\varepsilon_{\hat{T}_{n'}})-i\eta)\\ &= \sum_n \omega \pm i\eta - \lambda - \hat{T}|a_n\rangle\langle a_n| \end{aligned}\tag{D.3.40}$$

where we made use of the fact that the inverse of the diagonal matrix is equal to the matrix itself, and that $\hat{T}|p_n\rangle\langle p_n| = \varepsilon_{\hat{T}_n}|p_n\rangle\langle p_n|$ and $\hat{T}|h_n\rangle\langle h_n| = -\varepsilon_{\hat{T}_n}|p_n\rangle\langle p_n|$. In the end, considering Dyson equation (D.3.13), the proper Self Energy Σ^*, containing all the interaction of the system and so the two body V_{a_n,a_n}, the pairing $\Delta_{\bar{a}_n,a_n}$ and the phonon exchange $\hat{\Sigma}(a,\omega)$ described above, adding the kinetic term and the Fermi energy parameter $-\varepsilon_F$ we obtain the following equation for the dressed Green's function,

$$\hat{G}(a,\omega+i\eta) = \left[\omega+i\eta-\hat{H}_{HFB}-\hat{\Sigma}(a,\omega+i\eta)\right]^{-1} \tag{D.3.41}$$

where $\hat{H}_{HFB}$ is described by (A.1.1) and following. Since this gives new eigenvectors and eigenvalues used in (A.2.30) that diagonalize both $\hat{H}_{HFB}$ and $\hat{\Sigma}$ that are the new coefficient $\tilde{u}$ and $\tilde{v}$ to be taken into account in the vertexes in Fig. A.2, (A.2.8)-(A.2.11), the solution of $\hat{G}$ must be found iteratively.

D.4 Quasiparticle(s) Approximation

One of the most interesting properties of the Green's function is that if we define

$$\bar{G}(\mu,\omega) \equiv \lim_{\eta\to 0} \Re e\{G(\mu,\omega)\} \tag{D.4.1}$$

its poles are the eigenvalues of the total perturbed Hamiltonian, at the order of perturbation considered to "dressing" it. So it is interesting to consider the quasiparticle approximation, where we find the poles of the dressed Green's function denominator in order to

find the perturbed energies of the system without considering the full strength function. This approach can provide a good insight on the effects of the perturbation due to the phonon-induced self-energy and pairing by keeping the same weel-known formalism used in the independent-particle picture. A further sophistication can be made by considering the fact that the poles corresponding to a single state can be more than one, thus giving a fragmentation due to the coupling of the single particle energy level with the others via the phonons.

If we consider as starting point the HF calculation, in the usual Nambu spinor-field, the unperturbed Green's function can be taken as

$$G^0_{11}(\mu,\omega) = \sum_n \frac{|\langle\psi_{HF}|c_\mu|\psi_n\rangle|^2}{\omega - \varepsilon^{HF}_\mu + i\eta} + \frac{|\langle\psi_{HF}|c^\dagger_\mu|\psi_n\rangle|^2}{\omega + \varepsilon^{HF}_\mu - i\eta} \qquad = \frac{1}{\omega - |\varepsilon^{HF}_\mu| \pm i\eta}, \tag{D.4.2}$$

using the Lehmann representation (D.1.13), where $\varepsilon^{HF}_\mu = \epsilon^{HF}_\mu - \epsilon_F$, and the plus sign in the denominator is for particles ($\epsilon^{HF}_\mu > \epsilon_F$) while the minus sign is for holes ($\epsilon^{HF}_\mu < \epsilon_F$). The element on the (2,2) position, that has the denominator swapped respect to (1,1), is

$$G^0_{22}(\mu,\omega) = \sum_n \frac{|\langle\psi_{HF}|c^\dagger_\mu|\psi_n\rangle|^2}{\omega - \varepsilon^{HF}_\mu + i\eta} + \frac{|\langle\psi_{HF}|c_\mu|\psi_n\rangle|^2}{\omega + \varepsilon^{HF}_\mu - i\eta} \qquad = \frac{1}{\omega + |\varepsilon^{HF}_\mu| \mp i\eta}, \tag{D.4.3}$$

while the off-diagonal elements vanish, in pure HF approximation, since it is not possible to destroy and create the same particle from the same state due to the Pauli principle (if $\langle\psi_{HF}|c^\dagger_\mu|\psi_n\rangle \neq 0$ then $\langle\psi_n|c^\dagger_\mu|\psi_{HF}\rangle = 0$ and vice versa, so $\langle\psi_{HF}|c^\dagger_\mu|\psi_n\rangle\langle\psi_n|c^\dagger_\mu|\psi_{HF}\rangle = 0$ always). From that follows

$$G^0(\mu,\omega) = \begin{pmatrix} G^0_{11}(\mu,\omega) & 0 \\ 0 & G^0_{22}(\mu,\omega) \end{pmatrix} \tag{D.4.4}$$

$$(G^0(\mu,\omega))^{-1} = \begin{pmatrix} (G^0_{11}(\mu,\omega))^{-1} & 0 \\ 0 & (G^0_{22}(\mu,\omega))^{-1} \end{pmatrix} \tag{D.4.5}$$

$$= \begin{pmatrix} \omega - |\varepsilon^{HF}_\mu| \pm i\eta & 0 \\ 0 & \omega + |\varepsilon^{HF}_\mu| \mp i\eta \end{pmatrix}, \tag{D.4.6}$$

$$\tag{D.4.7}$$

in this way the Dyson equation (D.3.13) becomes

$$(G(\mu,\omega))^{-1} = \begin{pmatrix} \omega - |\varepsilon^{HF}_\mu| \pm i\eta - \Sigma_{11}(\mu,\omega) & -\Sigma_{12}(\mu,\omega) \\ -\Sigma_{21}(\mu,\omega) & \omega + |\varepsilon^{HF}_\mu| \mp i\eta - \Sigma_{22}(\mu,\omega) \end{pmatrix}, \tag{D.4.8}$$

and considering that we wants to find the poles of the real part of the Green's function, in other terms the roots of its inverse (so we have to solve $\lim_{\eta\to 0} \Re e\{(G(\mu,\omega))^{-1}\} = 0$),

$$\begin{pmatrix} \omega - |\varepsilon^{HF}_\mu| \pm i\eta - \Sigma_{11}(\mu,\omega) & -\Sigma_{12}(\mu,\omega) \\ -\Sigma_{21}(\mu,\omega) & \omega + |\varepsilon^{HF}_\mu| \mp i\eta - \Sigma_{22}(\mu,\omega) \end{pmatrix} = 0 \tag{D.4.9}$$

giving another known form of the Dyson equation, used in [16, 38], as an eigenvalue equation that well suits the perturbative nature of Σ,

$$\left[\begin{pmatrix} |\varepsilon^{HF}_\mu| & 0 \\ 0 & -|\varepsilon^{HF}_\mu| \end{pmatrix} + \Sigma(\mu,\omega)\right] \begin{pmatrix} x_0(\mu) \\ y_0(\mu) \end{pmatrix} = \omega \begin{pmatrix} x_0(\mu) \\ y_0(\mu) \end{pmatrix}. \tag{D.4.10}$$

In this picture it can be seen that the self energy perturbation implies an energy correction and the solutions of this eigenvalues equations are the perturbed energies of the original single particle state μ. For every single-particle state μ there can be more than one solution, where every solution corresponds to a fragment of the original single-(quasi-) particle. In fact there are as many fragments as the possible couplings though most of them are suppressed due to their tiny strength. Since the matrix Σ is Hermitian ($\Sigma_{12} = \Sigma_{21}^*$ cf. D.3.5) this equation have real eigenvalues ω_μ^n and the eigenvalues are symmetric $\omega_\mu(n) = -\omega_\mu(n')$ and eigenvectors can be chosen in order to form a complete orthonormal set (cf. Appendix A)

$$\sum_n \begin{pmatrix} x_0(\mu,n) \\ y_0(\mu,n) \end{pmatrix} (x_0(\mu,n) \quad y_0(\mu,n)) = \mathcal{I}. \tag{D.4.11}$$

so the solutions of the eigenvalue equation are

$$\left[\begin{pmatrix} |\varepsilon_\mu^{HF}| & 0 \\ 0 & -|\varepsilon_\mu^{HF}| \end{pmatrix} + \Sigma(\mu, \omega_\mu(n)) \right] \begin{pmatrix} x_0(\mu,n) \\ y_0(\mu,n) \end{pmatrix} = \omega_\mu(n) \begin{pmatrix} x_0(\mu,n) \\ y_0(\mu,n) \end{pmatrix}, \tag{D.4.12}$$

where $\omega_\mu(n)$ are the the quasiparticle energy of the fragments and $x_0(\mu,n), y_0(\mu,n)$ are the quasiparticle amplitudes that, following Eq. (D.4.11) are normalized as

$$\sum_n x_0^2(\mu,n) + y_0^2(\mu,n) = 1. \tag{D.4.13}$$

APPENDIX E

Particle Vibration Coupling with Separable Interaction

In this Appendix we give the basic expressions needed to compute the particle-vibration coupling vertex according to the collective model of Bohr and Mottelson [39]. This formalism is especially suitable to deal with the coupling of quasiparticles with low-lying collective density modes, making use of their experimental energies and transition strength, and I have used it extensively in ref. [16] to calculate the renormalization processes in ^{120}Sn. It is also used in Chapter 2 to calculate the renormalization of single-particles states in 132Sn. On the other hand, it is not convenient to deal with spin modes, and this is one of the reasons why results exposed in Chapter 1 make use instead of transition densities calculated with Skyrme interactions. The QRPA calculation will be carried out with the separable force

$$V(\vec{r}_1,\vec{r}_2) = -\kappa_{self}\ r_1\frac{\partial U}{\partial r_1}r_2\frac{\partial U}{\partial r_2}\sum_{\lambda\mu}\chi_\lambda Y^*_{\lambda\mu}(\theta_1)Y_{\lambda\mu}(\theta_2) \tag{E.0.1}$$

where $U(r)$ is a potential that gives a good reproduction of the experimental levels. In practice, we adopt the Woods-Saxon parametrization given in [47] (cf. Eq. (2-182)) together with an empirical pairing coupling constant adjusted to reproduce the pairing gap deduced from the experimental odd-even mass difference. The parameters χ_λ are determined so as to get a good agreement with the observed properties (energy and transition strength) of the low-lying surface modes. More precisely, we shall reproduce the polarizability $\beta^2_{\lambda 1}/\hbar\omega_{\lambda 1}$ of the low-lying modes, where $\beta_{\lambda\nu}$ denotes the experimental nuclear deformation parameter. In fact, the matrix elements of the phonon-induced pairing interaction for levels close to the Fermi energy are approximately proportional to the polarizability of the mode (cf. Eq. (1.22) below). The resulting values of χ_λ turn out to be close to 1, indicating that the QRPA coupling constant is close to the Bohr-Mottelson self-consistent coupling constant $\kappa_{self} = \left[\int r\frac{\partial\rho}{\partial r}r\frac{\partial U}{\partial r}r^2dr\right]^{-1}$.

This scheme then reduces to the collective particle-shape vibration (phonon) coupling scheme given by Bohr and Mottelson [39] (cf. Eqs. 6-207- 6-209). In fact the particle-hole matrix elements, neglecting the exchange terms (cf. on this point [43], Eq. (14.54) and Chap.16), are given by

$$F(abcd\lambda) = -\kappa_{self}\chi_\lambda < ab\lambda\mu|r_1\frac{\partial U}{\partial r_1}Y^*_{\lambda\mu}(\theta_1)|0><0|r_2\frac{\partial U}{\partial r_2}Y^*_{\lambda\mu}(\theta_2)|cd\lambda\mu > \tag{E.0.2}$$

where μ is any of the z-projections of the angular momentum λ. In this expression the QRPA-like single-particle indices (c,d) and the scattered particle indices (a,b) appear in separated factors, so that one gets the angular momentum reordering property

$F(abdc\lambda) = (-1)^{j_c - j_d + \lambda} F(abcd\lambda) = (-1)^{j_a - j_b + \lambda} F(bacd\lambda)$, and

$$V(ab\lambda\nu) = -\kappa_{self}\chi_\lambda(u_a u_b - v_a v_b) < ab\lambda\mu | r_1 \frac{\partial U}{\partial r_1} Y^*_{\lambda\mu}(\theta_1)|0> \left[\frac{2\lambda+1}{2j_a+1}\right]^{1/2}$$
$$\times \sum_{c\leq d}(1+\delta_{cd})^{-1/2}\left[(X_{cd}(\lambda\nu)+Y_{cd}(\lambda\nu))(u_c v_d + v_c v_d) < 0 | r_2 \frac{\partial U}{\partial r_2} Y^*_{\lambda\mu}(\theta_2)|cd\lambda\mu >\right] \quad \text{(E.0.3)}$$

The quantity in the summation is precisely the transition amplitude $M(\lambda\nu)$ of the $\hat{M} = r_2 \frac{\partial U}{\partial r_2} Y^*_{\lambda\mu}(\theta_2)$ operator, which is usually expressed in terms of the so-called collective deformation parameter as $M(\lambda\nu) = \alpha^o_{\lambda\nu}/\kappa_{self}$, assuming a collectively deformed density $\delta\rho = -r\frac{\partial\rho}{\partial r}\sum_{\lambda\mu} Y^*_{\lambda\mu}(\theta)\alpha_{\lambda\mu}$

In this way we can write

$$V(ab\lambda\nu) = -\chi_\lambda(u_a u_b - v_a v_b) < ab\lambda\mu | r_1 \frac{\partial U}{\partial r_1} Y^*_{\lambda\mu}(\theta_1)|0> \left[\frac{2\lambda+1}{2j_a+1}\right]^{1/2} \alpha^o_{\lambda\nu}. \quad \text{(E.0.4)}$$

Finally, following the notation in [39], Eqs.(6-207 to 6-209) using the reduced matrix element $< j_b||Y_\lambda||j_a >= (-1)^{j_a - j_b} < j_a j_b; \lambda\mu|Y_{\lambda\mu}|0 > \sqrt{2\lambda+1}$ and the relation $\alpha^o_{\lambda\nu} = \beta_{\lambda\nu}/\sqrt{2\lambda+1}$, we can write

$$V(ab\lambda\nu) = h(ab\lambda\nu)(u_a u_b - v_a v_b), \quad \text{(E.0.5)}$$

where

$$h(ab\lambda\nu) = -(-1)^{j_a - j_b}\beta^{eff}_{\lambda\nu} < a | r_1 \frac{\partial U}{\partial r_1}|b >< j_b||Y_\lambda||j_a > \left[\frac{1}{(2j_a+1)(2\lambda+1)}\right]^{1/2}, \quad \text{(E.0.6)}$$

which is the basic vertex in [39] corrected by our effective deformation parameter $\beta^{eff}_\lambda = \chi_{\lambda\nu}\beta_{\lambda\nu}$. Analogously one finds

$$W(ab\lambda\nu) = h(ab\lambda\nu)(u_a v_b + v_a u_b). \quad \text{(E.0.7)}$$

Bibliography

[1] D. R. Bès, R. A. Broglia, G. G. Dussel, R. J. Liotta, and H. M. Sofía, "The nuclear field treatment of some exactly soluble models," *Nucl. Phys. A*, vol. 260, p. 1, 1976.

[2] D. R. Bès, R. A. Broglia, G. G. Dussel, R. J. Liotta, and H. M. Sofía, "Application of the nuclear field theory to monopole interactions which include all the vertices of a general force," *Nucl. Phys. A*, vol. 260, p. 27, 1976.

[3] D. R. e. Bès, "On the many-body foundation of the Nuclear Field Theory," *Nucl. Phys. A*, vol. 260, p. 77, 1976.

[4] R. A. Broglia, B. R. Mottelson, D. R. Bès, R. Liotta, and H. M. Sofía, "Treatment of the spurious state in Nuclear Field Theory," *Physics Letters B*, vol. 64, p. 29, 1976.

[5] B. R. Mottelson, *Elementary Modes of Excitation in Nuclei, Le Prix Nobel en 1975*. Stockholm: Imprimerie Royale Norstedts Tryckeri, 1976. p. 80.

[6] P. F. Bortignon, R. A. Broglia, D. R. Bès, and R. Liotta, "Nuclear field theory," *Phys. Rep.*, vol. 30, p. 305, 1977.

[7] D. Bès and J. Kurchan, *The tratment of Collective Coordinates in Many–Body Systems*. Singapore: World Scientific, 1990.

[8] C. Mahaux, P. F. Bortignon, R. A. Broglia, and C. H. Dasso, "Dynamics of the shell model," *Phys. Rep.*, vol. 120, p. 1, 1985.

[9] W. Dickhoff and D. Van Neck, *Many-Body Theory Exposed!: Propagator Description of Quantum Mechanics in Many-Body Systems*. World Scientific, 2005.

[10] G. F. Bertsch, P. F. Bortignon, and R. A. Broglia, "Damping of nuclear excitations," *Rev. Mod. Phys.*, vol. 55, p. 287, Jan 1983.

[11] P. F. Bortignon, A. Bracco, and R. A. Broglia, *Giant Resonances*. Amsterdam: Harwood Academic Publishers, 1998.

[12] A. B. Migdal, "Interaction between electrons and lattice vibrations in a normal metal," *Sov. Phys. JETP*, vol. 7, p. 996, 1958.

[13] B. Jennings, "Non-observability of spectroscopic factors," *arXiv:1102.3721v1*.

[14] P. Avogadro, F. Barranco, A. Idini, and E. Vigezzi, "Medium polarization effects in the superfluidity of finite nuclei and of the inner crust of neutron stars," 2013.

[15] J. Schrieffer, *Superconductivity*. New York: Benjamin, 1964.

[16] A. Idini, F. Barranco, and E. Vigezzi, "Quasiparticle renormalization and pairing correlations in spherical superfluid nuclei," *Phys. Rev. C*, vol. 85, p. 014331, 2012.

[17] G. Gori, F. Ramponi, F. Barranco, P. F. Bortignon, R. A. Broglia, G. Colò, and E. Vigezzi, "Attractive and repulsive contributions of medium fluctuations to nuclear superfluidity," *Phys. Rev. C*, vol. 72, p. 011302, 2005.

[18] A. Pastore, F. Barranco, R. A. Broglia, and E. Vigezzi, "Microscopic calculation and local approximation of the spatial dependence of the pairing field with bare and induced interactions," *Phys. Rev. C*, vol. 78, p. 024315, 2008.

[19] S. Bogner, T. Kuo, and A. Schwenk, "Model-independent low momentum nucleon interaction from phase shift equivalence," *Physics Reports*, vol. 386, p. 1, 2003.

[20] K. Hebeler, T. Duguet, T. Lesinski, and A. Schwenk, "Non-empirical pairing energy functional in nuclear matter and finite nuclei," *Phys. Rev. C*, vol. 80, p. 044321, 2009.

[21] G. Colò, H. Sagawa, S. Fracasso, and P. Bortignon, "Spin–orbit splitting and the tensor component of the skyrme interaction," *Physics Letters B*, vol. 646, p. 227, 2007.

[22] G. Colò, H. Sagawa, and P. F. Bortignon, "Effect of particle-vibration coupling on single-particle states: A consistent study within the skyrme framework," *Phys. Rev. C*, vol. 82, p. 064307, Dec 2010.

[23] M. J. Bechara and O. Dietzsch, "States in $^{121}\mathrm{Sn}$ from the $^{120}\mathrm{Sn}(d,\ p)^{121}\mathrm{Sn}$ reaction at 17 mev," *Phys. Rev. C*, vol. 12, p. 90, 1975.

[24] E. Gerlic, G. Berrier-Ronsin, G. Duhamel, S. Galès, E. Hourani, H. Langevin-Joliot, M. Vergnes, and J. Van de Wiele, "Neutron-hole distributions in $^{111,115,119}\mathrm{Sn}$ as observed in the $(^3\mathrm{He}, \alpha)$ reaction," *Phys. Rev. C*, vol. 21, p. 124, 1980.

[25] S. Dickey, J. Kraushaar, R. Ristinen, and M. Rumore, "The $^{120}\mathrm{Sn}(p, d)^{119}\mathrm{Sn}$ reaction at 26.3 MeV," *Nuclear Physics A*, vol. 377, p. 137, 1982.

[26] G. Potel, F. Barranco, F. Marini, A. Idini, E. Vigezzi, and R. A. Broglia, "Calculation of the transition from pairing vibrational to pairing rotational regimes between magic nuclei $^{100}\mathrm{Sn}$ and $^{132}\mathrm{Sn}$ via two-nucleon transfer reactions," *Phys. Rev. Lett.*, vol. 107, p. 092501, 2011.

[27] G. Bassani, N. M. Hintz, C. D. Kavaloski, J. R. Maxwell, and G. M. Reynolds, "$(p,\ t)$ ground-state $L = 0$ transitions in the even isotopes of Sn and Cd at 40 MeV, $N = 62$ to 74," *Phys. Rev.*, vol. 139, p. B830, 1965.

[28] P. Guazzoni, M. Jaskola, L. Zetta, A. Covello, A. Gargano, Y. Eisermann, G. Graw, R. Hertenberger, A. Metz, F. Nuoffer, and G. Staudt, "Level structure of ^{120}Sn: High resolution (p, t) reaction and shell model description," *Phys. Rev. C*, vol. 60, p. 054603, 1999.

[29] P. Guazzoni, L. Zetta, A. Covello, A. Gargano, B. F. Bayman, T. Faestermann, G. Graw, R. Hertenberger, H.-F. Wirth, and M. Jaskola, "$^{118}\mathrm{Sn}$ levels studied by the $^{120}\mathrm{Sn}(p, t)$ reaction: High-resolution measurements, shell model, and distorted-wave born approximation calculations," *Phys. Rev. C*, vol. 78, p. 064608, 2008.

[30] K. L. Jones, A. S. Adekola, D. W. Bardayan, J. C. Blackmon, K. Y. Chae, K. A. Chipps, J. A. Cizewski, L. Erikson, C. Harlin, R. Hatarik, R. Kapler, R. L. Kozub, J. F. Liang, R. Livesay, Z. Ma, B. H. Moazen, C. D. Nesaraja, F. M. Nunes, S. D. Pain, N. P. Patterson, D. Shapira, J. F. Shriner, M. S. Smith, T. P. Swan, and J. S. Thomas, "The magic structure of ^{132}Sn explored through the single–particle states of ^{133}Sn," *Nature*, vol. 465, p. 454, 2010.

[31] P. Cottle, "Doubly Magic Tin," *Nature*, vol. 465, p. 430, 2010.

[32] J. Beene, R. Varner, C. Baktash, A. Galindo-Uribarri, C. Gross, J. G. del Campo, M. Halbert, P. Hausladen, Y. Larochelle, J. Liang, J. Mas, P. Mueller, E. Padilla-Rodal, D. Radford, D. Shapira, D. Stracener, J.-P. Urrego-Blanco, and C.-H. Yu, "Coulomb excitation studies of 132,134sn," *Nuclear Physics A*, vol. 746, p. 471, 2004. ¡ce:title¿Proceedings of the Sixth International Conference on Radioactive Nuclear Beams (RNB6)¡/ce:title¿.

[33] D. Radford, C. Baktash, J. Beene, B. Fuentes, A. Galindo-Uribarri, J. G. del Campo,

C. Gross, M. Halbert, Y. Larochelle, T. Lewis, J. Liang, J. Mas, P. Mueller, E. Padilla, D. Shapira, D. Stracener, R. Varner, C.-H. Yu, C. Barton, M. Caprio, D. Hartley, and N. Zamfir, "Nuclear structure studies with heavy neutron-rich ribs at the hribf," *Nuclear Physics A*, vol. 746, p. 83, 2004. ¡ce:title¿Proceedings of the Sixth International Conference on Radioactive Nuclear Beams (RNB6)¡/ce:title¿.

[34] B. Fogelberg, M. Hellström, D. Jerrestam, H. Mach, J. Blomqvist, A. Kerek, L. O. Norlin, and J. P. Omtvedt, "Detailed spectroscopy of the doubly closed shell nucleus ^{132}Sn : first observation of octupole collectivity," *Phys. Rev. Lett.*, vol. 73, p. 2413, Oct 1994.

[35] T. Björnstad, L.-E. D. Geer, G. Ewan, P. Hansen, B. Jonson, K. Kawade, A. Kerek, W.-D. Lauppe, H. Lawin, S. Mattsson, and K. Sistemich, "Structure of the levels in the doubly magic nucleus 50132sn82," *Physics Letters B*, vol. 91, p. 35, 1980.

[36] H. Liang, P. Zhao, L. Li, and J. Meng, "Spin-orbit and orbit-orbit strengths for the radioactive neutron-rich doubly magic nucleus ^{132}Sn in relativistic mean-field theory," *Phys. Rev. C*, vol. 83, p. 011302, 2011.

[37] B. Fogelberg, H. Gausemel, K. A. Mezilev, P. Hoff, H. Mach, M. Sanchez-Vega, A. Lindroth, E. Ramström, J. Genevey, J. A. Pinston, and M. Rejmund, "Decays of ^{131}In, ^{131}Sn, and the position of the $h_{11/2}$ neutron hole state," *Phys. Rev. C*, vol. 70, p. 034312, 2004.

[38] V. Van der Sluys, D. Van Neck, M. Waroquier, and J. Ryckebusch, "Fragmentation of single-particle strength in spherical open-shell nuclei: Application to the spectral functions in ^{142}Nd," *Nucl. Phys. A*, vol. 551, p. 210, 1993.

[39] A. Bohr and B. R. Mottelson, *Nuclear Structure, Vol.II*. New York: Benjamin, 1975.

[40] A. Fetter and J. Walecka, *Quantum Theory of Many-Particle Systems*. Dover Books on Physics, Dover Publications, 1971.

[41] R. A. Broglia, "From phase transitions in finite systems to protein folding and non–conventional drug design," *La Rivista del Nuovo Cimento*, vol. 28, no. 1, p. 1, 2005.

[42] R. Mattuck, *A Guide to Feynman Diagrams in the Many-Body Problem*. Dover Books on Physics & Chemistry, Dover Publ., 1976.

[43] D. J. Rowe, *Nuclear Collective Motion. Models and Theory*. London: Methuen & Co., 1970.

[44] J. Terasaki, J. Engel, M. Bender, J. Dobaczewski, W. Nazarewicz, and M. Stoitsov, "Self-consistent description of multipole strength in exotic nuclei: Method," *Phys. Rev. C*, vol. 71, p. 034310, 2005.

[45] J. Terasaki and J. Engel, "Self-consistent description of multipole strength: Systematic calculations," *Phys. Rev. C*, vol. 74, p. 044301, 2006.

[46] A. Idini, F. Barranco, R. A. Broglia, and E. Vigezzi, "Contribution of nuclear field theory medium effects to the pairing gap," *Journal of Physics: Conference Series*, vol. 336, no. 1, p. 012012, 2011.

[47] A. Bohr and B. R. Mottelson, *Nuclear Structure, Vol.I*. New York: Benjamin, 1969.

List of Publications

This work of thesis mostly consist in non-published, very present-state work. In the following list of publications can be found other works and arguments I have engaged during the course of my studies.

Refereed publications

- "Quasiparticle renormalization and pairing correlation in spherical superfluid nuclei"
  A. Idini, F. Barranco, E. Vigezzi, *Phys.Rev. C* 85:014331 (2012)
- "Calculation of the Transition from Pairing Vibrational to Pairing Rotational Regimes between Magic Nuclei Sn and Sn via Two-Nucleon Transfer Reactions"
  G. Potel, F. Barranco, F. Marini, **A. Idini**, E. Vigezzi, R. A. Broglia, *Phys. Rev. Lett.* 107:092501 (2011)

Publications under review

- "Quantitative study of coherent pairing modes with two neutron transfer: Sn-isotopes"
  G. Potel, **A. Idini**, F. Barranco, E. Vigezzi, R.A. Broglia, *arXiv:1210.5085 [nucl-th]*.
- "Nuclear Field Theory predictions for Li and Be: shedding light on the origin of pairing in nuclei"
  G. Potel, **A. Idini**, F. Barranco, E. Vigezzi, R.A. Broglia, *arXiv:1212.2437 [nucl-th]*.

Publications in preparation

- "Single Cooper pair transfer in stable and exotic nuclei"
  G. Potel, **A. Idini**, F. Barranco, E. Vigezzi, R.A. Broglia, *arXiv:0906.4298v3 [nucl-th]*.
- "Magicity of $^{132}_{50}\mathrm{Sn}_{82}$ not better than about one half?"
  A. Idini, G. Potel, F. Barranco, E. Vigezzi, R.A. Broglia. (cf. Ch. 2)
- "Renormalization effects and transfer reactions in ^{120}Sn"
  A. Idini, G. Potel, F. Barranco, E. Vigezzi, R.A. Broglia. (cf. Ch. 1)

Publications in conference proceedings and contributions to volumes

- "Medium Polarization Effects on the Superfluidity of Finite Nuclei and of the Inner Crust of Neutron Stars"
  P. Avogadro, F. Barranco, **A. Idini**, E. Vigezzi, *50 years of Nuclear BCS*, eds. R. A. Broglia and V. Zelevinsky, chapter 18, pag. 243-262, World Scientific Press, Singapore.

- "Reaction mechanism of two–neutron transfer in DWBA"
  G. Potel, **A. Idini**, F. Barranco, E. Vigezzi, R.A. Broglia, *EPJ Web of Conf.* 17, 01004 (2011)

- "Nuclear surface dynamics and pairing correlations" F. Barranco, R.A. Broglia, **A. Idini**, E. Vigezzi, *J. Phys.: Conf. Ser.* 321 012019 (2011)

- "Dyson treatment of NFT medium polarization processes in superfluid nuclei"
  A. Idini, F. Barranco, E. Vigezzi, R. A. Broglia, *J. Phys.: Conf. Ser.* 312 092032 (2011)

- "Contribution of Nuclear Field Theory medium effects to the pairing gap"
  A. Idini, F. Barranco, R.A. Broglia, E. Vigezzi, *J. Phys.: Conf. Ser.* 336 012012 (2011)

- "Investigation of the self-activity and high energy γ-rays response of a 1" x 1" and 3" x 3" $LaBr_3$:Ce scintillators"
  F. Camera, N. Blasi, S. Brambilla, F.C.L. Crespi,**A. Idini**, C. Maiolino, R. Nicolini, S. Riboldi, D. Santonocito, M. Sassi, O. Wieland, *Nuclear Science Symposium Conference Record. IEEE* 10.1109/NSSMIC.2007.4437258 (2007)

List of Figures

List of Tables